CARDIAC RECONSTRUCTION WITH ORGAN SPECIFIC EXTRACELLULAR MATRIX

by

John Michael Wainwright

Bachelor of Science in Chemical Engineering, University of Florida, 1999

Master of Engineering in Bio-Medical Engineering, University of Florida, 2004

Submitted to the Graduate Faculty of

Swanson School of Engineering in partial fulfillment

of the requirements for the degree of

Doctor of Philosophy

University of Pittsburgh

2010

UNIVERSITY OF PITTSBURGH

SWANSON SCHOOL OF ENGINEERING

This dissertation was presented

by

John Michael Wainwright

It was defended on

April 5th, 2010

and approved by

William Wagner, PhD, Professor, Department of Surgery

Kimimasa Tobita, MD, Assistant Professor, Department of Developmental Biology

Thomas Gilbert, PhD, Assistant Professor, Department of Surgery

Sanjeev Shroff, PhD, Professor, Department of Bioengineering

Dissertation Director: Stephen Badylak, DVM, MD, PhD, Professor, Department of Surgery

CARDIAC REMODELING WITH ORGAN SPECIFIC EXTRACELLULAR MATRIX

John Michael Wainwright, PhD

University of Pittsburgh, 2010

Surgical reconstruction of congenital heart defects is often limited by the non-resorbable material used to approximate normal anatomy. In contrast, non-crosslinked extracellular matrix (ECM) biologic scaffold materials have been used for tissue reconstruction of multiple organs and are replaced by host tissue. Preparation of whole organ ECM by vascular perfusion can maintain much of the native three-dimensional (3D) structure, strength, and tissue specific composition. A 3D Cardiac-ECM (C-ECM) biologic scaffold material would logically have structural and functional advantages over materials such as Dacron™ for myocardial repair, but the *in vivo* remodeling characteristics of C-ECM have not been investigated to date.

Intact porcine and rat hearts were decellularized through retrograde aortic perfusion to create a 3D C-ECM biologic scaffold material. C-ECM biochemical and structural composition were evaluated. C-ECM was not different in cell survival assays from a standard ECM material, urinary bladder matrix (UBM), and supported cardiomyocytes in both 2D and 3D culture. Finally, a porcine C-ECM or Dacron™ patch was used to reconstruct a full thickness right ventricular outflow tract (RVOT) defect in a rat model with a primary endpoint of 16 wk The Dacron patch was encapsulated by dense fibrous tissue and showed little cellular infiltration. Echocardiographic analysis showed that the Dacron patched heart had dilated right ventricular minimum and maximum dimensions at 16 wk compared to pre-surgery baseline values. The C-ECM patch remodeled into dense, cellular connective tissue including: collagen, endothelium,

smooth muscle, and small islands of cardiomyocytes. The C-ECM patch showed no ventricular dimensional or functional differences to baseline values at either the 4 or 16 wk time point.

The porcine and rat heart can be efficiently decellularized using perfusion in less than 10 hours. The potential benefit of the 2D and 3D C-ECM was shown to support cardiomyocytes with an organized sarcomere structure. The C-ECM patch was associated with better function and histomorphology compared to the Dacron™ patch in this rat model of RVOT reconstruction. While there is much work to be done, the methodology described herein provides a useful step to fully realizing a functional cardiac patch.

TABLE OF CONTENTS

LIST OF TABLES

LIST OF FIGURES

PREFACE

I have grown tremendously in my understanding of bioengineering during my time at University of Pittsburgh. I would first like to thank Dr. Stephen Badylak for taking me into his lab and providing guidance during my graduate studies. I would also like to thank my wonderful committee members: Dr. William Wagner, Dr. Kimimasa Tobita, Dr. Thomas Gilbert, and Dr. Sanjeev Shroff for their time and great feedback.

I would like to thank everyone that has helped me in the Badylak lab. Donald Freytes for helping me with experiments, helping me with edits, and introducing me to people. Ann Stewart-Akers, Scott Johnson, and John Freund for showing me around the lab and helping me with projects. Urvi Patel, Caitlin Czajka, Denver Faulk, Kathryn Kukla and Bora Janicijevic for their help on summer projects and throughout the year. Nathaniel Remlinger for help with isolations and GFP rats. Neill Turner, Vineet Agrawal, Brian Brown, Ellen Brennan, Hongbin Jiang, and Li Zhang for their advice and help with different projects. Jennifer DeBarr and Deanna Rhoads for their help with histology preparation and slides. Jocelyn Runyon, Renee Atkinson, Dawn Roberts, and Eve Blasko for all of their help scheduling meetings, conference rooms, and everything else that came up. I would also like to thank everyone else I have worked with during my time here; I appreciate your time and willingness to help.

I would also like to acknowledge our collaborators that contributed to the work presented in this dissertation. Ryotaro Hashizume and Kazuro Fujimoto for their surgical expertise and

time performing surgeries and answering my questions on the rat studies. William Anderson and Giovanni Speziali, William Katz, Pietro Bajona, Stefano Salizzoni, Stephen Stewart, Mike Anselmi, for their collaboration and for performing the ASD procedures. All of the people at the animal facility Joe Hanke, Terri Gasser, Buffie Kerstetter, Mike Firda, Aaron Dean, and Shawn Bengston for all of their help on the different projects. Thank you very much!

To the Bioengineering faculty and staff you have made my learning experience very beneficial. Special thanks to Lynette Spataro, Joan Williamson, Judy Repp, and Jason Vey for answering all of my unending questions. To Harvey Borovetz and Rosa Pinkus for the opportunity to be their teaching assistant; I learned the difficulties and benefits of being a mentor.

My family for their support. My wife, Amanda Wainwright, for her love, understanding, and support of my long and strange hours and frequent waking in the middle of the night to work. My parents, Dee and Mike Wainwright, for their love and great vacations that helped me keep my sanity. To all my other family that has been there to talk with over the long years.

I am also thankful for my funding sources:

NIH-NIBIB small research grant (1R03EB009237-01A1) entitled “Cardiac Remodeling with Organ Specific Extracellular Matrix Scaffolds.”

NIH-NHLBI training grant (T32-HL76124) entitled “Cardiovascular Bioengineering Training Program.”

I truly appreciate everyone’s help that has assisted in my years here in Pittsburgh, without you I would not have accomplished this goal.

1.0 INTRODUCTION

‘‘Nature impresses us with a great variety of reactive possibilities in the adaptation of its tissues to new conditions and substances. Sound progress in medicine is easiest when we work along with the physiological currents of beneficial reaction and adaptation. To understand the direction and the limits of nature’s reactions is always the first step toward progress in tissue engineering (1).’’ As stated by Wolter and Meyer, tissue engineering’s role is to understand and modify the body’s response to injury by using the tools nature provides. To this end, scaffolds, cells, and cytokines by themselves or in combination can be used to persuade the injured tissue towards functional remodeling. Specifically, by using an organ specific biologic scaffold material derived from extracellular matrix (ECM) by itself or in combination with cells, one can provide a template for beneficial reconstruction and remodeling.

1.1 DISEASE OVERVIEW

The function of the heart to pump blood continuously to the whole body was first described by William Harvey in 1628 (2). While this elucidated the function of the heart, the mechanisms are still being investigated; even more mysterious are the origins, progression, and resolution of cardiovascular disease. Approximately 81 million Americans have cardiovascular disease

(CVD) accounting for 37% of all deaths and 5.3 million Americans with CVD have heart failure (HF) (3).

There is even less information on the causes of congenital heart defects. Approximately 3 in 1000 infants require corrective surgery for congenital heart defects (CHD) within the 1st yr of life (3). The most common CHD defects include ventricular septal defects (VSDs) (20%), Atrial septal defects (18.8%), coarctation of the aorta (7.6%), tetralogy of Fallot (6.1%), transposition of the great arteries (2.6%), hypoplastic left heart syndrome (2.2%) (4-5). Repairing the defects with functional tissue would increase quality of life and life expectancy.

1.2 CURRENT TREATMENTS

Current treatments of CHD and HF include: pharmacological intervention, heart transplant, surgical ventricular reconstruction (SVR), and mechanical assist devices all have shortcomings. The treatments often lead to continued progression of the disease, need for reoperations, lack of donor organs, lack of sufficient cell source/unproven benefits, and sepsis/device failure (6-9). While these treatments have decreased the 5 year age-adjusted mortality rate for HF by approximately 10% over the past 40 years, the 5 yr mortality rates are still 59% in men and 45% in women (10).

The first line of defense against heart disease is pharmacological intervention. Statins or low-dose aspirin are often given to prevent myocardial infarctions (11). Aspirin can also be used to aide in closure of a patent foramen ovale in newborn babies. After a myocardial infarction, angiotensin converting enzyme, ACE, inhibitors and angiotensin II type I receptor antagonists

are beneficial in improving symptoms and prolonging a LV dysfunctional patient's life (6). In many patients though, pharmacological intervention does not stop the progression of HF.

The gold standard for HF patients is heart transplantation, however not enough organs exist for the number of patients. Currently the international society of heart lung transplantation reports approximately 3200 heart transplants per year worldwide (12); which is far short of even 292,000 US deaths caused by HF (13). Heart transplantation is also limited in its longevity as the median survival after transplantation just over 10 years (14).

Because of the lack of donor hearts, surgical reconstruction is an alternative. For CHD the defects in structure can be reconstructed using synthetic grafts or homografts. Pediatric cardiac reconstruction often requires a repeat surgery because the synthetic materials or cross-linked homografts do not remodel as the patient grows. About 50% of patients who undergo repair of tetralogy of fallot (TOF) require reoperation within 40 yrs of the surgery (15-16). In one study 20% of patients required a reoperation due to stenosis or aneurism within 16 months (17). Homografts additionally have issues with sensitization and rejection (18-19).

In HF, the dilated ventricle can undergo surgical ventricular reconstruction (SVR) with a synthetic graft to improve the developed pressure in the heart. The RESTORE group investigated SVR in 439 patients using the Dor procedure with a Dacron graft. In the Dor procedure a portion of the infarcted heart is resected and the ventricle is reformed into a conical shape using a Dacron graft (20). They concluded that SVR "is a safe and effective operation in the treatment of the remodeled dilated anterior ventricle after anterior myocardial infarction (21)." However, the Dacron graft only reinforces the weakened portion of the heart and is not functional tissue or remodel over time. Therefore, a patch that could constructively remodel the defect would be beneficial over current surgical reconstruction techniques.

Ventricular assist devices (VADs) do provide active support for the failing heart; they can be used to support the left, right, or both ventricles. Complications include hemolysis, thrombosis, stroke, sepsis, and device failure (9). There have been ongoing improvements to the VADs since their implementation in the 1970's. In a recent trial, 67.4% of patients survived one year after VAD implantation at experienced centers (22). New devices in trials use an impeller with no bearings, which should reduce the possibilities of thrombosis and improve outcomes further (23). Even for patients that survive, the VADs still require constant anticoagulation, battery changes, and check-ups which impact patient quality of life (23).

1.3 INVESTIGATIONAL TREATMENTS

A tissue engineering approach to HF and CHD may be able to improve patient life expectancy while minimizing impact on quality of life. Most tissue engineering approaches involve a single procedure or surgery, do not require long term drug support including anticoagulation or immune suppression, and have no external power requirements. Therefore, patients should have an improved quality of life over current treatments.

1.3.1 Cell based therapies

Cell based therapies for CHD and HF hold great interest but to date functional cardiac tissue has not been formed in human clinical trials. There have been small functional improvements found by injecting stem cells into the infarcted area, but the exact mechanism of functional improvement is unknown (8). Similar small improvements have been found by injecting mesenchymal stem cells (MSCs) into the circulation after an acute myocardial infarction (24) but greater clinical improvements are needed. Recently, multiple groups have reported differentiation of human embryonic stem cells (H-ESC) into cardiomyocytes with structural (organized sarcomere structure) and functional (synchronous beating) properties (25-26). One group has even implanted a poly-1-lactic acid (PLLA) and polylactic glycolic acid (PLGA) scaffold including the H-ESC derived cardiomyocytes with endothelial cells and fibroblasts onto a rat heart in a non-defect model and showed integration with native vasculature (27). However, this was a non-infarct model and amount of surviving cardiomyocytes was not assessed. While there are many possible cell sources and methods, no stem cell therapy to date has proved effective in treating heart failure.

1.3.2 Cytokines

Many tissue engineering strategies include the use of growth factors directly or indirectly. Granulocyte colony-stimulating factor (G-CSF) was shown to reduce LV remodeling after an infarction in a mouse model (28). Angiotensin-(1–7), a biologically active metabolite of

Angiotensin I and II, preserved cardiac function, coronary perfusion, and aortic endothelial function in a rat model for heart failure (29), however it did not show any vasodilation properties in humans (30). The combination of hepatocyte growth factor with an ECM patch showed improved electrical activity and local shortening compared to ECM alone or Dacron patch (31). However, administration of growth factors has to be closely monitored as they can cause unintended severe consequences such as neurologic impairment from ectopic bone formation (32). Again, these improvements require more research before they reach clinically relevant efficacy for cardiac applications.

1.3.3 Scaffolds

Scaffolds are an integral part of tissue many engineering strategies. As described above, scaffolds can provide a substrate for the delivery of cells and cytokines, but can also singularly change the physical and biological remodeling cues (33).

1.3.3.1 Synthetic Scaffolds

Dacron™ and Teflon™ have been used for years for SVR, but are associated with complications such as stenosis and aneurism (34-35). Polylactic acid (PLA) and polyglycolic acid (PGA) polymers are some of the earliest and widely used biodegradable scaffolds because they break down into natural byproducts and their mechanical properties can be tuned by incorporating different percentages and changing the anisotropy of the polymers. Cardiomyocytes have been shown to form sarcomeric structures *in vitro* on electrospun PLA scaffolds (36). Unlike the stiffer PLA structure, polyester urethane urea (PEUU) has been shown to have tunable elastic properties that can be manipulated to closely match a variety of native tissues (37). PEUU

scaffolds have been used for right ventricle outflow tract (RVOT) repair and showed replacement with fibrous tissue with no indications of thrombosis (38). While it is possible to use these synthetic scaffolds for mechanical support or combine them with cell, drug, or cytokine therapies, they do not provide beneficial bioactivity on their own.

1.3.3.2 ECM Biologic Scaffolds

One regenerative medicine approach that has been successful for tissue restoration has been the development of "bioinductive" scaffold materials such as those composed of naturally occurring extracellular matrix scaffolds (ECM). The ECM scaffolds that have been most widely used have been those derived from the porcine small intestinal submucosa (SIS), bovine dermis (TissueMend^{TM}), human dermis (e.g., AlloDerm), and porcine urinary bladder (UBM). This approach has led to the formation of site-specific tissue reconstruction in several body systems, including myocardial repair (39-43). Naturally occurring extracellular matrix (ECM) scaffolds have been successfully used to augment or replace diseased or injured tissues from a variety of body systems in pre-clinical studies and clinical practice. Non-crosslinked ECM scaffolds have been shown to degrade rapidly and completely (44-45) and are associated with a robust host cellular response and deposition of neomatrix that remodels in response to host factors such as growth or change in mechanical loading (an important concept in myocardial reconstruction). Degradation of an ECM scaffold is an essential component of the remodeling process. Several *in vitro* studies have shown that degradation products of ECM scaffolds have inherent bioactivity, including antibacterial and chemotactic properties (46-48). These findings are consistent with the results from *in vivo* studies that showed infection resistance in intentionally contaminated surgical sites treated with ECM (49-52) and recruitment of bone marrow derived cells to the site of ECM remodeling (53-54). The recruitment of progenitor cells to participate in the

remodeling response may partially explain the observed site-specific remodeling (55). Non-crosslinked ECM scaffolds have been shown to promote differentiation of macrophages towards an anti-inflammatory phenotype consistent with tissue remodeling and accommodation (56). The positive bioactive and mechanical properties of ECM lead to many potential beneficial applications.

Since ECM has been shown to have many chemical components that have chemo-attractant, anti-microbial, and bioactive properties, it has been investigated for use in place of the synthetic patches in the Dor procedure (57-60). The ECM remodeled into partially organized densely cellular collagenous tissue with small islands of cardiomyocytes. The ECM showed an improvement in regional contractility and recruited hematopoietic cells as shown by labeling of CD 45 marker but did not fully restore myocardial structure or function (61-62). Alternatively, ECM gel has been used *in vitro* as part of a scaffold for a contractile cardiac patch (63). These cardiac applications are promising, but they lack the three dimensional (3D) structure needed to reconstruct complex geometries.

(a) Organ Specific ECM Scaffolds

Given the highly specific composition, organization, and function of the ECM of each individual organ, a xenogeneic ECM scaffold derived from the organ that is targeted for repair (i.e., the heart) may provide the optimal biomechanical behavior and biological signals for site specific remodeling to occur in that location. Bornstein first described the term “dynamic reciprocity” to suggest that secreted matrix macromolecules could modulate the structure and function of the cells that produced them (64-66) Bissell further elucidated the term to describe the interaction between an ECM and an organ’s cells in development, differentiation, and regulation (67-69). One study showed organ specific ECM scaffolds have the advantage of maintaining a

differentiated cell phenotype *in vitro* (e.g., hepatic sinusoidal endothelial cells of the liver), whereas other ECM did not maintain differentiation (70). Multiple other authors have described the role of Cardiac-ECM (C-ECM) in normal and diseased hearts (71-72). ECM scaffolds largely retain the 3-D tissue architecture and composition of the tissue from which they are isolated (73-77), it would be logical that C-ECM possesses potential benefits for myocardial tissue engineering applications. Within the last two years, C-ECM has been produced by several laboratories and has shown multiple structural and functional benefits (78-81). A detailed method to decellularize an intact porcine heart in less than 10 hours has been described (78). Whole heart C-ECM in an *in vitro* perfusion system has been shown to support contractile cardiomyocytes that generated aortic pressure (80). Singelyn et al. showed angiogenesis after injection of a gel form of C-ECM in a non-infarct cardiac rat model (81). While each of these studies showed the potential benefits of C-ECM, none were in an *in vivo* defect model. The unique ECM microstructure and ultrastructure provide distinct signals for the resident cells that reside within the tissue (67-69). It is this reciprocal role between ECM structure and composition and resident cell function that make organ specific ECM an appealing biologic scaffold for functional remodeling. ***Therefore, the goal of the present study is to evaluate cardiac extracellular matrix (C-ECM) for reconstruction of myocardial tissue.*** These goals will be accomplished through the successful completion of three specific aims.

1.4 SPECIFIC AIMS

SPECIFIC AIM No. 1: To decellularize an intact heart and characterize composition, microstructure, and tissue properties.

Rationale: The heart is a well vascularized and densely cellular tissue. Unlike the small intestine or urinary bladder, cardiac tissue cannot be physically delaminated into a thin sheet due to the presence of long spiral fibers (82). A more rigorous chemical decellularization method which utilizes the native vasculature of the heart can deliver reagents to all regions of the heart.

Hypothesis$_1$: An intact heart can be chemically decellularized with retrograde aortic perfusion.

SPECIFIC AIM No. 2: To determine the ability of C-ECM to support proliferation of endothelial cells and myoblast cells and maintain phenotype of cardiomyocytes.

Rationale: The reconstruction of functional tissue requires multiple cell types including muscle, endothelial, and progenitor cells. The ability of C-ECM to support cells *in vitro* will be assessed in the sheet and gel form as well as an intact decellularized rat heart.

Hypothesis$_2$: C-ECM scaffold will support cell survival and maintain cardiomyocyte phenotype.

SPECIFIC AIM No. 3: To compare the ability of a 6 mm C-ECM patch and Dacron patch in a rat model to reconstruct the right ventricle outflow tract (RVOT).

Rationale: RVOT reconstruction is often needed for congenital heart defects. Current synthetic patches often need a second surgery being the patches do not remodel (15); therefore

there is a clinical need for an improved patch material. C-ECM structure and composition is unique to the heart, it is hypothesized that it will provide superior reconstruction than synthetic materials.

Hypothesis$_3$: The C-ECM patch will result in more cardiomyocyte, smooth muscle, and endothelial cells in the patched area compared to Dacron and will not cause stenosis or dilation of the RVOT or negatively impact the global function of the LV.

2.0 DECELLULARIZATION AND CHARACTERIZATION OF PORCINE HEART

2.1 INTRODUCTION

Biologic scaffolds composed of extracellular matrix (ECM) have been shown to promote the constructive remodeling of numerous tissue types in preclinical studies and in clinical practice (41-42, 44, 54, 83-87). The most widely studied ECM scaffold materials include those derived from small intestine (SIS) (44, 88), urinary bladder (UBM) (41, 54, 86), and dermis (89-90). The ECM of each tissue is synthesized by the resident cells and is in a state of dynamic equilibrium in response to environmental cues (68-69). Convincing arguments can be made for the advantages of tissue specific ECM scaffolds for tissue specific repair (91-98). Logically, a biologic scaffold derived from the targeted tissue source would possess the ideal 3-dimensional (3-D) architecture and biochemical composition to support tissue specific cell phenotype, cell proliferation, and tissue biomechanical properties. If organs can be decellularized and still maintain their 3-D integrity, the resulting scaffold would possibly represent the ideal scaffold for all components of the organ including: vascular and lymphatic structures, nerves, and the parenchymal cells.

Most commercially available biologic scaffold materials are manufactured as thin sheets. The source tissues are typically decellularized by immersion and agitation in a combination of salt solutions, detergents, and enzymatic solutions. Due to the density, mass, and 3-D

architecture of most whole organs such as the heart, liver, and kidney, these approaches are ineffective at removing cellular material (42, 99). Recently, Ott et al. described the decellularization of rat hearts by vascular perfusion (80). Decellularization of a porcine heart was shown to be possible, but a comprehensive, reproducible, and time-effective decellularization technique was not provided.

The purpose of specific aim one is to describe a decellularization method for a complex organ, specifically the porcine heart, by pulsatile retrograde aortic perfusion to generate cardiac extracellular matrix (C-ECM). Decellularization was confirmed by immunohistochemical (IHC) methods and DNA quantification. The C-ECM was characterized by IHC analysis, scanning electron microscopy (SEM), and mechanical testing.

2.2 MATERIALS AND METHODS

2.2.1 Preparation of C-ECM

Porcine hearts weighing approximately 300g were obtained immediately following euthanasia of adult pigs. Excess fat and connective tissue were removed and the ventricles were rinsed with water to remove coagulated blood. Each heart was frozen at -80ºC for at least 16 hours for storage and to aide in cell lysis. The hearts were then thawed in type 1 reagent grade water at room temperature. The aorta was cannulated with a ½" to ¼" straight barbed reducer and connected to ¼" ID silicone tubing. Each heart was placed in a 4 L beaker containing 3 L of hypotonic Type 1 water that was recirculated using a peristaltic pump (L/S® Drive EW-07550-30**,** Cole-Parmer**,** Vernon Hills, Illinois) for 15 minutes at one L/min. The Type 1 water was

replaced with 2X phosphate buffered saline (PBS) at one L/min each for 15 min. Three liters of 0.02% trypsin/0.05% EDTA/ 0.05% NaN_3 solution was warmed to 37°C using a digital hotplate and then perfused through the myocardial vasculature at one L/min for two hrs. A 3% Triton X-100/0.05% EDTA/ 0.05% NaN_3 was then used for perfusion followed by a 4% deoxycholic acid solution at 1.3 L/min each for two hours at room temperature. After each chemical solution was used as a perfusate, Type 1 reagent grade water was perfused through the heart for approximately five min with no recirculation followed by recirculating 2X PBS for 15 min to aide in cell lysis and removal of cellular debris and chemical residues. Disinfection was accomplished by perfusion of 0.1% peracetic acid (PAA)/4% EtOH at 1.7 L/min for one hour. The acid was neutralized and removed from the ECM by perfusing the intact matrix with PBS (pH 7.4) two times and type 1 water three times for 15 min each at 1.7 L/min. Fluid pressure was measured at the aorta during the entire decellularization process. The free walls of the left ventricle (LV) and right ventricle (RV) were excised and were either used immediately for mechanical properties testing in the hydrated state or, were laid flat on non-stick aluminum foil, frozen at -80°C for at least two hours, and then lyophilized until dry for biochemical analysis. See appendix A for C-ECM preparation SOP.

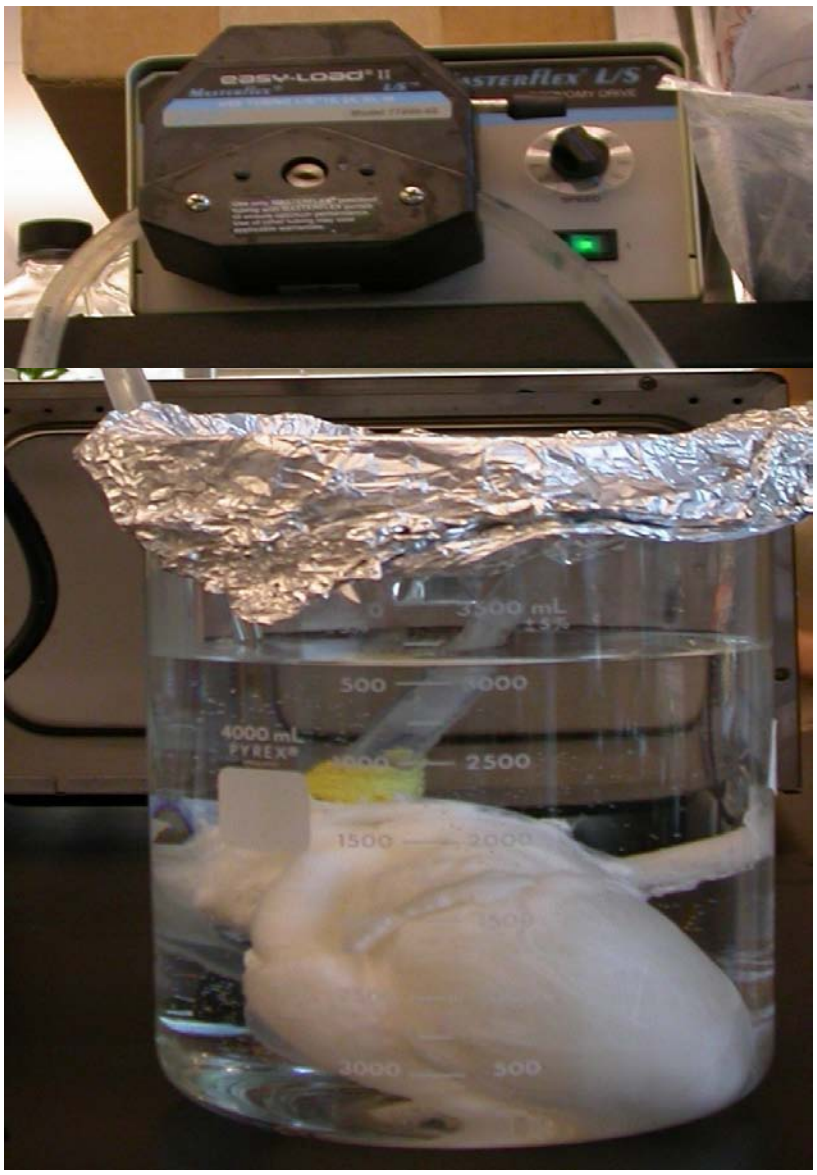

Figure 1. Porcine heart during decellularization

2.2.2 *Immunohistochemistry and Immunofluorescence Studies*

Full thickness samples of C-ECM and native (non-decellularized) ventricles were fixed in 10% formalin and then paraffin embedded. Eight micron thick sections were cut and deparaffinized. Hematoxylin and eosin (H&E) and 4', 6-diamidino-2-phenylindole (DAPI) were used to evaluate the presence of nuclear material. Movat's Pentachrome stain was used to allow visualization of

the distribution of nuclei, elastic fibers, collagen, glycosaminoglycans, fibrin/fibrous structures, and muscle. Herovici stain was used to discriminate and visualize collagen I and III in the ECM scaffolds. In addition, collagen IV, a basement membrane component, was visualized using a mouse anti-human collagen IV antibody. Slides were imaged using a Nikon™ E600 microscope with 4X and 20X objectives and captured using MetaVue™ Software package (Molecular Devices, Sunnyvale, CA).

2.2.3 *Scanning Electron Microscopy*

C-ECM ventricle and native ventricle were fixed with 2.5% glutaraldehyde followed by dehydration by 1 % Osmium tetroxide. The samples were then dehydrated in a graded series of ethanol concentrations in PBS. The samples were sputter coated with 3.5 μm of gold and visualized using a JEOL 9335 field emission gun SEM (JEOL Ltd., Tokyo, Japan) to capture standard scanning electron digitized images at 1000 and 30X.

2.2.4 *DNA Quantification*

Approximately 10 mg of native and ventricular C-ECM were digested with 0.1 mg Proteinase K (Sigma-Aldrich Corp. St. Louis, MO) in one ml of PBS at 37°C on a rocker overnight. The digest was then purified using Phenol/chloroform/Isoamyl alcohol (100). The Quant-iT™ PicoGreen® dsDNA assay (Molecular Probes, Inc., Eugene, OR) was used for quantification of the amount of DNA using the manufacturer's instructions. Samples were evaluated in triplicate. Equal volumes of digest were separated by gel electrophoresis in a 1% agarose gel with Ethidium Bromide at 60V for approximately 1 hour and the gel was visualized under ultraviolet transillumination to determine the fragment size of residual DNA.

2.2.5 *Glycosaminoglycans and Elastin Quantification*

Total sulfated glycosaminoglycans (GAGs) and cross-linked elastin within the C-ECM were determined using the manufacturer's instructions (Biocolor Ltd., Carrickfergus UK). One sample of three lots each of lyophilized C-ECM LV and RV as well as one sample of LV and RV from native ventricle were digested with papain for the GAG and elastin assay. Samples were evaluated in duplicate and all values were normalized to 1 mg dry sample for comparison. A two-tailed students t-test was performed to determine whether differences existed between the GAG and elastin contents of native ventricle versus C-ECM with the p-value set at 0.05 (Minitab® version 15.1.1.0, Minitab, State College, PA).

2.2.6 *Mechanical Testing*

Suture retention testing was performed per ANSI/AAMI VP20–1994 Guidelines for Cardiovascular Implants-Vascular Prostheses (101). A 2-0 Prolene suture was passed through a square piece of C-ECM from the right and left ventricle (n=5 for each) with a 2-mm bite depth. Suture retention testing was performed on a Test Bench System (Bose, Eden Prairie, Minnesota) at 10 cm/min and the load was measured using a 10 lb model 31 load cell (Honeywell, Columbus, O). Minitab® version 15.1.1.0 was used to calculate the one sided t-test ($p<0.05$) with the hypothesis that each of the LV and RV C-ECM had a greater maximum force to failure than UBM.

A MTS Tytron 250 with a 500g MTS load cell model 118-02 (MTS, Eden Prairie, MN) was used to obtain uniaxial maximum force measurements of C-ECM. A dog bone shaped piece of ECM measuring 1 cm by 3 cm of the left ventricle and right ventricle orientated lengthwise along the short and long axis of the porcine heart, and UBM (n=5). The ECM was then

preconditioned by pulling the sample to 10 % of its length 5 times followed by measuring force to failure. A one-tailed student's t-test was performed to determine whether differences existed between the maximum force to failure for the LV and RV C-ECM as compared to UBM with the p-value set at 0.05. (Minitab® version 15.1.1.0, Minitab, State College, PA).

In vitro cell culture

A MTS Insight with a 2000 N MTS load cell model 569327-03 (MTS, Eden Prairie, MN) was used with a ball-burst compression cage (Instron, Norwood, MA) to measure the biaxial burst strength of native LV and RV and the C-ECM derived from each ventricle. The test was performed in accordance with ASTM D3787-07 Test Method for Bursting Strength of Textiles-Constant-Rate-of-Traverse (CRT) Ball Burst with deviations for sample geometry. Similar methodology has been used in multiple published studies to describe the biaxial strength of synthetic and biologic scaffolds (99, 102-104). The native ventricles were excised and tested the same day as euthanasia. The C-ECM was tested within 48 hours of the completion of decellularization. For all groups, the specimen was clamped in the fixture such that the polished ball contacted the endocardium. A 25.4mm polished steel ball was advanced at a constant rate (25.4 mm/min) through the test material. Each experiment was conducted three separate times for each ventricle in the native and decellularized form. A two-tailed student's t-test was performed to determine whether differences existed between the maximum force to failure and extension at maximum force for the LV and RV C-ECM as compared to the values for native LV and RV with the p-value set at 0.05. (Minitab® version 15.1.1.0, Minitab, State College, PA).

2.3 RESULTS

2.3.1 *Preparation of C-ECM*

At the beginning of the decellularization process, the mean perfusion pressure was recorded as approximately 150 mmHg. During the Trypsin step, the hearts lost some of their red-brown coloration and became more flaccid, and the reagent became pinkish in appearance. With each subsequent reagent change, the hearts became whitish in appearance and expanded to approximately twice the original volume. Although the flow rate was increased throughout the decellularization process, the mean perfusion pressure dropped to approximately 50 mmHg by the time of the final rinses. 16 porcine hearts have been successfully decellularized using the method described.

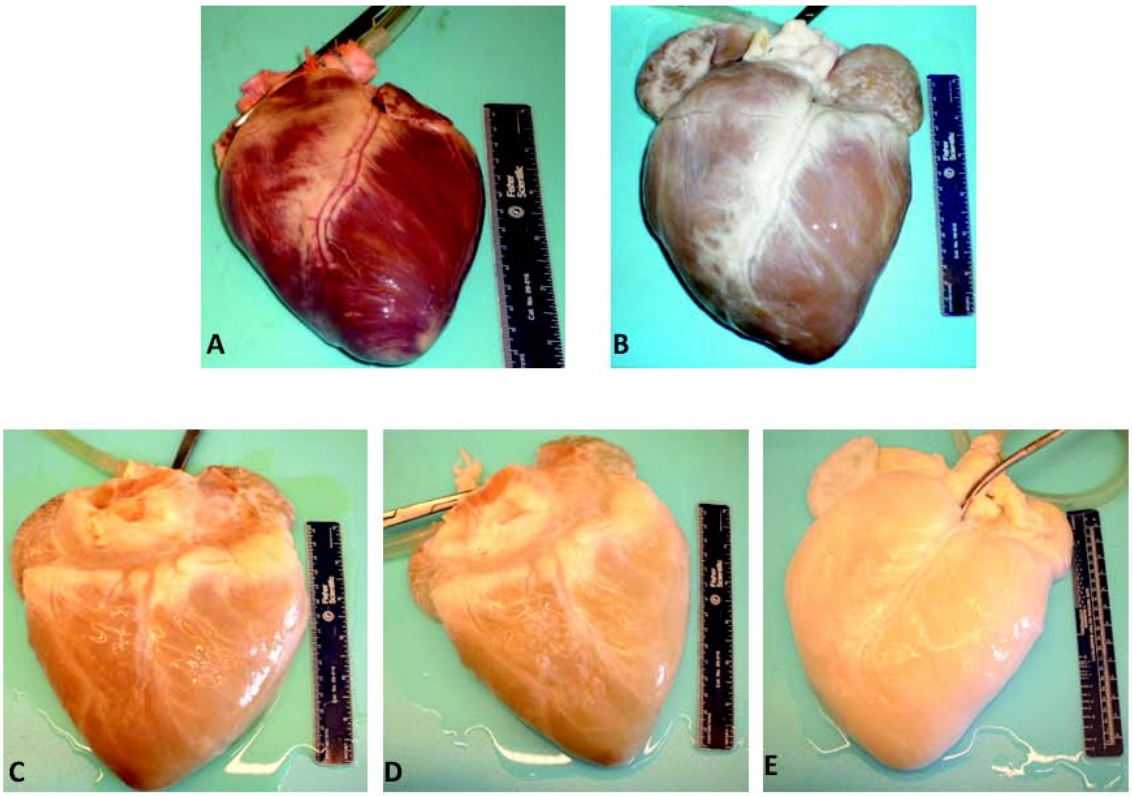

Figure 2. Representative images of the gross appearance of intact porcine hearts subjected decellularization by retrograde perfusion. A: Before Decellularization, B: After 0.02% Trypsin, C: After 3% Triton X-100, D: After 4 % Sodium Deoxycholate, E: After 0.1% Peracetic Acid.

2.3.2 *Immunohistochemistry*

H&E and DAPI showed no visible cell nuclei or double stranded DNA at 40X and 200X magnification, respectively, whereas the native heart showed dense cellularity.

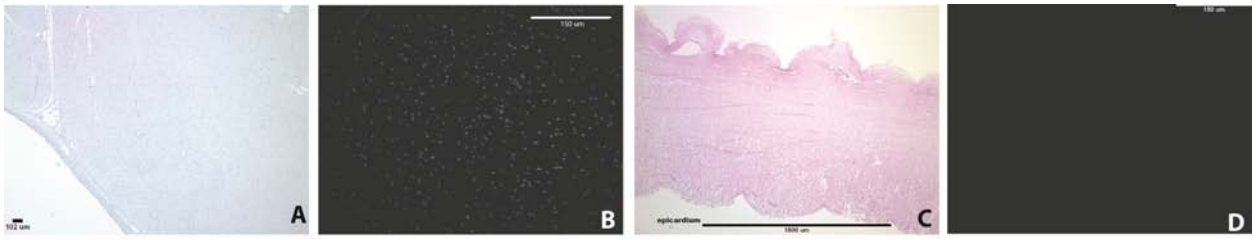

Figure 3. Representative photomicrographs showing no nuclear staining after perfusion decellularization. A: Native ventricle H&E Scale: 102 µm, B: Native ventricle DAPI Scale: 150 µm, C: C-ECM H&E Scale: 1000 µm, D:C-ECM DAPI Scale: 150 µm.

Movat's Pentachrome staining of the C-ECM showed the absence of muscle cells after decellularization.

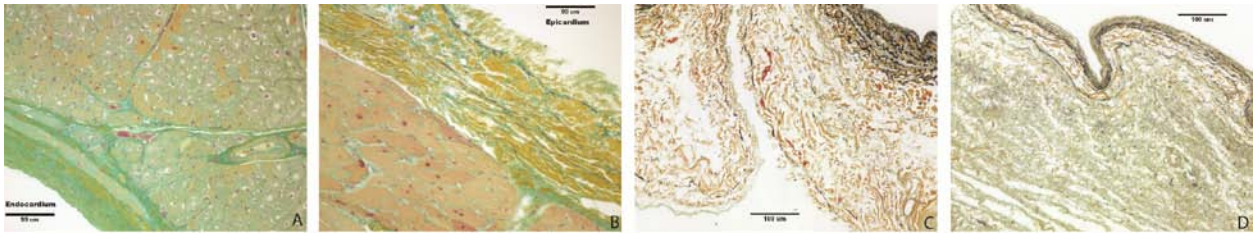

Figure 4. Movat's Pentachrome photomicrographs of A: Native ventricle epicardial surface Scale: 99 µm, B: Native ventricle endocardial surface Scale: 99 µm , C: C-ECM endocardial surface with coronary Scale: 100 µm, D: C-ECM epicardial surface Scale: 100 µm. All at 200X Nuclei: purple/black, Elastic fibers: black, Collagen: yellow, Proteoglycan: green, Muscle: light red, Fibrin/Fibrous structures: vibrant red.

Movat's and Herovici's staining showed the presence of collagen type I and III as well as elastin, with particularly dense collagen structure localized at the epicardium and endocardium.

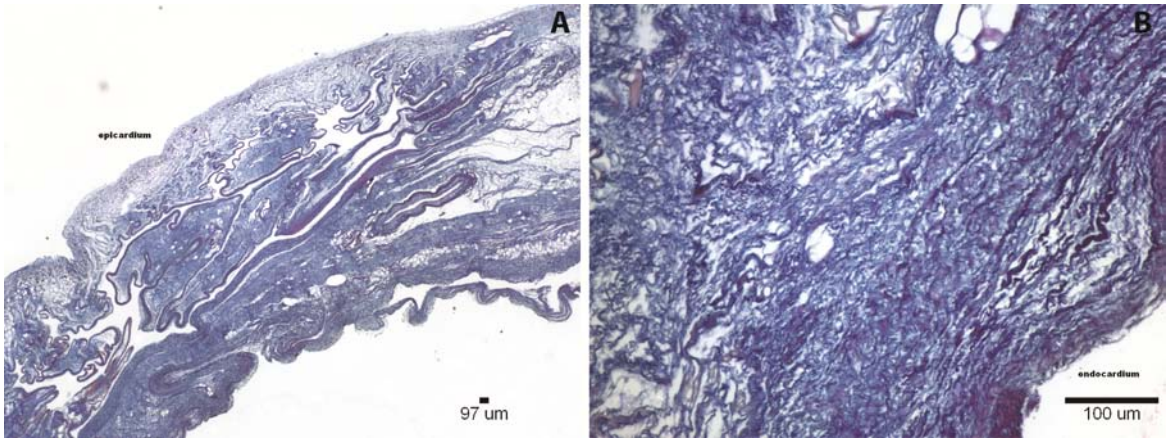

Figure 5. Herovici Stain of C-ECM A:40X epicardial surface labeled Scale: 97 µm, B: 200X endocardial surface Scale: 100 µm. Collagen I: blue and Collagen III: pink.

The basement membrane structures present within native ventricle tissue and C-ECM were identified by the positive staining for collagen IV, a basement membrane component, on the endocardium, myocardium and coronary arteries.

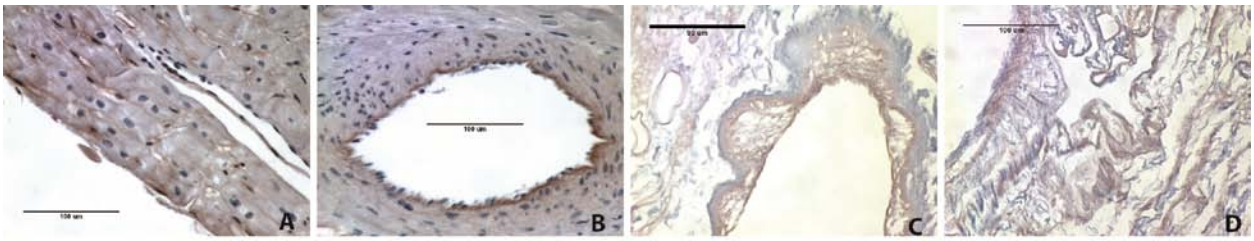

Figure 6. Collagen IV staining of A: Native LV endocardium Scale: 100 µm, B: Native LV Coronary Artery Scale: 100 µm, C: C-ECM endocardium Scale: 99 µm, D: C-ECM coronary artery Scale: 100 µm. All at 400X.

2.3.3 *Scanning Electron Microscopy*

The native and C-ECM epicardium and endocardium both showed a dense collagen layer with topographic variances. The native ventricle has a densely cellular myocardium whereas the C-ECM shows a more open configuration within the myocardium. Intact vascular matrix was

evident throughout the C-ECM. The SEM shows a 0.5 mm diameter coronary artery in the cross-sectional view. No cells were visible in any of the SEM samples for C-ECM, but they were apparent in the native samples.

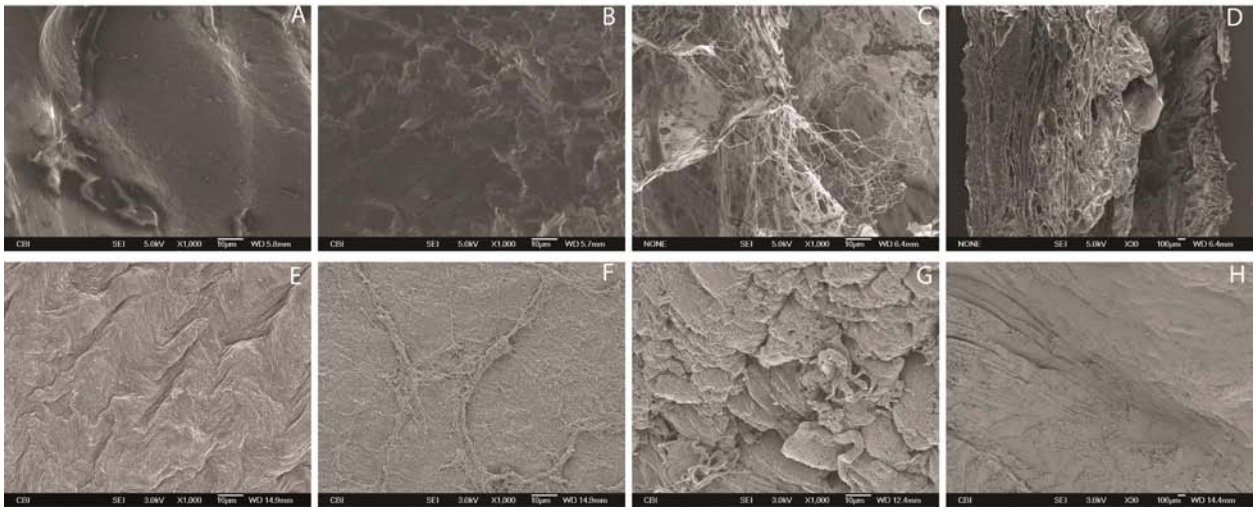

Figure 7. SEM of Native and lyophilized C-ECM from the LV. A: C-ECM Epicardium 1000X, B: C-ECM Endocardium 1000X, C: Cross-section of C-ECM 30X D: Cross-section of C-ECM 1000X E: Native Epicardium 1000X, F: Native Endocardium 1000X, G: Cross-section of Native 30X H: Cross-section of Native 1000X. 1000X image scale: 10 µm. 30X image scale: 100 µm.

2.3.4 *DNA Quantification*

Quantitative analysis of DNA content within the C-ECM with the Pico Green assay showed a significant decrease in the amount of DNA compared to the DNA present in the native ventricles (31.48 ng DNA/mg sample vs. 484.36 ng DNA/mg sample ($p=0.014$)). This value represents a 94% decrease in the amount of the double stranded DNA found in the tissue as a result of decellularization.

Table 1. ECM component quantification. Values are normalized to 1 mg lyophilized sample.

Sample	DNA (ng)	GAG (µg)	Elastin (µg)
Native Heart	484.4	4.7	38.7
STDV	53.5	0.4	38.2
C-ECM	31.5	5.4	19.7
STDV	2.2	0.2	3.4

The ethidium bromide gel showed no DNA bands or smears associated with the decellularized C-ECM whereas the native ventricle showed a large band above 1500 base pairs.

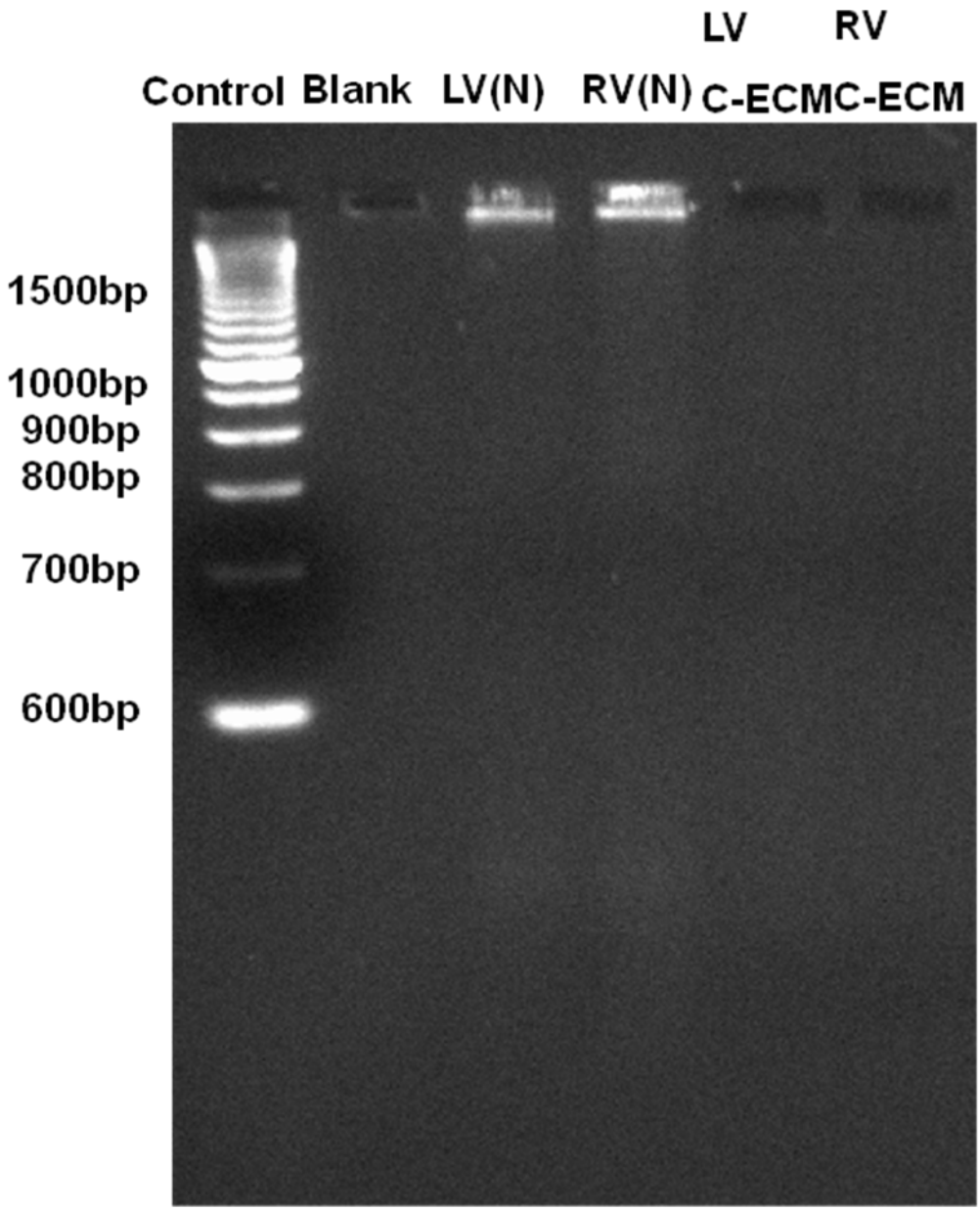

Figure 8. DNA fragment size as determined by ethidium bromide gel. (N) denotes native.

2.3.5 *GAG and Elastin Quantification*

The amount of GAGs and elastin in C-ECM was not different than that measured in the native ventricle tissue ($p < 0.05$).

2.3.6 *Mechanical Testing*

C-ECM from the LV showed suture retention strength (SRS) of 2.48N ± 1.09N and C-ECM RV showed a SRS of 2.78N ± 1.05N, while UBM had a SRS value of 1.23N ± 0.35N (n=5 per group). C-ECM from the LV and RV had a statistically higher SRS than UBM ($p < 0.004$).

The load to failure for the C-ECM from the LV was 3.02N ± 0.99N in the longitudinal direction and 6.82N ± 3.40N in the circumferential direction. The load to failure for C-ECM from the RV was 4.44N ± 0.13N in the longitudinal direction and 8.80N ± 1.37N in the circumferential direction. Whereas UBM had a maximum failure force of 1.28N ± 0.27N. C-ECM from the LV and RV in both longitudinal and circumferential orientations had a statistically higher load to failure than UBM ($p < 0.001$).

Table 2. Table of Suture and Uniaxial Pull Tests

	ECM Type	AVG Max (N)	STDEV
Suture Pull	UBM	1.23	0.35
	C-ECM LV	2.39	0.54
	C-ECM RV	2.67	0.30
Uniaxial Pull	UBM	1.28	0.27
	C-ECM LV Longitudinal	3.02	0.99
	C-ECM LV Circumferential	6.82	3.40
	C-ECM RV Longitudinal	4.44	0.13
	C-ECM RV Circumferential	8.80	1.37

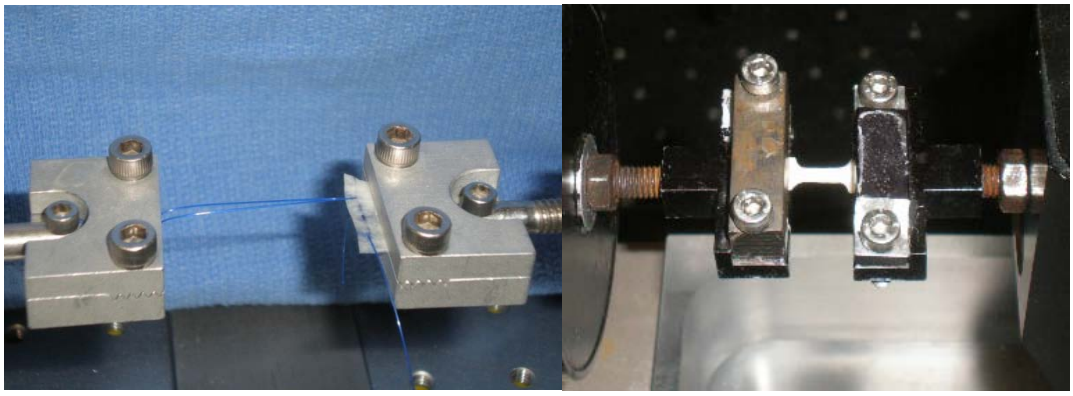

Figure 9. Picture of Suture and Uniaxial Pull Tests

The maximum force or extension at maximum force of C-ECM for the respective ventricle was not different than the native ventricle ($p<0.05$), although the average extension at maximum force was greater for the native ventricles. The native ventricles showed multiple sub-failure peaks that were associated with failure of layers within the tissue, while the C-ECM showed a smoother curve consistent with rotation and extension of fibers that likely occurred as a result of dilation of the heart during decellularization. Failure was observed as the ball penetrated through the epicardium in all groups.

Table 3. Maximum force and extension at maximum force with standard error and p value of t-test comparing native ventricle to C-ECM ventricle.

	Native LV	C-ECM LV	Native RV	C-ECM RV
Avg Max Force (N)	130.77	113.99	132.49	125.00
Std error	14.68	22.80	8.98	19.86
t-test between Native and C-ECM	0.58		0.76	
Avg extension at Max force (mm)	30.26	26.30	34.72	26.10
Std error	5.52	0.60	6.46	1.27
t-test between Native and C-ECM	0.55		0.32	

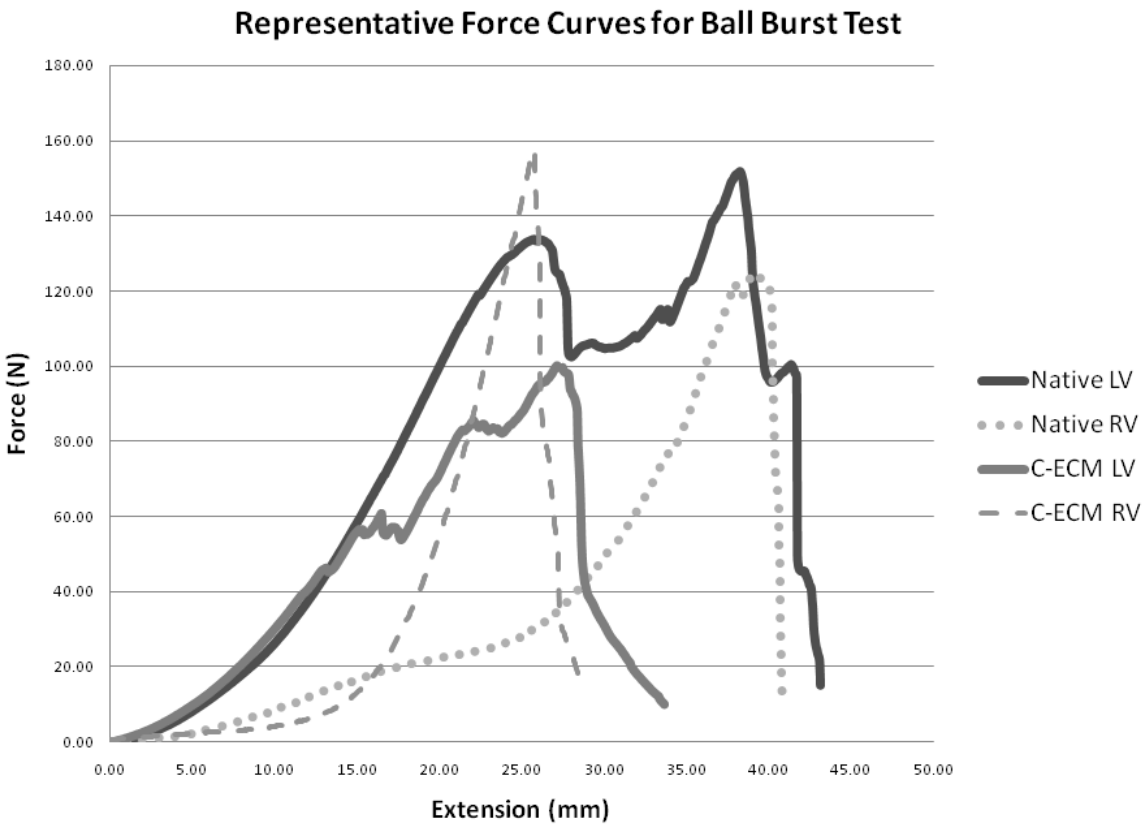

Figure 10. Graph of representative force curves for ball burst test.

2.4 DISCUSSION

The present study described a reproducible and time-efficient decellularization technique for the intact porcine heart. The technique utilized retrograde aortic perfusion with successive hypertonic, hypotonic, enzymatic, acid, and detergent solutions to maximize the distribution of chemicals throughout the tissue, maximize the disruption of cells, and minimize the damage to the ECM. The protocol took less than 10 hours to complete, and effectively removed DNA from the tissue to levels comparable to other commercially available ECM products (100, 105) and passed decellularization criteria (106).

It is important to limit the tissue exposure time and concentration of Trypsin, Triton® X-100, deoxycholic acid, sodium dodecyl sulfate (SDS), PAA, or other commonly used decellularizing agents, as each solution can have a disruptive effect on the ECM structure while removing the cellular components (107). By appropriate utilization of the series of reagents described in the present method, the decellularization time was significantly reduced from the time reported for decellularization of porcine heart valves, sliced porcine heart and intact rat hearts (80-81, 108-109). The systematic decellularization method was setup so that each step preformed a specific task. By flushing the heart with a hypotonic solution (type I water) the cells swell which increases the effectiveness of cell lysis caused by freezing the heart at -80 °C. Trypsin cleaves the peptide bonds on the C-side of Argenine and Lysine (110); this aides in breaking the bonds between the cell membranes and the ECM resulting in more open spaces so the remaining solutions can infuse the entire heart. Triton® X-100 disrupts lipid–lipid and lipid–protein bonds leading to the breakdown of the cell membrane (107). Sodium deoxycholate then is able to permeate the cell membrane easier and solubilizes cytoplasmic and nuclear cellular membranes helping to remove cellular material. While peracetic acid (PAA) also disrupts the cell membranes and intracellular organelles, its main purpose in this application is to inactivate a wide range of bacteria, fungi, and viruses (111-113). The hypotonic (type I water) followed by hypertonic (2X PBS) washes between each of the solutions causes and remaining cells to swell and then shrink which aides in cell lysis as well as removal of chemical and cellular residues. The final water and PBS washing steps neutralize PAA and degrade it into water, carbon dioxide, and oxygen. In the trypsin and Triton X-100 solutions 0.05% of ethylene-diamine-tetra-acetic acid (EDTA) and sodium azide (NaN_3) were added. The EDTA was added to aide in cell removal by chelating calcium. NaN_3 was added to prevent formation of pyrogens/endotoxins

(114-115). The remaining solutions were used to remove EDTA and NaN_3. In the present study, the systematic perfusion decellularization maintained much of the chemical and structural components of the ECM including GAGs and elastin as shown by IHC, SEM, and mechanical data.

A previous study on the decellularization of heart valves with trypsin and Triton X-100 found that collagen and elastin structure were severely disrupted and that stable suture lines for anastomosis could not be formed (116), but C-ECM prepared by the described method had a statistically higher suture pull out strength compared to UBM. Earlier attempts to decellularize cardiac tissue have not been able to remove all cellular remnants due to the densely cellular cardiac tissue (117-118). Gratzer's group investigated serial decellularization of anterior cruciate ligaments (ACL) with Triton X-100 in combination with SDS or tributyl phosphate (TnBP) and found that both decellularized the tissue, but SDS disrupted the collagen matrix, removed GAGs, and impacted fibroblast ingrowth (119-120). Rieder et al. saw a cytotoxic effect of aortic valves decellularized with SDS on endothelial cells but did not with sodium deoxycholate (121). Based on these two studies plus cells were not attaching *in vitro* to C-ECM initially decellularized with SDS, SDS was avoided as a decellularization solution. TnBP alone was tried for decellularization of C-ECM but few changes were seen in cellularity, therefore sodium deoxycholate was chosen for the decellularization. By using the described protocol, much of the complex 3-D architecture of the heart was maintained including vasculature and basement membrane structures.

While Brendel et al. first described by whole organ decellularization in 1978, it was used as a laboratory tool to investigate basement membrane permeability in the kidney (122). When this study was started, there were no publications on ventricular decellularization for tissue

engineering applications. Since then C-ECM has been produced by several laboratories (79-81). Eitan et al. sliced the left ventricle into 3 mm rings and then treated with trypsin for 2 days, Triton X-100 for 8 days, and ethanol overnight to decellularize the ventricle. Whole rat heart C-ECM was produced by Taylor's group by serial perfusion with SDS, Triton X-100 and antibiotics for a total of 5.7 days (80). Singelyn et al. used the same solutions as Taylor, but cut a porcine heart into 2 mm thick slices and treated with SDS for 4-5 days followed by Triton X-100 and deionized water washes overnight (81). While Eitan and Singelyn did decellularize porcine ventricles, they destroyed much of the macroscopic structure which could be beneficial in reconstruction surgeries. Although Taylor's group did show a picture of a decellularized porcine heart, they only published the method and detailed analysis for the decellularized rat heart. The method described is unique in that it decellularizes the intact heart in less time while maintaining the macroscopic 3D organization.

Much of the C-ECM structure was maintained which led to favorable mechanical properties. C-ECM suture retention strength (SRS) and uniaxial pull strength (UPS) were compared to UBM since published data on the values of UBM exist (99, 101-102) and because this ECM material has been used in several preclinical trials for full wall thickness ventricular repair (83, 123-126). The higher SRS and UPS strength of C-ECM verse UBM showed that C-ECM should be able to withstand initial pressure of the left or right ventricle; this is further substantiated by the fact that the biaxial rupture strength of the C-ECM (119 N) was not different from the native tissue (128 N). This result is especially impressive as the dry weight of the C-ECM samples tested was approximately 1/3 of the native samples. The biaxial rupture strength of the C-ECM was also significantly larger than that reported for 4 layers of UBM (35 N) (99); which has successfully patched a full thickness left ventricular defect in preclinical evaluations

(126). The combination of the mechanical testing data indicates that the C-ECM scaffold should withstand ventricular pressures while remodeling progresses.

2.5 SUMMARY AND CONCLUSION

The innovative portion of the decellularization method described in this chapter is the optimization of systematic decellularization solutions in combination with retrograde aortic perfusion to produce a biologic scaffold that maintained much of the macroscopic and microscopic structures as well as the C-ECM composition. Since the C-ECM biaxial rupture strength force was not different than the native tissue and was significantly larger than 4 layers of UBM, the mechanical integrity of C-ECM should be sufficient to withstand the pressure of the right or left ventricle as constructive remodeling progresses. While there is much work to be done, the methodology described herein provides a useful step to fully realizing an engineered complex organ.

2.6 FUTURE WORK

It may be possible to further optimize the decellularization process based on the desired use. For instance, C-ECM slices have recently been produced with trypsin and Triton® X-100 being used for longer periods of time as the main decellularization steps (79). Using only trypsin and Triton® X-100 may leave more of the biologically active molecules in the ECM as it would eliminate the ionic detergent but could negatively impact the mechanical strength (107, 109).

This method could be beneficial in producing a C-ECM gel similar to ones previously described (81, 127), as mechanical strength is not essential but minimizing effects on growth factors could be beneficial.

Although the method described is specific to cardiac tissue, the technique could be systematically modified for decellularization of other tissues and organs. New methods for decellularization would need to be systematically analyzed for effectiveness of decellularization, remaining biochemical components, and mechanical strength. In terms of mechanical strength an ECM device must be designed with an understanding that there is an initial decrease in strength and then an increase in strength above the original implant as the tissue remodels. In one study of a body wall repair in a dog, the 8 layer SIS device had a burst strength of 73 lbs before implantation (128). The SIS device reached a minimum burst strength at 10 days (40 lbs) and continued to increase strength for the next two years (157 lbs) where it reached a biaxial failure force greater than the original tissue (33 lbs) (128). Physiologic mechanical loading is also critical in constructive ECM scaffold remodeling. Without physiologic loading ECM will constrict and often forms granulation tissue (129). When designing an ECM device one must consider the initial degradation of strength to about 50% of the originally implanted device so the scaffold could be physiologically loaded and lead to constructive remodeling.

3.0 *IN VITRO* C-ECM EVALUATION OF CELL COMPATIBILITY

As shown in the previous chapter, perfusion decellularization can maintain much of the 3D integrity and biochemical composition of the native cardiac ECM (78). Being the ECM of each tissue is synthesized by the resident cells and is in a state of dynamic equilibrium in response to environmental cues (68-69), convincing arguments can be made for the advantages of tissue specific ECM scaffolds for organ repair (91-98). Logically, a biologic scaffold derived from the targeted tissue source would possess the ideal 3-dimensional (3-D) architecture and biochemical composition to support tissue specific cell phenotype, cell proliferation, and tissue biomechanical properties. Therefore the C-ECM scaffold should have beneficial physical and biochemical cues for cell seeding.

Another advantage of using an organ specific matrix is the three-dimensional (3D) structure (ventricles, valves, coronaries, and etc.). The vasculature can be used as conduits for cell seeding and perfusion making it possible to reseed a decellularized heart. If the decellularized heart could be reseeded with a clinically relevant cell and matured *in vitro* to obtain physiologic structures and pressures, then it could be possible to use the tissue as a contractile cardiac patch, a bio-ventricular assist device (bio-VAD), or possibly a total implant.

The goal of this specific aim is to determine the ability of C-ECM to support proliferation of endothelial cells and progenitor cells as well as the viability and phenotype maintenance of cardiomyocytes. These experiments used endothelial cells, progenitor cells, and cardiomyocytes

as they are some of the cells required for functional myocardium. *In vitro* cell culture was used to compare C-ECM and UBM. UBM was chosen as a comparison to C-ECM because UBM has shown beneficial remodeling in previous cardiac studies (83, 123-124, 126). The intact decellularized rat heart was also reseeded and incorporated into a perfusion culture system to show some of the benefits of the 3D structure.

3.1 METHODS

3.1.1 C-ECM Preparation

An intact porcine heart was perfusion decellularized to produce a C-ECM biological scaffold as previously described (78). Briefly, porcine hearts weighing approximately 300g were obtained immediately following euthanasia of adult pigs. Excess fat and connective tissue were removed and the ventricles were rinsed with water to remove coagulated blood. Each heart was frozen at -80ºC for at least 16 hours for storage and to aide in cell lysis. The hearts were then thawed in type 1 reagent grade water at room temperature. The aorta was cannulated with a ½" to ¼" straight barbed reducer and connected to ¼" ID silicone tubing. Each heart was placed in a 4 L beaker containing 3 L of hypotonic Type 1 water that was recirculated using a peristaltic pump (L/S® Drive EW-07550-30**,** Cole-Parmer**,** Vernon Hills, Illinois) for 15 minutes at one L/min. The Type 1 water was replaced with 2X phosphate buffered saline (PBS) at one L/min each for 15 min. Three liters of 0.02% trypsin/0.05% EDTA/ 0.05% NaN_3 solution was warmed to 37°C using a digital hotplate and then perfused through the myocardial vasculature at one L/min for two hrs. A 3% Triton X-100/0.05% EDTA/ 0.05% NaN_3 was then used for perfusion followed

by a 4% deoxycholic acid solution at 1.3 L/min each for two hours at room temperature. After each chemical solution was used as a perfusate, Type 1 reagent grade water was perfused through the heart for approximately five min with no recirculation followed by recirculating 2X PBS for 15 min to aide in cell lysis and removal of cellular debris and chemical residues. Disinfection was accomplished by perfusion of 0.1% peracetic acid (PAA)/4% EtOH at 1.7 L/min for one hour. The acid was neutralized and removed from the ECM by perfusing the intact matrix with PBS (pH 7.4) two times and type 1 water three times for 15 min each at 1.7 L/min. Fluid pressure was measured at the aorta during the entire decellularization process. The free walls of the left ventricle (LV) and right ventricle (RV) were excised and were either used immediately for mechanical properties testing in the hydrated state or, were laid flat on non-stick aluminum foil, frozen at -80°C for at least two hours, and then lyophilized until dry for biochemical analysis.

3.1.2 UBM Preparation

The preparation of UBM has been previously described (130). In brief, porcine urinary bladders were harvested from market weight pigs (108-118 kg) immediately following euthanasia and placed in ice. The excess connective tissue and residual urine were removed. The tunica serosa, tunica muscularis externa, the tunica submucosa, and majority of the tunica muscularis mucosa were mechanically removed. The urothelial cells of the tunica mucosa were dissociated from the luminal surface by soaking the tissue in phosphate-buffered saline solution with a pH of 7.4 (PBS). The resulting biomaterial, which was composed of the basement membrane of the urothelial cells plus the subjacent lamina propria, was referred to as urinary bladder matrix (UBM). UBM sheets were placed in a solution containing 0.1% (v/v) peracetic acid (Sigma), 4%

(v/v) ethanol (Sigma), and 95.9% (v/v) sterile water for two hours while agitating. Peracetic acid residue was then removed with one PBS wash, followed by two washes with sterile water, followed by a final PBS wash all for 15 minutes each. The decellularized UBM sheets were then lyophilized using a FTS Systems Bulk Freeze Dryer Model 8-54 and used in the sheet form or comminuted to a powder form using a Wiley Mini Mill.

3.1.3 ECM Gel Preparation

C-ECM and UBM sheet and gels were produced as previously described (78, 101, 127). One gram of UBM or C-ECM powder was digested with 100 mg pepsin (~2,000-2,300 Units/mg, Sigma-Aldrich, St. Louis, MO) in sterile 100 ml 0.01 N HCl. This solution was stirred constantly at room temperature (25°) for 48 hours. The resultant viscous solution of digested UBM or pre-gel solution had a pH of approximately 3.0-4.0. The activity of pepsin was irreversibly inactivated when the pH was raised to 7.4 by mixing 0.1 N NaOH (1/10 of the volume of pre-gel solution) and 10X PBS (1/9 of the volume of pre-gel solution) at 4°C. The solution was brought to the 6 mg ECM/ml solution using cold (4°C) 1X PBS and placed at 37°C for approximately 15 minutes for gelation to occur.

3.1.1 Chick Fetal Cardiomyocytes Cell Description

Hamburger-Hamilton Stage 31 (day 7) White Leghorn Chicken Embryonic Cardiomyocytes (CCMs) were provided by Dr. Kimimasa Tobita. As previously described, CCMs were isolated using collagenase and trypsin digests and preplated for one hour to selectively isolate cardiomyocytes (131-132). CCMs were cultured in DMEM with 10% FBS, 1% chick embryo

extract, and 100 U/ml Penicillin/100 μg/ml Streptomycin under a humidified atmosphere in 95% air/5% CO_2.

3.1.2 Human Aortic Endothelial Cell Description

HAECs were obtained from Cambrex (CC-2535). HAECs were cultured in EGM-2 medium (Lonza, Walkersville, MD) under a humidified atmosphere in 95% air/5% CO_2.

3.1.3 Mouse C2C12 Myoblasts Cell Description

C2C12 mouse myoblasts were purchased from the American Tissue Culture Collection (ATCC). The C2C12 population was expanded in Dulbecco's modified Eagle medium (DMEM) (Invitrogen Corporation, Grand Island, NY), supplemented with 10% calf serum (Hyclone, Logan, UT), and 100 U/ml Penicillin/100 μg/ml Streptomycin (Invitrogen Corporation, Grand Island, NY). C2C12s were culture under a humidified atmosphere in 95% air/5% CO_2.

3.1.4 Human Fetal Cardiomyocytes Cell Description

Human fetal cardiomyocytes (HCMs) were provided by Dr. Amit Patel at the University of Pittsburgh. Hearts were collected at approximately week 14 gestational age, within 1 hour of medically induced termination. Hearts were dissected out and washed 3X in DPBS (-) at 4°C. The hearts were finely minced in a solution of DPBS (-)/0.01% EDTA and incubated at 4°C for 10 minutes. This was followed by enzymatic digestion in a solution of DPBS (-)/0.01% EDTA containing 1 mg/ml collagenase 1A and 20 units/ml of DNase 1 at 37°C for 30 minutes. After

digestion, fetal bovine serum (FBS) was added at the final concentration of 10%. Undigested tissues and cell clumps were separated by passing the cell suspension through a 100 μm cell strainer. Dissociated cells were washed 3X by centrifugation at 400 g for 10 min. Cells were plated and expanded until approximately 10 million cells were obtained. The cells were trypsinized, counted, spun down and re-suspended in 1 ml of DMEM/F-12 complete.

3.1.5 Rat Neonatal Cardiomyocytes Cell Description

Rat neonatal (day 1-4) cardiomyocytes (RCMs) were isolated using a similar method as previously described (131). Briefly, hearts were excised and diced into 1 mm pieces. Collagenase and trypsin were diluted with calcium free buffer to obtain concentrations listed below. Pieces were transferred to a 50 ml conical with 4 ml/litter of pups of 3 mg/ml collagenase type II for 30 minutes (min) followed by six 0.1% trypsin (Gibco, Carlsbad, California) digestions for 7 min at 37 °C while mixed with a stir bar at approximately 1 rev/sec. Supernatant was filtered through a 100 um cell filter and neutralized in Rat Cardiac Myocyte Growth Medium (RCGM, Lonza, Switzerland), 1% Penicillin-Streptomycin, and 1% fungizome (Gibco, Carlsbad, California). Cells were spun down for 5 min at 1000 g and resuspended in 10 ml DMEM/F12 complete. The first two trypsin digests were preplated twice for 1 hr each in plasma etched 60 mm petri dishes and the remaining trypsin digest supernates were preplated for one hr to purify for RCMs. After the preplate time elapsed the supernate was removed from the petri dishes and the cells in the supernate were counted were counted using a coulter counter (Bekman Coulter, Brea, Ca) per manufacturer's instructions. RCMs were spun down again and resuspended in 1 ml of RCGM.

3.1.6 Initial Cardiomyocyte Cell Seeding Experiment

Lyophilized C-ECM and UBM sheets were packaged in sterilization pouches and terminally sterilized using ethylene oxide (EtO). CCMs were seeded on the luminal side of ECM sheets or the top of ECM gels. Approximately 500,000 cells/cm^2 were cultured on the ECM scaffolds for 4 days in DMEM with 10 % fetal bovine serum, 1% chick embryo extract, and 1 % penicillin and streptomycin. The scaffolds were then fixed in 4% paraformaldehyde for 20 min followed by rinsing with PBS. Monoclonal Anti-α-Actinin antibody (clone EA-53, Sigma-Aldrich Corp. St. Louis, MO) and anti-beta Tubulin antibody (TU-06, Abcam, Cambridge, MA) were used to distinguish CCMs from other cell types (131). The scaffolds were placed between two cover slips and imaged using an inverted Olympus Fluoview 1000 confocal microscope (Olympus, Center Valley, PA).

3.1.7 Proliferation Assay and Histological Assessment

A proliferation assay (ViaLight Plus Kit, Lonza, Rockland, ME) was used to quantitatively assess the relative number of cells on the scaffold per the manufactures instructions (133-134). Either 10,000 C2C12 or 20,000 HAEC cells in 200 µl of media without serum was pipetted onto the luminal surface of the C-ECM and UBM as well as the surface of C-ECM and UBM gels in a 96 well plate. Experiments were run in triplicate along with a single negative control for each construct. The negative control consisted of the ECM with media only. After 48 hrs the cell lysis buffer was applied and luminesence of the supernatant was measured to determine relative ATP quantities. This assay was run four times for each cell line.

Visual immunofluorescent analysis was performed on all scaffolds using HAECs at a seeding density of 500,000 cells/cm^2 for 8 days and C2C12 at a density of 200,000 cells/cm^2 for 3 days. At the end of the cell culture period, the scaffolds were fixed in 4% paraformaldehyde for 20 min followed by rinsing. HAECs and C2C12 cells were stained with Rhodamine Phalloidin to image f-actin fibers and Hoechst to stain nucleic DNA. The scaffolds were placed between two cover slips and imaged using an inverted Olympus Fluoview 1000 Confocal Microscope (Olympus, Center Valley, PA).

3.1.8 Decellularization Rat C-ECM

Rat C-ECM was produced in a similar manner as porcine C-ECM described earlier in this chapter (78). Due to the size of the rat heart a lower flow rate and time were needed for decellularization. The time for the trypsin, Triton X-100, and Deoxycholate acid perfusion was 1 hour and PAA solution was perfused for 30 min. The initial flow rate was set at 5 ml/min increasing to 12 ml/min through the decellularization process. The intact decellularized rat heart ECM was terminally sterilized with 2 million Rads of gamma irradiation for cell seeding experiments.

3.1.9 Verification of Decellularization of Rat C-ECM

Full thickness samples of C-ECM were fixed in 10% formalin and then paraffin embedded. Eight micron thick sections were cut and deparaffinized. Hematoxylin and eosin (H&E) and 4', 6-diamidino-2-phenylindole (DAPI) were used to evaluate the presence of nuclear material.

Approximately 50 mg of native ventricle and ventricular C-ECM were digested with 10 µl Proteinase K (Cat # 25530-049 Invitrogen) in 50 ml of 10 mM Tris-HCL, 100 mM NaCl, 25 mM EDTA, 0.5% SDS in water at 50°C on a rocker overnight. The digest was then purified using Phenol/chloroform/Isoamyl alcohol (100). The Quant-iT™ PicoGreen® dsDNA assay (Molecular Probes, Inc., Eugene, OR) was used for quantification of the amount of DNA using the manufacturer's instructions. Samples were evaluated in triplicate. Equal volumes of digest were separated by gel electrophoresis in a 1% agarose gel with Ethidium Bromide at 60V for approximately 1 hour and the gel was visualized under ultraviolet transillumination to determine the fragment size of residual DNA.

3.1.10 HCM 3D culture

The decellularized rat heart was then placed into a sterile perfusion chamber under a humidified atmosphere of 95% air/5% CO_2 with 50 ml of DMEM/F-12 supplemented with 10% FBS and 1% P/S 100 U/ml Penicillin/100 µg/ml Streptomycin (DMEM/F-12 complete) and perfusion started at 2 ml/min.

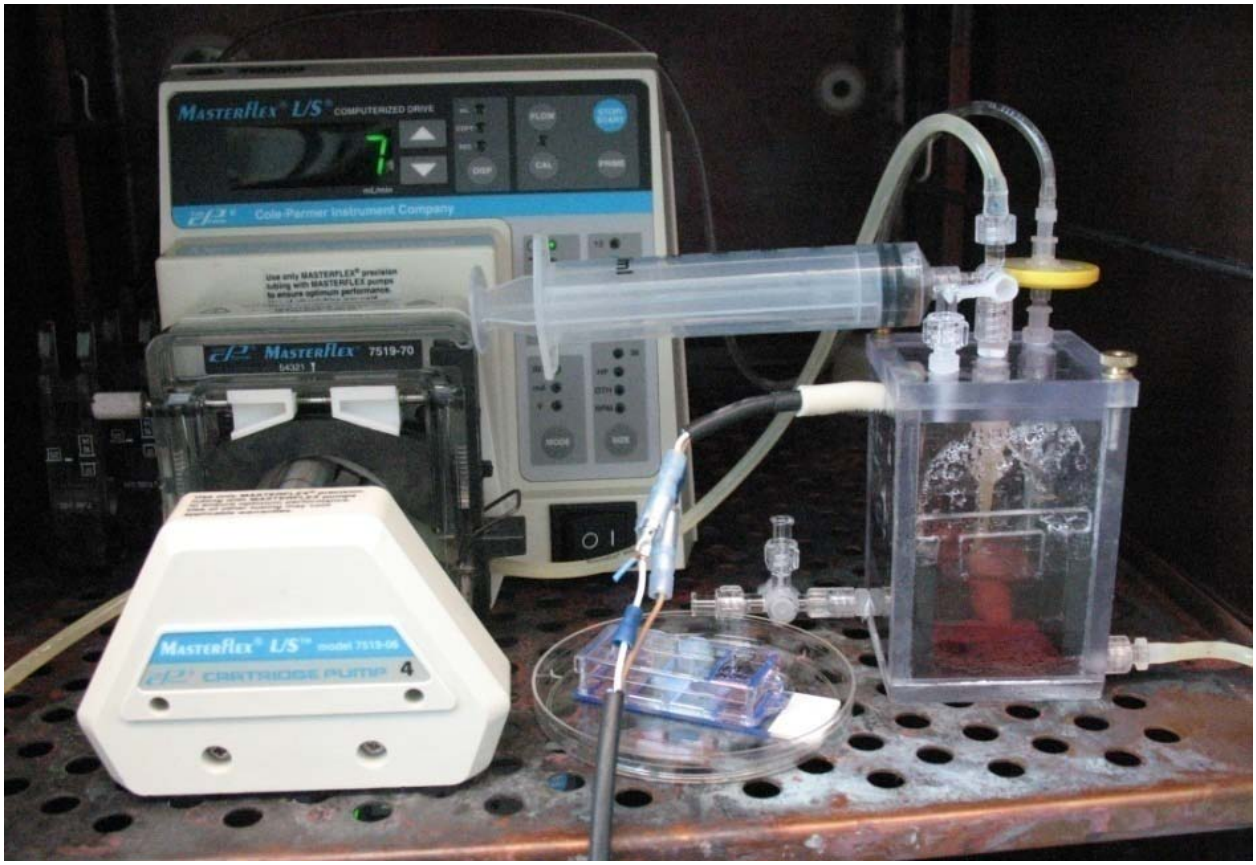

Figure 11. Picture of perfusion chamber and peristaltic pump

This was a pilot study that included the reseeding of one heart at one and two week time points. To reseed the rat heart, the perfusion pump was stopped while approximately 20 million HCMs re-suspended in 1 ml of DMEM/F-12 complete were injected into the aortic cannulae. Perfusion was restarted for 1 min and then constantly perfused at 2 ml/min after 30 min. Perfusion was increased from 2 ml/min to 8 ml/min by 2 ml/min increments each day. At one or two weeks the reseeded heart was perfused with 4% PFA in PBS for 20 min. The heart was bisected along the long axis. Half was paraffin fixed, sectioned, and stained with hematoxylin and eosin (H&E) and imaged using Nikon™ E600 microscope (Nikon Instruments Inc. Melville, NY). The remaining tissue was further sectioned and stained with Rhodamine Phalloidin and Hoechst, or anti-alpha actinin, anti-Histone H3 (Millipore, Billerica, MA), and Hoechst.

Sections were imaged on an Olympus Fluoview 1000 confocal microscope (Olympus, Center Valley, PA).

3.1.11 RCM 3D culture

The perfusion pump was stopped and approximately 30 million RCMs were injected into the aortic cannulae at approximately 5 ml/min. Perfusion was restarted for 1 min and then constantly perfused at 2 ml/min after 30 min. Perfusion was increased to 8 ml/min by 2 ml/min increments each day. The first experiment was stopped at 3 days to show that the RCMs were throughout the 3D rat C-ECM. The second experiment was carried out for 7 days; at day 2 the media was changed to RCGM with 100 µM BrdU to prevent the proliferation of fibroblasts (135). On day 3 the electrical stimulation was started using carbon blocks (136-137). Stimulation was provided using a Grass stimulator (S88X, Grass Technologies, West Warwick, RI) at 1beat per second, 5 volts, and 10 ms. At the end of the experiment, the recellularized 3D C-ECM was perfused with 4% PFA in PBS for 20 min followed by serial perfusion of 5 ml of PBS three times followed by optimal cutting temperature solution (Ted Pella, Redding, Ca). After freezing, the heart was sectioned through the short axis near the apex, papillary muscles, and valves and slides obtained. Slides were stained with H&E, Masson's Trichrome, or anti-alpha actinin, anti-cardiac troponin T, and Hoechst and imaged.

3.1.12 Statistical analysis

A one way ANOVA with a Tukey's post hoc analysis was performed to determine whether differences existed between the relative fluorescent units (RFU) of cells seeded on the surface of C-ECM and UBM sheets and gels with the p-value set at 0.05. A power analysis was also performed for the one way ANOVA using the maximum difference between means and a pooled standard deviation (Minitab® version 15.1.1.0, Minitab, State College, PA).

3.2 RESULTS

3.2.1 Initial Cardiomyocyte Cell Seeding Experiment

CCMs are identified by positive α-actinin staining and positive *β*-tubulin staining (green-yellow). Non-CCMs are recognized by negative α-actinin staining and positive *β*-tubulin staining (red). CCMs were the primary population of cells observed on the ECM scaffolds. CCMs attached to all forms of the ECM biologic scaffolds and survived for the 4 day culture period. The α-actinin fibers showed no global preferred orientation on any of the ECM scaffolds. Only the C-ECM sheet and C-ECM gel supported the formation of organized CM sarcomere structure, as indicated by striations of the α-actinin fibers by day four of culture (138).

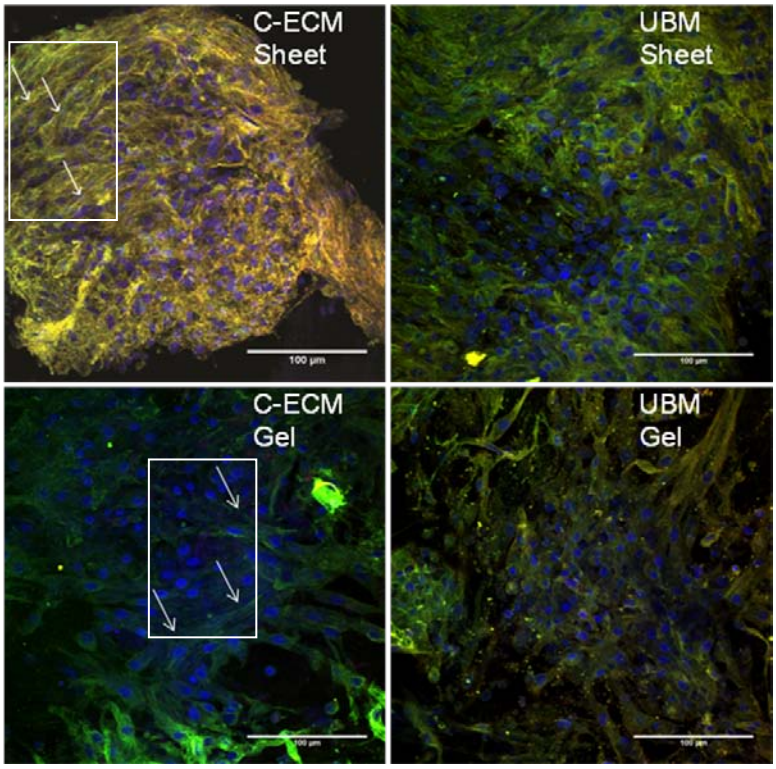

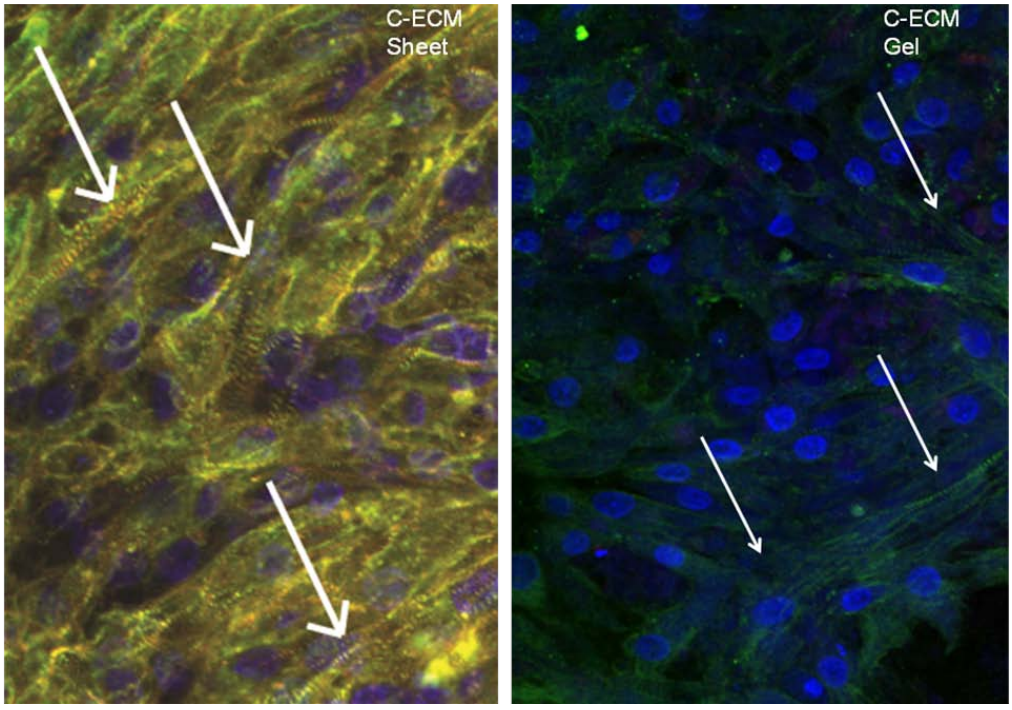

Figure 12. CCMs seeded on surface of C-ECM and UBM sheet and gel. *α*-actinin red and *β*-tubulin staining green. 400X scale: 100 µm.

3.2.2 Proliferation Assay and Histological Assessment

As seen by the confocal images of the HAECs, the cells attached and survived on all forms of the ECM scaffolds for the 8 day culture period. The f-actin fibers (red) appear to have preferred alignment direction on the C-ECM sheet, on all the other constructs, the actin fiber orientation seems to be random.

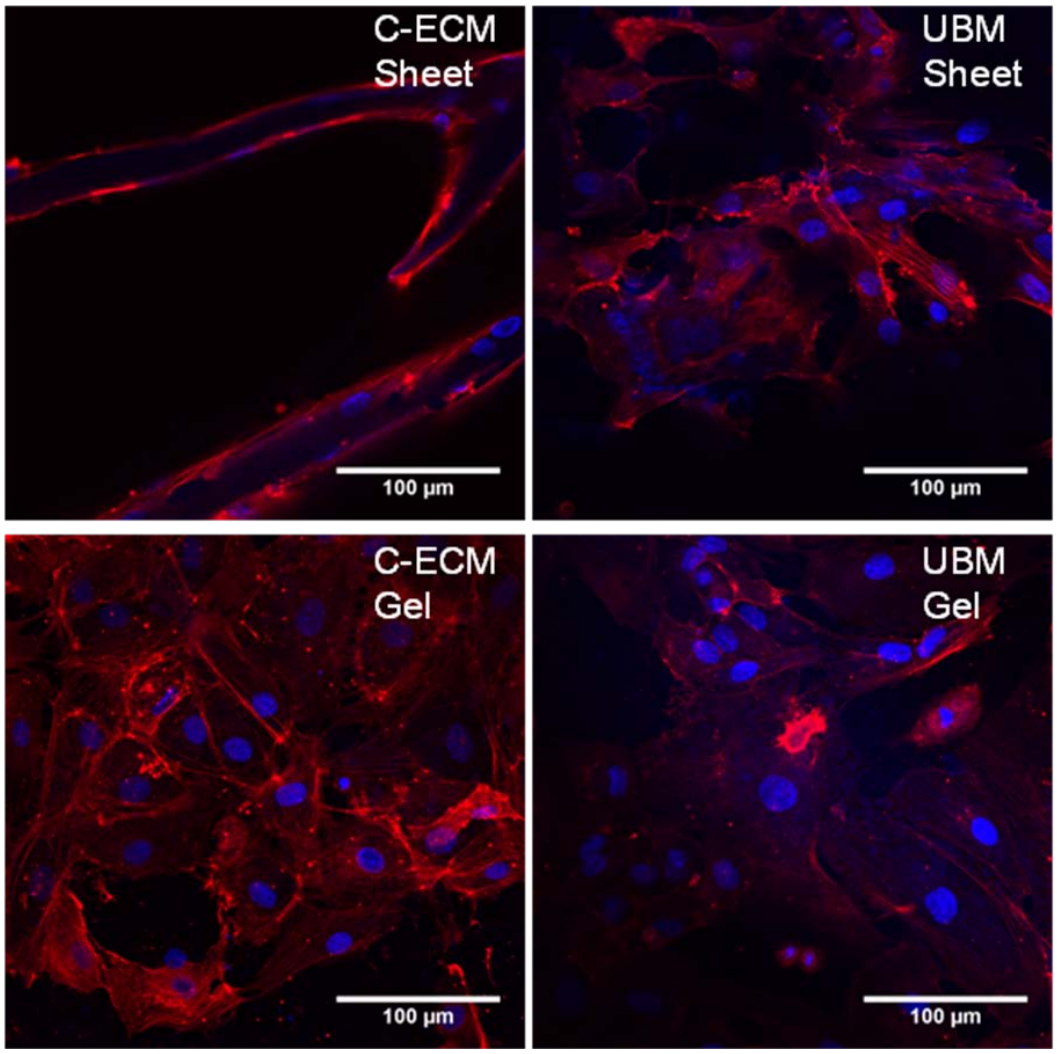

Figure 13. HAECs seeded on surface of C-ECM and UBM sheet and gel. Rhodamine Phalloidin red and DAPI blue. Scale: 100 µm.

The average and the standard deviation (stdv) for relative fluorescent units (RFU) between the three repetitions for each ECM scaffold are shown in the figure below. The UBM gel had a statistically higher RFU value than the UBM sheet or C-ECM sheet, but was not statistically different from the Cardiac gel. There were no differences between the amounts of ATP/cells on any of the other ECM scaffold forms. The power of this test was 0.88.

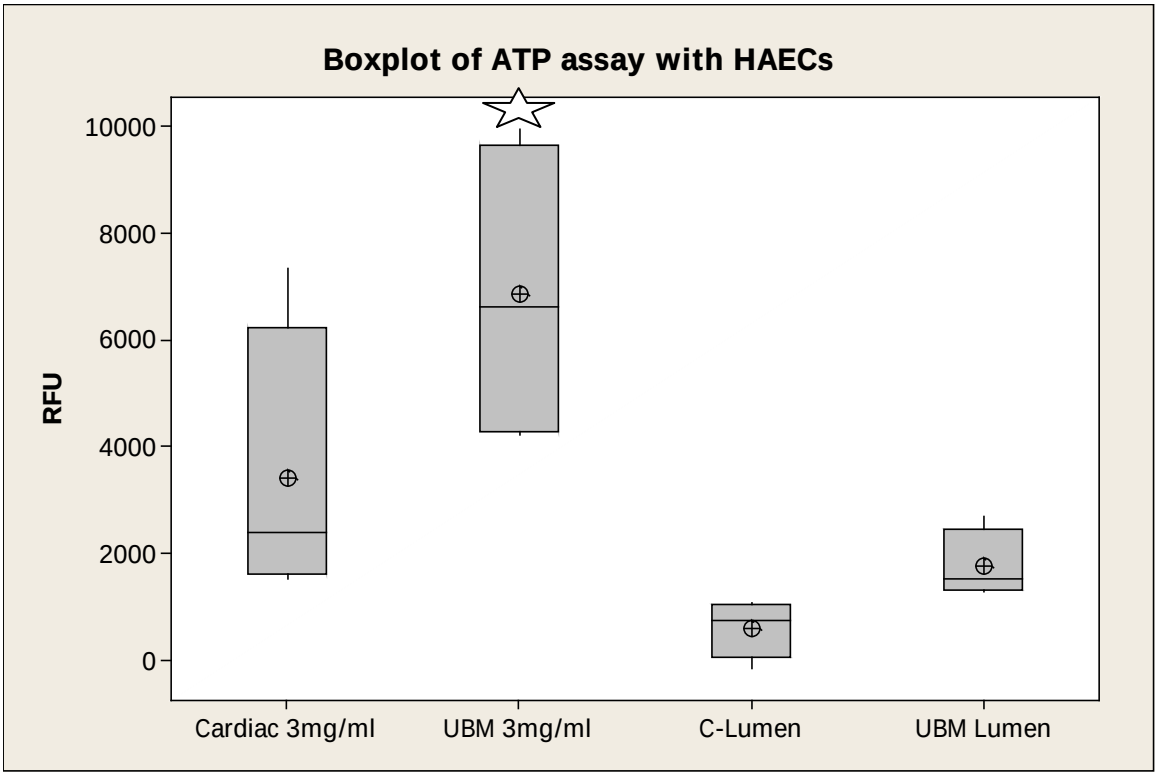

Figure 14. Boxplot of ATP assay RFU results for HAECs seeded on surface of C-ECM and UBM sheet and gel.* UBM gel had a statistically higher RFU value than the UBM sheet or C-ECM sheet, but was not statistically different from the Cardiac gel.

The C2C12s also attached and survived on all of the ECM scaffolds for the 3 day culture period. The morphology of the C2C12 cells are different on each of the scaffolds. C2C12s on the cardiac lumen appear to be present in more layers. The nuclei on the UBM lumen are more rounded. The nuclei on both gels are elongated and there appears to be some local alignment of the f-actin fibers on the UBM gel.

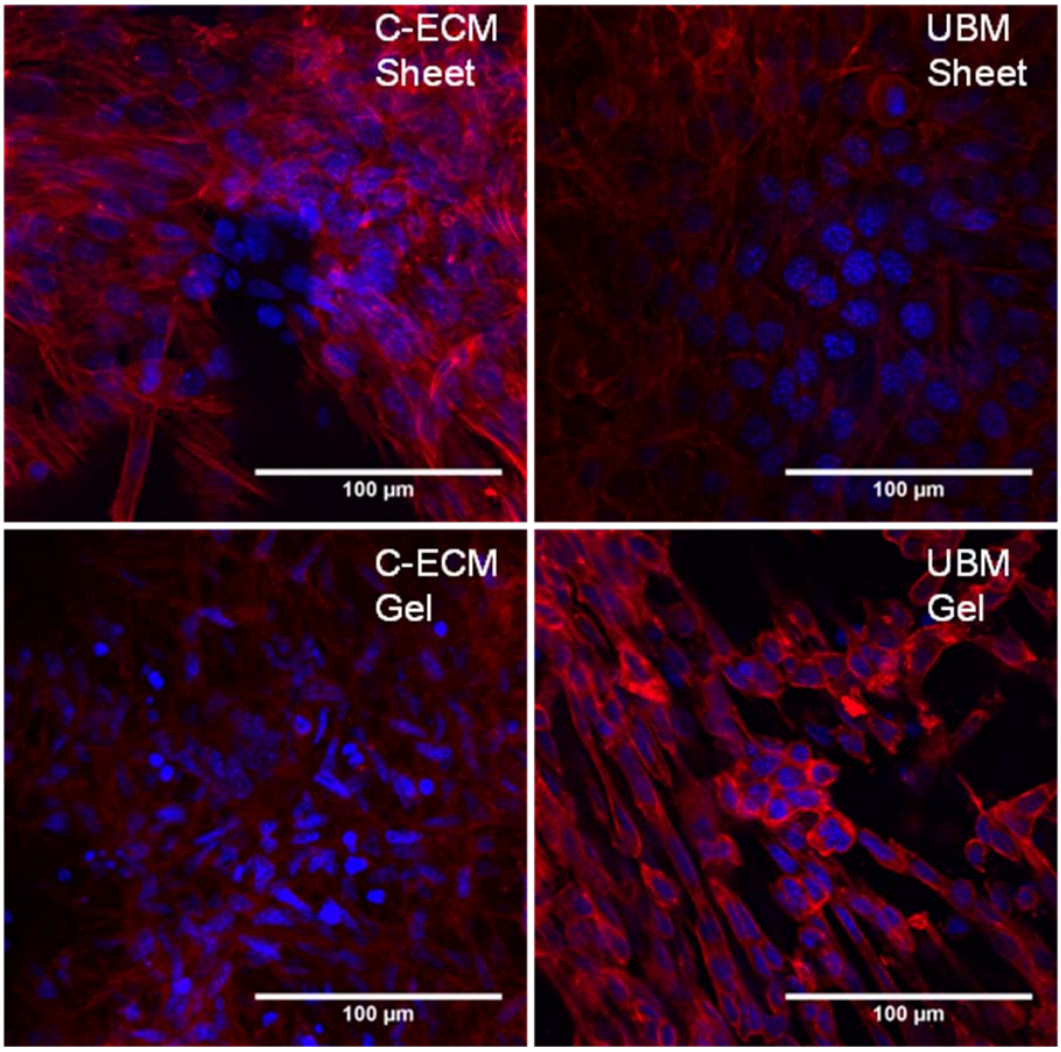

Figure 15. C2C12s seeded on surface of C-ECM and UBM sheet and gel. Rhodamine Phalloidin red and DAPI blue. 600X scale: 100 µm.

There were no statistical differences in the ATP assay RFU values between the C2C12s seeded on any of the ECM scaffolds. The power of this experiment was 0.54.

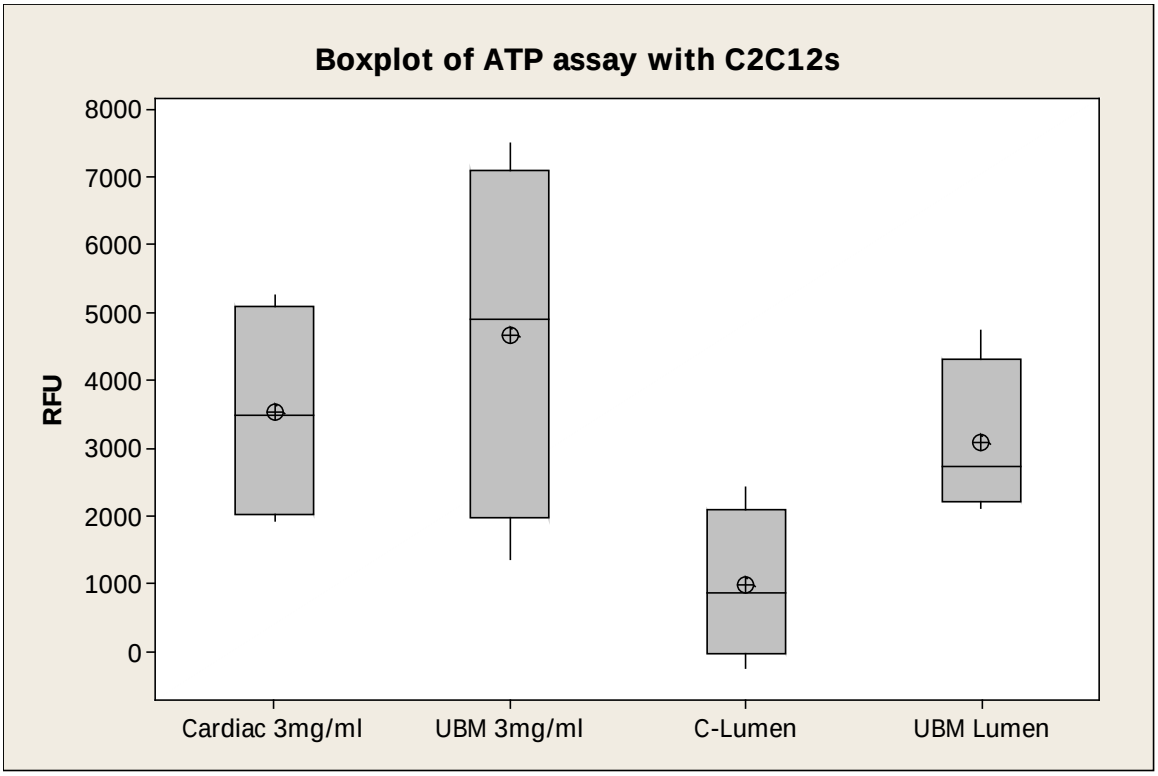

Figure 16. Boxplot of ATP assay RFU results for C2C12s seeded on surface of C-ECM and UBM sheet and gel.

3.2.3 Three Dimensional Culture of Cardiomyocytes

3.2.3.1 Decellularization Rat C-ECM

It was possible for the rat heart to be decellularized in a similar manner as the porcine heart and the decellularized rat heart maintained some of the vascular structures.

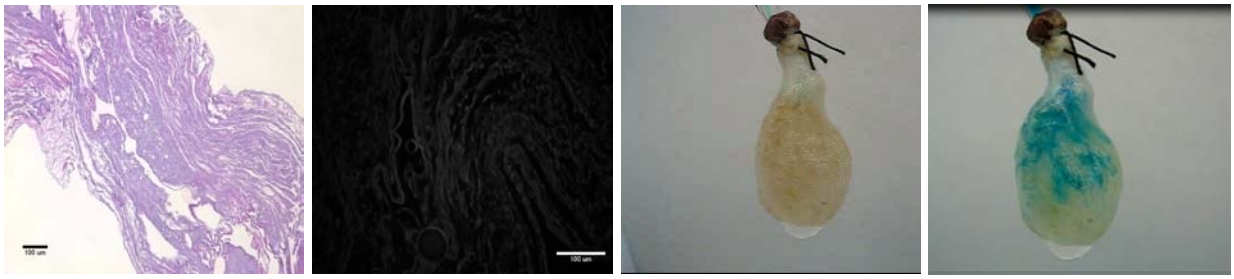

Figure 17. Microscopic view of decellularized rat heart H&E: 100X. DAPI: 200X. Macroscopic view of decellularized rat heart injected with dye at 2 ml/min. Scale: 100 µm.

The Quant-iT™ PicoGreen® dsDNA assay (Molecular Probes, Inc., Eugene, OR) and 1% agarose gel with Ethidium Bromide quantification showed remaining double stranded DNA was comparable with or less than other FDA approved ECM devices (100, 105). Both decellularized rat hearts had more than 50 ng DNA/mg ECM and one decellularized rat heart had a faint DNA streak starting about 600 base pairs in the gel.

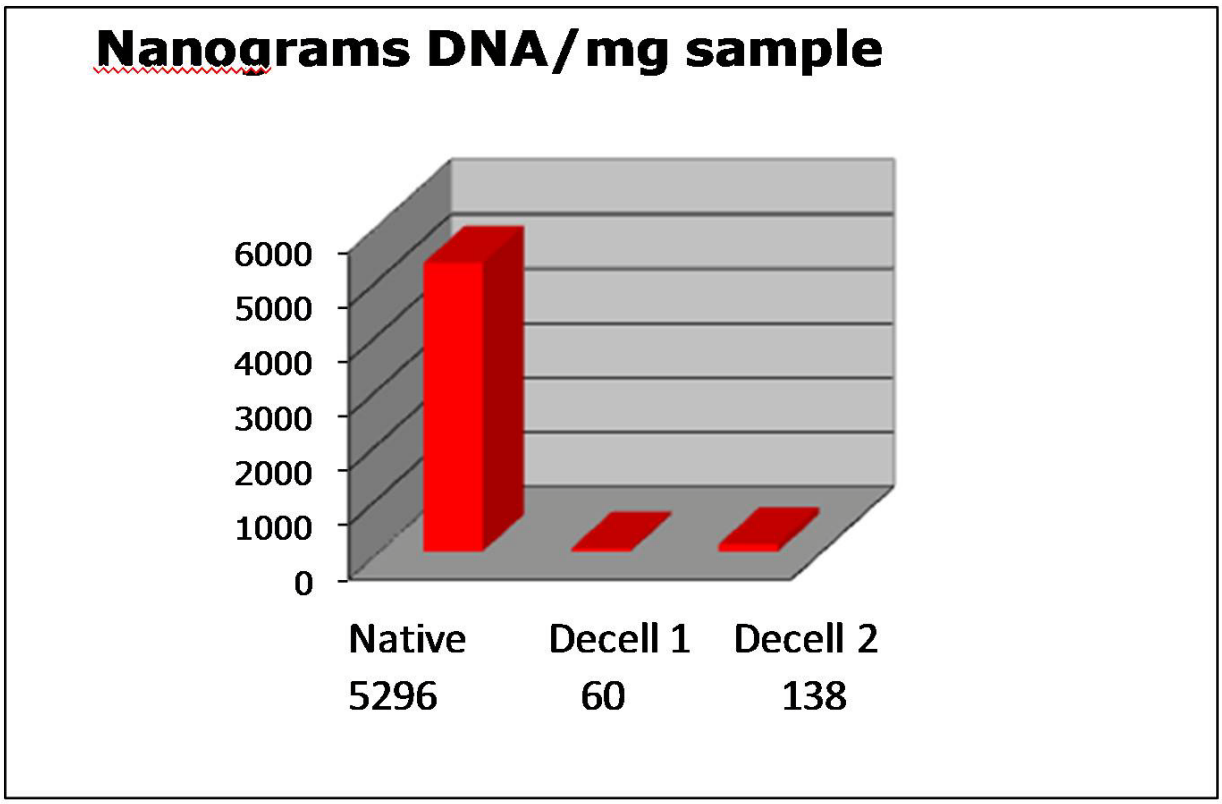

Figure 18. Quant-iT™ PicoGreen® dsDNA assay results for one native and two decellularized rat hearts.

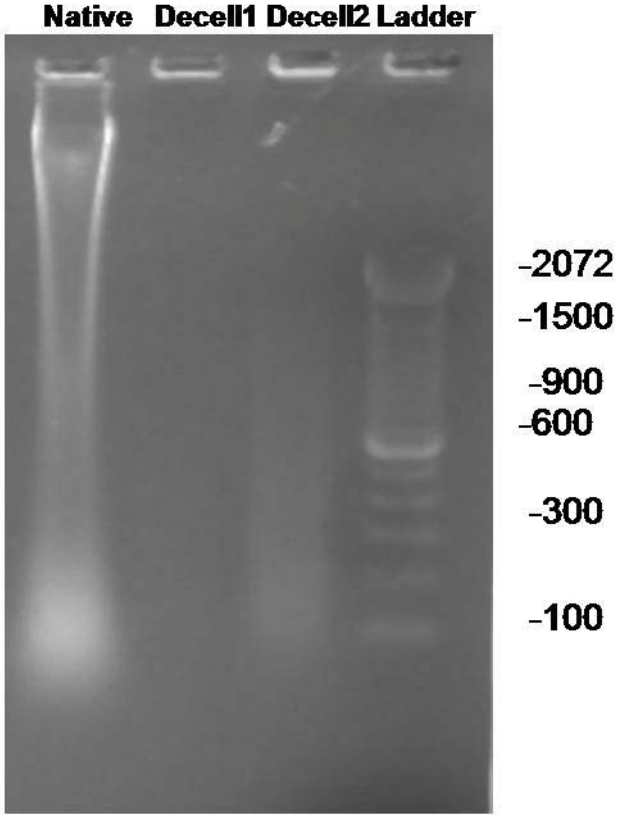

Figure 19. Quantification of DNA by 1% agarose gel with Ethidium Bromide for one native and two decellularized rat hearts. DNA base pair ladder shown for relative comparison.

3.2.3.2 HCM 3D culture

There is a large change in color and texture between the decellularized and reseeded heart at 2 weeks of culture. The decellularized heart is white/clear and the reseeded heart is beige. The decellularized heart also collapses into a sheet when cut in half (data not shown) but the free wall of the reseeded ventricles maintains its spherical shape when cut longitudinally.

Figure 20. Macroscopic view of rat heart before and after cultured with HCM for 2 weeks. Apex to aorta length 22 mm for both hearts.

H&E and DAPI microscopic images show major changes in cellularity between the decellularized and reseeded heart. The decellularized heart shows no nuclei in the H&E and only the ECM matrix is visible in the DAPI image. The recellularized heart shows nuclei and DNA throughout the ventricle wall.

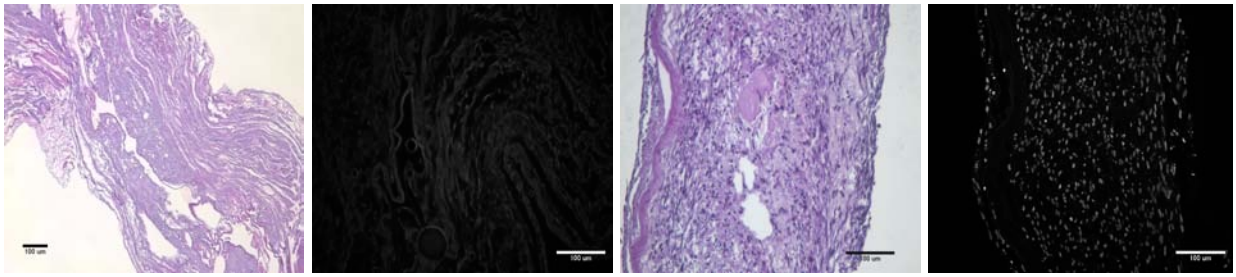

Figure 21. Microscopic view of rat heart before and after cultured with HCM for 1 week. H&E of decellularized heart at 100X all others at 200X. Scale: 100 µm.

The recellularized heart shows local alignment of the HCMs on the endocardial surface. The rhodamine phalloidin staining shows alignment of the f-actin HCM fibers within the 200X field of view at both one and two weeks.

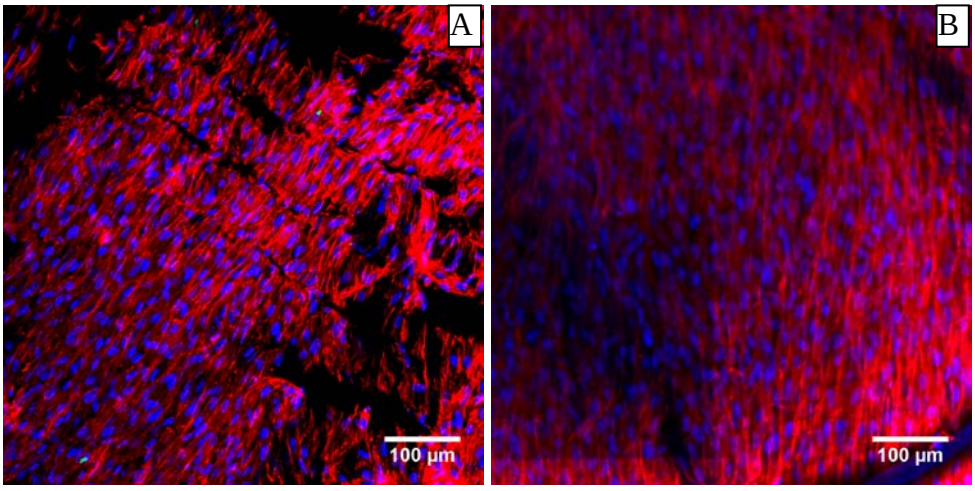

Figure 22. Reseeded heart after cultured with HCM for 1 week (A) and 2 weeks (B). Cells stained with rhodamine phalloidin (red) and Hoechst (blue) 200X. Scale: 100 µm.

Many of the HCMs present in the reseeded scaffold at 1 week showed evidence of proliferation. The colocalization of Histone H3, a proliferation marker (139), and alpha-actinin, a striated muscle marker, shows that many of the HCMs are actively dividing after 1 week in culture. An organized sarcomere structure cannot be seen.

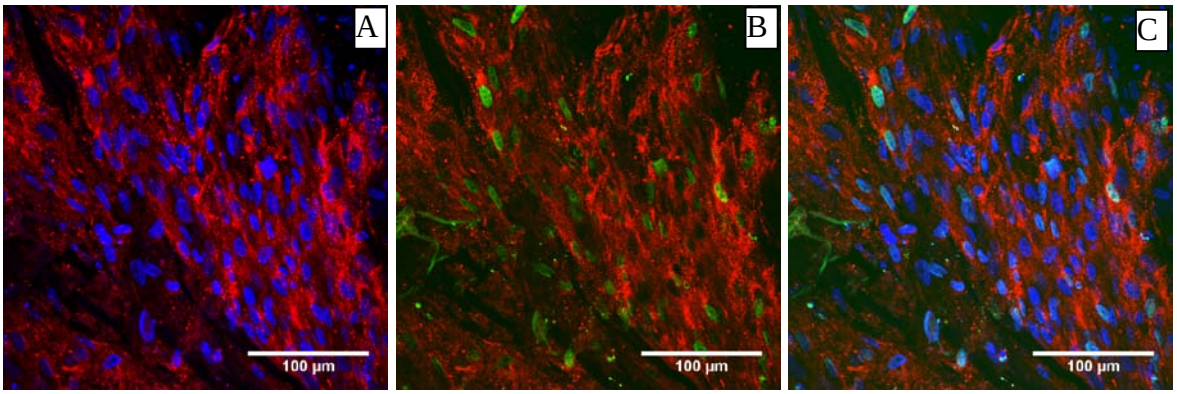

Figure 23. Reseeded heart after cultured with HCM for 1 week. DAPI for Nuclei: Blue. Anti-α-actinin for muscle specific actinin: Red. Histone H3 for proliferation/mitosis: Green. 400X A: DAPI and anti α-actinin. B: Histone H3, and anti α-actinin. C: Combined DAPI, Histone H3, and anti-α-actinin. Scale: 100 µm.

3.2.3.3 RCM 3D culture

RCMs were visualized throughout the reseeded heart. One reseeded heart was fixed after three days of culture to visualize cell location. Clusters of cells were seen in circumferential heart slices near the apex, papillary muscle, and atrioventricular (AV) valves. The cells were seen in what appeared to be vasculature as well as between ECM fibers. About 90% of cells were retained in the heart as determined from cell counts of the media and perfusion chamber.

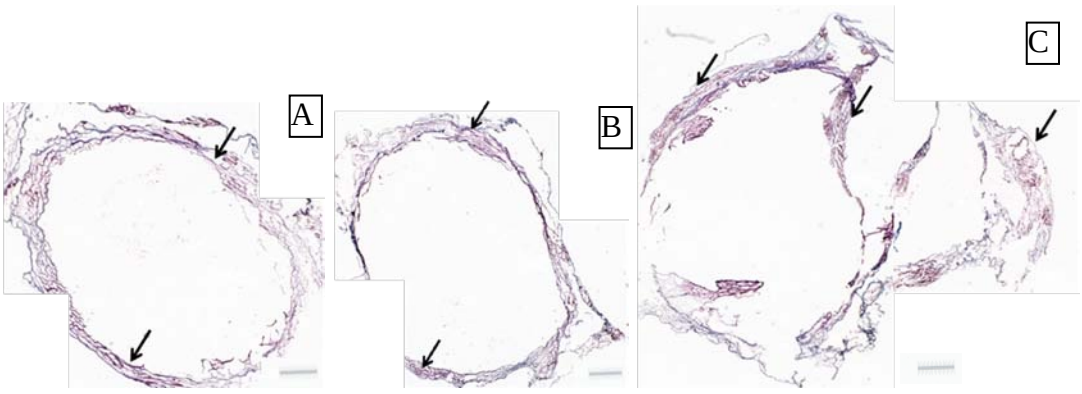

Figure 24. Reseeded heart after cultured with RCM for 3 days. A: Apex of heart. Masson's trichrome 20X. B: Near papillary muscles of the heart. Masson's trichrome 20X. C: Near AV valves of the heart. Masson's trichrome 20X. Scale: 1000 µm.

One can see RCMs with an organized sarcomere structure within the ECM in a reseeded heart that was fixed after 7 days of culture. The H&E images show that the cells are within the ECM of the RV and LV. From the immunofluorescence one can see striated patterns of the RCMs. The cells stained positive for cardiac troponin T but very few of these cells expressed the proliferation marker Histone H3. The immunofluorescent image also shows that the RCMs are within the C-ECM; the C-ECM shows up as the light grey using the transmission light capture on the confocal microscope. These images show that the intact decellularized rat heart is capable of maintaining RCMs in culture for up to one week.

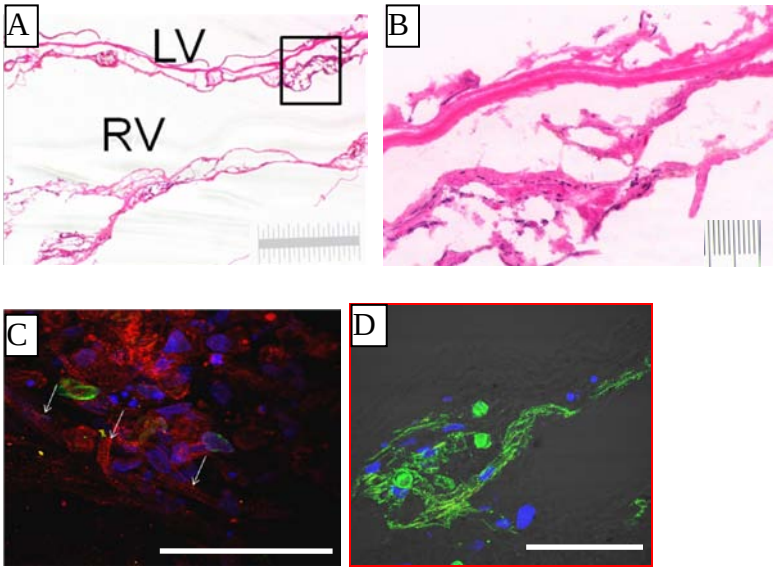

Figure 25. Reseeded heart after cultured with RCM for 7 days A: Middle of heart. H&E 40X scale: 1000 µm. B: Higher magnification of inset from A. H&E 200X scale: 100 µm. C: 1000X magnification from inset from A scale: 100 µm. DAPI: blue, Histone H3: green, and α-actinin: red 100 µm scale bar. D: 600X magnification from inset from A with transmission light to visualize matrix DAPI: blue, α-actinin: green, and cardiac troponin T: red. Scale: 100 µm.

3.3 DISCUSSION

The *in vitro* cultures showed that C-ECM produced by our method maintained a differentiated cardiomyocyte phenotype unlike UBM, supported cell survival of endothelial and progenitor cells similar to UBM, and enabled 3D culture of cardiomyocytes in a perfusion system. A more vigorous series of decellularization solutions compared to UBM were needed to decellularize the tissue because of the densely cellular and thick nature of the myocardium. Therefore, *in vitro* cell culture was used to compare C-ECM and UBM to verify C-ECM enabled similar proliferation. C-ECM was comparable to UBM for the culture of cardiomyocytes, endothelial cells, and myoblast cells with the exception that only an organized sarcomere structure shown by striated cardiomyocytes were seen on the C-ECM sheet and C-ECM gel. UBM has been used in multiple cardiac reconstruction studies and showed some local contraction (83, 123-124, 126); the fact that C-ECM produced by the method described was not different to UBM is promising. In multiple *in vitro* investigations ECM has been shown to support synchronously contractile cardiomyocytes (63, 79-80, 140-141). C-ECM has a further benefit compared to other ECM scaffolds because of C-ECM's complex 3D structure that was shown to support viable cardiomyocytes with an organized sarcomere structure.

Cardiomyocytes, endothelial, and progenitor cells were used for the *in vitro* culture and morphology was compared between the scaffolds as these would be some of the cells required to regenerate functional myocardial tissue. While the scaffolds for reconstruction are implanted as

a sheet, it has been shown that 60% of the mass of ECM is degraded and lost within the 1st month and remodeled with native tissue (44, 142). One way to obtain degraded ECM is to subject it to pepsin digestion. Pepsin degraded ECM products have been shown to be chemo-attractant, anti-microbial, and bioactive (57-58, 143). Therefore cells were seeded on the surface of the ECM gels in the *in vitro* assays to assess the effects of the ECM degradation products. Because the primary isolation of cardiomyocytes contains fibroblasts, quantitative cardiomyocyte cell counts could not be obtained. Therefore myoblasts and endothelial cells were used to quantify relative *in vitro* cell counts on the C-ECM and UBM scaffolds.

Only on C-ECM sheet and gel was an organized sarcomere structure seen for CCM culture; this showed the maintenance of cardiac phenotype. Organization of the sarcomere structure is one component required for cardiomyocyte contraction. While multiple experiments have shown the phenotype maintenance and contraction of cardiomyocytes on non-organ specific ECM (63, 140-141), the endpoint of the initial cardiomyocyte seeding (4 days) in the described experiment was shorter. It could be possible that the C-ECM composition allowed for faster reorganization of the cardiomyocytes after the isolation procedure. In fact, cardiomyocytes plated on extracellular matrix produced by cardiac fibroblasts (Cardiogel) were shown to adhere more rapidly after plating, exhibit spontaneous contractility earlier, undergo cytoskeletal and myofibrillar differentiation earlier, and grow larger than their counterparts plated on laminin or fibronectin alone (144-145). More experiments looking at the time course of cardiomyocyte organization on C-ECM would be needed to confirm the benefit of organ specific ECM on cardiomyocyte structure and function.

The cell morphology and cell quantity of endothelial and myoblast cells on C-ECM sheet or gel was similar to the same form of UBM. There was an obvious alignment of HAECs only

on C-ECM sheet. The HAEC alignment on the C-ECM could be related to the trabeculae of the heart as patterning has been show to align endothelial cells (146). The ViaLight® Plus Bioassay Kit (Lonza, Allandale, NJ) was chosen to determine the metabolic activity because the amount of ATP measured correlates well to the cell number (133-134). The higher proliferation on the UBM gel compared to the ECM sheets could be due to composition, as ECM degradation products have been shown to be a chemoattractant for endothelial cells *in vitro* (47), but there were structural differences between the sheet and gel that could have impacted proliferation. The power for the HAEC ANOVA was 0.88 (β=0.12) so there was a high probability that differences in cell number between the scaffolds would be detected. The power (0.54) for the C2C12 analysis was much lower, so differences between cell survival/proliferation between the scaffolds may have been missed. Running the experiment again for the C2C12s may have increased the power, but the large standard deviation could have been caused by differences in myoblast differentiation. While C-ECM did not show an advantage over UBM in the quantitative portion of the study, the comparable results are encouraging being UBM has been shown to beneficially remodel in multiple organ systems (41, 83, 147).

A market weight pig has a heart that is approximately the same size as the adult human heart but the decellularized rat heart was chosen for reseeding experiments because of the number of cells required for reseeding; the adult human heart contains 2-4 billion cells (148-149). Minimizing the number of cells required for these initial reseeding experiments is critical because contractile cardiomyocytes have limited proliferation (150) and can only be isolated from fetal or neonatal hearts. Cardiomyocytes were seeded into an intact decellularized rat heart to show that C-ECM scaffold is capable of maintaining cells *in vitro* by using the native vasculature to provide nutrients. While the ng DNA/mg ECM and base pair streak for the

decellularized rat heart were higher than the lab standard for decellularization (106), the scaffolds were sufficiently decellularized that no nuclei or DNA could be seen at high magnification and had approximately the same amount of remnant DNA as described by Taylor's group (80) accounting for the high percentage of water in the decellularized rat heart (~95% water). Therefore the amount of remnant DNA did not impact the microscopic evaluation of the reseeded rat heart.

The human fetal cardiomyocytes were originally used for reseeding experiments because of the relevance of the species to clinical applications. The local alignment of the HCMs may be due to the pulsatile flow of the perfusate as CMs have been shown to align in parallel to the direction of tension (151). The proliferation of the HCMs and presence throughout the entire matrix would make reseeding a larger matrix feasible however, these cells are not contractile in culture and are difficult to obtain. Further experiments using neonatal rat cardiomyocytes were performed to show that it is possible to seed and maintain striated cardiomyocytes within a 3D C-ECM scaffold *in vitro* by using the native vasculature. In the cross section of the reseeded 3D C-ECM, one can see the RCMs within the matrix throughout the heart and maintenance of cardiomyocyte phenotype.

This is the first experiment to show the recellularization of the decellularized heart with cardiomyocytes using the coronary arteries. In Taylor's work, they injected cells directly into the anterior LV of the C-ECM which led to approximately 50% loss of cells in the first 20 min and only a partial reseeding of the LV. They suggested that cells could not permeate the blood vessel walls as they state "endothelial cells formed single layers in both larger and smaller coronary vessels throughout the wall (80)." It is unknown exactly how the cells migrate from the vessel to the myocardial ECM, but it is logical that pores would have to form in the vessel walls

during decellularization. While the average width for a day 3 rat neonatal cardiomyocyte is about 6.2 μm (150), they tend to form clumps during the isolation so pores would probably need to be larger than the average CM width. The additional steps compared to Taylor's work in the decellularization method described here that maybe responsible for the permeability of the blood vessel walls are the initial freezing, pulsatile flow with higher peak pressures, and the use of trypsin. The ice crystals formed in the initial freezing step helped with cell lysis, but also may have ruptured the vessels as the water expanded. The pulsatile flow used in the described method obtained higher peak pressures than the 77.4 mmHg reported by Taylor and may have torn through the vessel walls during the decellularization process. The trypsin step specifically breaks the collagen peptide bonds on the C-side of Argenine and Lysine which could have opened/increased pores in the vessel wall. The large and small coronary arteries and veins could be isolated and the size of pores investigated through SEM and immunohistochemistry after the freezing, trypsin, and final step to specifically determine how and where the pores in the vessel wall are formed.

3.4 CONCLUSION

C-ECM supported *in vitro* culture of cardiomyocytes, endothelial and myoblast cells. Only on the C-ECM scaffold did the cardiomyocytes show an organized sarcomere structure showing maintenance of their differentiated state. The 3D C-ECM was shown to be a suitable substrate for cardiac cell attachment with maintenance of cardiomyocyte phenotype and is suitable for *in vivo* experimentation.

3.5 FUTURE WORK

Ultimately transplantation of a total tissue engineered heart is the goal, but transplantation of a single chamber as a bio-VAD or a physiologically contracting cardiac patch would be beneficial. Some of the barriers to clinical translation of a 3D cardiomyocyte scaffold are cell source, cell seeding, organization of multiple cell types, physiologic pressure generation, adequate perfusion, and immunogenicity. While it has been shown that a 3D decellularized heart can produce about 10 mmHg of aortic pressure if recellularized by neonatal rat cardiomyocytes (80), these cells are not clinically relevant. Human stem cells are clinically relevant and have been differentiated into cardiomyocytes (25-27, 152); these cells could be implanted in a non-differentiated or differentiated form. If induced pluripotent stem (IPS) cells were used (153-156), the original fibroblasts to be differentiated could be harvested from the same patient being treated; this would address many of the immunogenicity issues. If non-differentiated stem cells were used to reseed the 3D C-ECM, they could be expanded and then differentiated toward a cardiac lineage within the scaffold. The presence of an organ specific extracellular matrix may provide signals to seeded cells to enhance their differentiation and function (144-145, 157-158). There are multiple possible ways to deliver cells for reseeding. Cardiac stem cell therapy studies have used coronary artery, coronary sinus, systemic infusion or direct injection into the myocardium of many different cell types to treat CVD (24, 155-157, 159-165). It is more difficult to inject cells through the coronary sinus in the decellularized rat heart, but this method is much easier and may be required to reseed the much larger porcine heart. Direct injection has issues with cell lose, but again it should be easier to perform this method with the decellularized porcine heart due to the increased myocardium thickness. These techniques may be useful in conjunction with retrograde aortic cell perfusion especially if multiple cell types were used for reseeding. Taylors

group did inject both cardiomyocytes and endothelial cells into the decellularized rat heart (80), but many more cells would be needed for a fully functional heart. Addition of fibroblasts and myofibroblasts would be required for ECM production and remodeling (72), but can proliferate quickly in culture and impact the cardiomyocyte contraction. Use of multiple plating steps and cell aggregation can limit the number of fibroblasts (131) and the addition of BrdU can prevent all proliferation including fibroblasts but would also stop stem cell proliferation (135). Some of the other cardiac structures that would require site specific cells are the heart valves: fibroblasts, interstitial cells, and valve specific endothelial cells, arteries: smooth muscle and endothelium, and myocardium: cardiomyocytes including pacing, perkinje fibers, atrial, and ventricle cells. It may also be required to have a local stem cell source for replacement of cardiomyocytes (166) such as isl1+ cells (152, 167-170). The organization of all of these specific cells would be extremely difficult *in vitro*. Partial organization of the cardiomyocytes could be obtained through physical (171-173) and electrical (174-175) stimuli, but it would be difficult to provide all of the environmental cues needed. An *in vivo* culture through a heterotopic implantation may provide better biological and physiologic cues for differentiation and organization (176-177). The right side of the heart could be end-to-end anastomosed to the vena cava and the left side to the descending aorta (proximal aorta to the left atrium and the ascending aorta of the tissue engineered heart to the distal aorta of the recipient). It is likely many of the cell types or at least stem cells would need to be seeded in the scaffold prior to implantation. Thus combining the *in vitro* with an *in vivo* culture could provide the optimal maturation conditions before final implantation. It may even be possible to differentiate stem cells toward a cardiac lineage and increase vascularization *in vivo* by adding growth factors in a localized controlled manor as part of an *in vivo* bioreactor. Much work would be required to determine the optimal culture

conditions for recellularization of 3D C-ECM with appropriate cellular diversity and restored tissue function before transplantation of a tissue engineered patch or heart becomes clinically feasible but the possibilities are exciting.

4.0 RIGHT VENTRICULAR OUTFLOW TRACT REPAIR WITH A CARDIAC BIOLOGIC SCAFFOLD

4.1 INTRODUCTION:

Approximately 3 in 1000 infants require corrective surgery for congenital heart defects (CHD) within the first year of life (13). Currently available homografts and synthetic biomaterials for surgical reconstruction are typically associated with rejection, stenosis, aneurysm formation, and calcification (16-17, 19, 178-179). Even if corrective surgery is not required for the complications listed above, additional surgery may be required to accommodate the growth of the patient since available non-resorbable materials do not remodel over time as the surrounding tissue develops proportionally with the patient (16-17). In contrast, non-crosslinked biologic scaffold materials composed of extracellular matrix (ECM) are typically degradable, associated with a robust host cellular response and deposition of neomatrix that does remodel in response to host factors such as growth or change in mechanical loading. Use of such biologic scaffold materials has been shown to promote a site appropriate constructive remodeling response of numerous tissue types including the heart (39, 41, 43).

Since the surface characteristics (180), mechanical properties (101-102), and ultrastructure (77-78) of the ECM harvested from each tissue is distinct and unique, it is logical and plausible that a Cardiac ECM (C-ECM) material would be best suited to facilitate the

constructive remodeling of cardiac tissue. C-ECM has been produced by several laboratories and has shown multiple structural and functional benefits over synthetic materials (78-81). A detailed method to decellularize an intact porcine heart in less than 10 hours with maintenance of mechanical strength and chemical composition was described in specific aim 1 (78). Specific aim 2 showed C-ECM's ability to maintain a differentiated cardiomyocyte phenotype in 2D and 3D culture. Whole heart C-ECM in an *in vitro* perfusion system was shown to support contractile cardiomyocytes that generated aortic pressure (80). Singelyn et al. showed angiogenesis after injection of a gel form of C-ECM in a non-infarct cardiac rat model (81). While each of these studies showed the potential benefits of C-ECM, none compared C-ECM to a clinically used material for ventricular reconstruction.

The objective of the present study was to assess the ability of C-ECM as a patch material to replace and remodel a full thickness right ventricular outflow tract (RVOT) defect in a Lewis rat model. Results were compared to a Dacron patch which is commonly used for myocardial reconstruction.

4.2 METHODS

4.2.1 *Overview of Experimental Design*

C-ECM was compared to Dacron for myocardial reconstruction in a right ventricular defect model. Specifically, a 6 mm C-ECM patch and Dacron patch were used to replace a full thickness RVOT defect in a rat model. The primary endpoints of the study were histomorphology and echocardiographic assessment. Eleven rats were included in each group

and eight of these animals were sacrificed at 16 wk post surgery. One additional rat from each group was sacrificed at 2, 4, and 8 wk to evaluate the remodeling process over time. Cell phenotype and morphology were evaluated at all time points using immunohistochemistry and immunolabeling techniques. Heart dimensions and function were quantified using echocardiography prior to surgery and at 4 and 16 wk post-surgery.

4.2.2 *Preparation of C-ECM*

Intact porcine hearts were perfusion decellularized to produce a C-ECM biological scaffold as previously described (78). Briefly, porcine hearts were obtained immediately following euthanasia and frozen at -80°C for at least 16 hrs and thawed. The aorta was cannulated and alternately perfused with type 1 reagent grade (Type 1) water and 2X PBS at 1L/min for 15 min. each. Serial perfusion of 0.02% trypsin/0.05% EDTA/ 0.05% NaN_3 at 37°C, 3% Triton X-100/0.05% EDTA/ 0.05% NaN_3, and 4% deoxycholic was conducted, each for 2 hrs at approximately 1.2 L/min. Finally, the heart was perfused with 0.1% peracetic acid /4% EtOH at 1.7 L/min for one hour. After each chemical solution, Type 1 water and 2X PBS were flushed through the heart to aide in cell lysis and removal of cellular debris and chemical residues. Decellularization was verified by removal of all visible nuclear material via hematoxylin and eosin (H&E) staining, decrease of measurable double stranded DNA to less than 50 ng/mg dry weight ECM, and showing that any remaining nuclear material consisted of DNA remnants less than 200 base pairs (106).

4.2.3 *Preparation of RVOT Patches*

The free wall of the decellularized porcine right ventricle (RV) was lyophilized and 6mm diameter patches were cut using a tissue punch. The 6 mm Dacron™ patch was cut from the

Bard®DeBakey® Woven Fabric (Bard Peripheral Vascular, Inc. Tempe, Az.). The average C-ECM patch thickness was 2.5 mm and the Dacron patch was 0.25 mm. All patches were packaged in sterilization pouches and terminally sterilized using ethylene oxide (EO gas sterilizer Series 3 Plus, Anderson Products, Haw River, NC).

4.2.4 *RVOT Surgical Procedure*

Adult female syngeneic Lewis rats (Harlan Sprague Dawley Inc, Indianapolis, IN) weighing 175 g to 200 g were used for the RVOT replacement procedure as previously described (38). Briefly, a surgical plane of anesthesia was obtained using isoflurane (approx 2.5%)/oxygen. The animals were intubated with a 16G catheter and respiration maintained at 60 cycles/min and a tidal volume of 1.5 ml. Using aseptic techniques with sterile instruments the skin of the chest was sterilized with povidone-iodine solution and the heart was exposed through a median sternotomy. A purse-string suture with a diameter slightly larger than 6.0 mm was placed in the free wall of right ventricular outflow tract (RVOT) with Surgipro II 7-0 polypropylene sutures (Covidien, Mansfield, MA). Both ends of the stitch were passed through a 22-gauge plastic vascular cannulae, which was used as a tourniquet. The tourniquet was tightened and the distended part of the RVOT wall inside the purse-string stitch was resected. The tourniquet was briefly released to determine whether massive bleeding occurred, which indicated that a transmural defect had been created in the RVOT. A 6 mm C-ECM or Dacron patch was sutured along the margin of the purse-string suture with 7-0 polypropylene over-and-over sutures to cover the defect in the RVOT. After completion of suturing, the tourniquet was released and the purse-string stitch was removed. After the expansion of lungs using positive end-expiratory pressure, the sternum was closed parasternally with four interrupted Surgipro 5-0 polypropylene sutures (Covidien, Mansfield, MA). The muscle layer and skin were closed with Polysorb 4-0 absorbable suture

(Covidien, Mansfield, MA). The first 3 days after surgery, buprenorphine (0.5 mg/kg) analgesia and cefuroxime (100 mg/kg) antibiotic were administered twice a day, subcutaneously and intramuscularly, respectively. One animal in each group was sacrificed at 2, 4, and 8 wk post surgery and 8 animals from each group were sacrificed at 16 wk post surgery. At the time of sacrifice, animals were anesthetized by inhalation of isoflurane (5%) in oxygen. Cardiac arrest solution (68 mM NaCl, 60 mM KCl, 36 mM NaHCO3, 2.0 mM MgCl2, 1.4 mM Na2SO4, 11 mM dextrose, 30 mM butanedione monoxime, 10,000 U/L of heparin) was administered intravenously and hearts were excised after death was confirmed. The research protocol followed the National Institutes of Health guidelines and was approved by the Institutional Animal Care and use committee at the University of Pittsburgh.

4.2.5 *Immunohistochemistry and Immunolabeling Methods*

The hearts were fixed in 4% paraformaldehyde for 20 min followed by rinsing in PBS. The hearts were then placed in a 30% sucrose solution for at least 16 hrs. Hearts were bisected along the short axis midway through the patch with a razor and placed in optimal cutting temperature solution (OCT, Sakura Finetek USA, Inc. Torrance, CA). Five micron thick frozen sections were cut for mounting, staining, and histological evaluation. Masson's Trichrome stain was used to visualize muscle, fibrous tissue, and nuclei using a Nikon™ E600 microscope (Nikon Instruments Inc. Melville, NY). Von Kossa stain was used to visualize calcification. Monoclonal anti-α-actinin (Sarcomeric) antibody (1:200, Sigma-Aldrich, St. Louis, MO) and cardiac troponin T antibody (1:100, Abcam, Cambridge, MA) were used to label cardiomyocytes. Von Willebrand factor (VWF) antibody (1:100, Abcam, Cambridge, MA) was used to identify endothelial cells. Smooth muscle myosin heavy chain 2 (SMMHCII) antibody (1:75 Abcam, Cambridge, MA) was used to label smooth muscle cells. Connexin

43/GJA1 antibody (1:200, Abcam, Cambridge, MA) was used to visualize gap junctions. All primary antibodies were incubated for 2 hrs at room temperature in 1% bovine serum albumin (BSA) followed by five 1% BSA washes. All Alexa Fluor secondary antibodies (Life Technologies, Carlsbad, Ca) were used at a concentration of 1:200 in 1% BSA for 2 hrs at room temperature followed by five 1% BSA washes. Nuclei were counterstained with 4', 6-diamidino-2-phenylindole (DAPI) and/or DRAQ5™ (Biostatus Limited, Shepshed Leicestershire, UK). Immunofluorescent (IF) slides were imaged on a confocal microscope.

4.2.6 *Echocardiographic Analysis*

Echocardiographic measurements were obtained pre-operatively, and at 4 and 16 wk post operatively. A surgical plane of isoflurane anesthesia (approximately 1.5% maintenance through nose cone) was established before echocardiography was performed. RV and LV minimum and maximum diameters and LV fractional shortening (FS) were calculated using Image J (NIH, Bethesda, Maryland).

4.2.7 *Statistical Analysis*

A repeated measures ANOVA with a Tukey's post hoc analysis was performed to determine whether differences existed between the pre-operative, the 4 wk post-operative, and 16 wk post-operative echocardiographic values within each patch group with the p-value set at 0.05. (Minitab® version 15.1.1.0, Minitab, State College, PA).

4.3 RESULTS

4.3.1 *Surgical Observations*

Macroscopic and scanning electron microscopy (SEM) images of the patches can be seen in Figure bellow. The 6 mm patches replaced about 25% of the RV freewall.

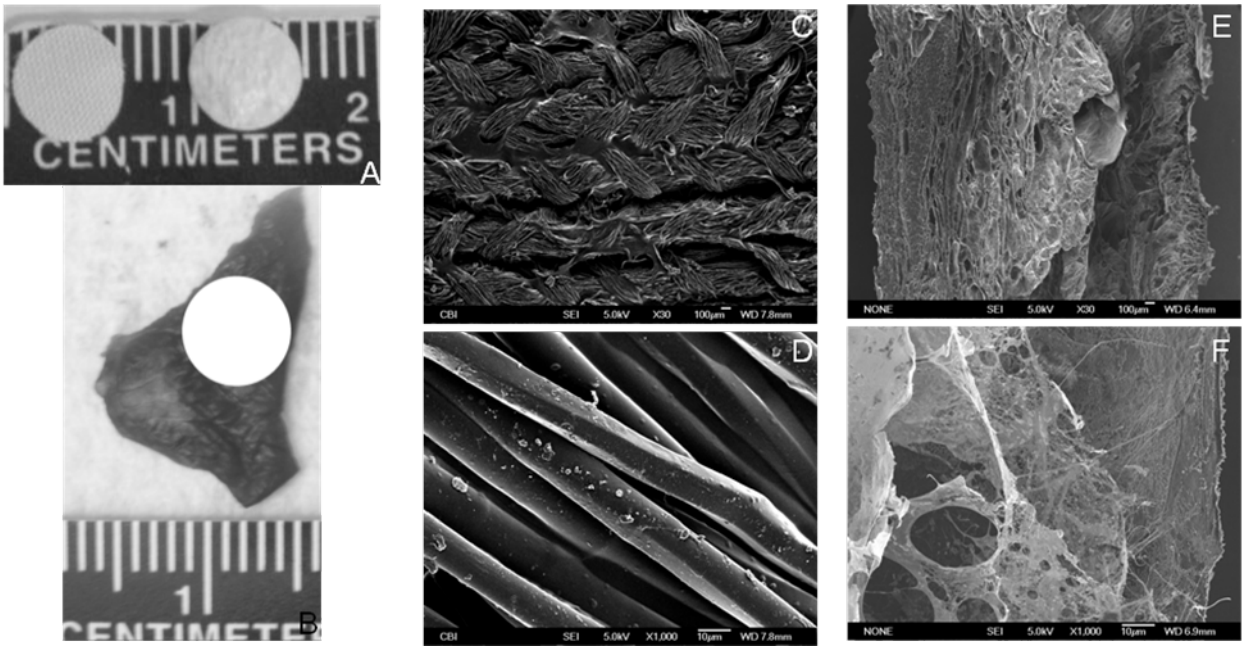

Figure 26. Dacron and C-ECM patches. A: Macroscopic photo of patches. Dacron on left and C-ECM on right. B: Approximate placement of 6 mm patch in RVOT shown on excised RV free wall. SEM of Dacron C:30X scale: 100 µm D: 1000X scale: 10 µm. SEM of C-ECM with endocardium on right side E: 30X scale: 100 µm F: 1000X scale: 10 µm.

At the time of implant, it took longer to achieve hemostasis with the Dacron™ patch than the C-ECM patch. There was one postoperative death in each of the Dacron and C-ECM groups. Due to the 2.5 mm thickness of the C-ECM patch, it protruded above the epicardial surface of the RV at implantation, but the difference was minimal as remodeling progressed to the 16 wk time point. At all end time points, there were dense fibrous adhesions on the epicardial surface on almost all of the Dacron patched hearts that were adhered to the sternum, but there were fewer adhesions with the C-ECM patched hearts.

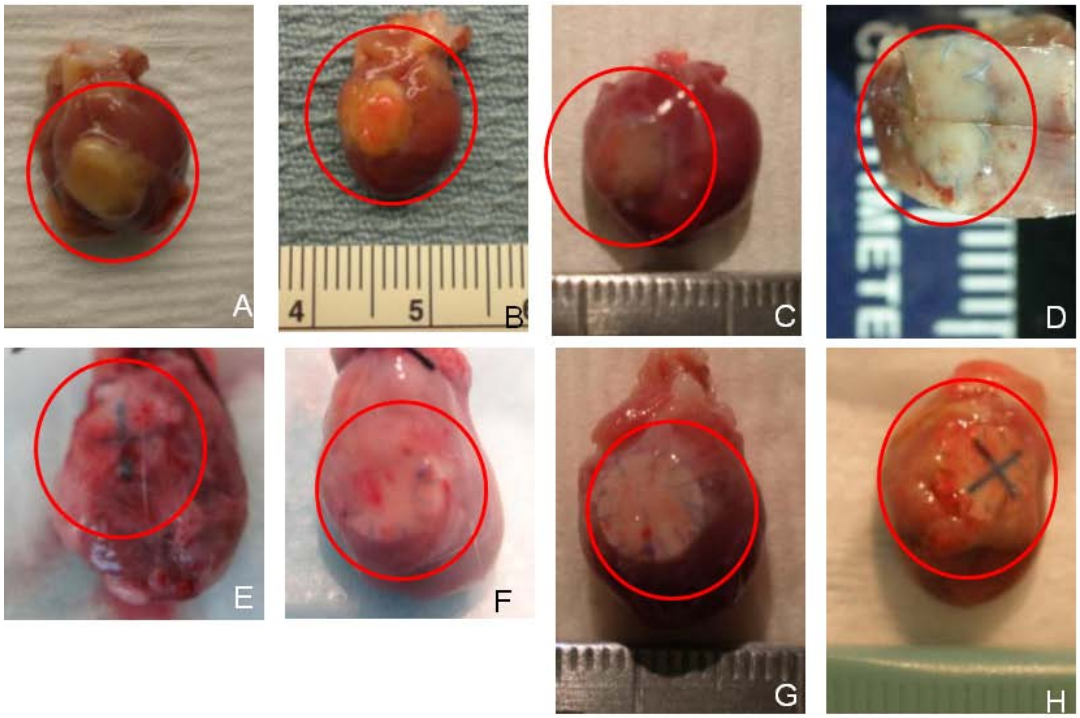

Figure 27. Macroscopic patch images at 2, 4, 8 and 16 wk post surgery. The C-ECM patch decreased in thickness as it remodeled. Fibrous adhesions can be seen at 2 and 4 wk on the Dacron patched hearts. The adhesions were removed from the later timepoints so that the patch could be better visualized. A: 2 wk C-ECM, B: 4 wk C-ECM, C: 8 wk C-ECM, D: 16 wk C-ECM after fixation, E: 2 wk Dacron, F: 4 wk Dacron, G: 8 wk Dacron, H: 16 wk Dacron.

4.3.2 *Immunohistochemistry and Immunolabeling Analysis of RVOT*

The Dacron material successfully patched the RVOT defect, but was encapsulated by fibrous tissue and there were very few cells that infiltrated the polyester weave of the Dacron patch. There were minimal histological differences in the patched region between the 2, 4, 8, and 16 wk time points.

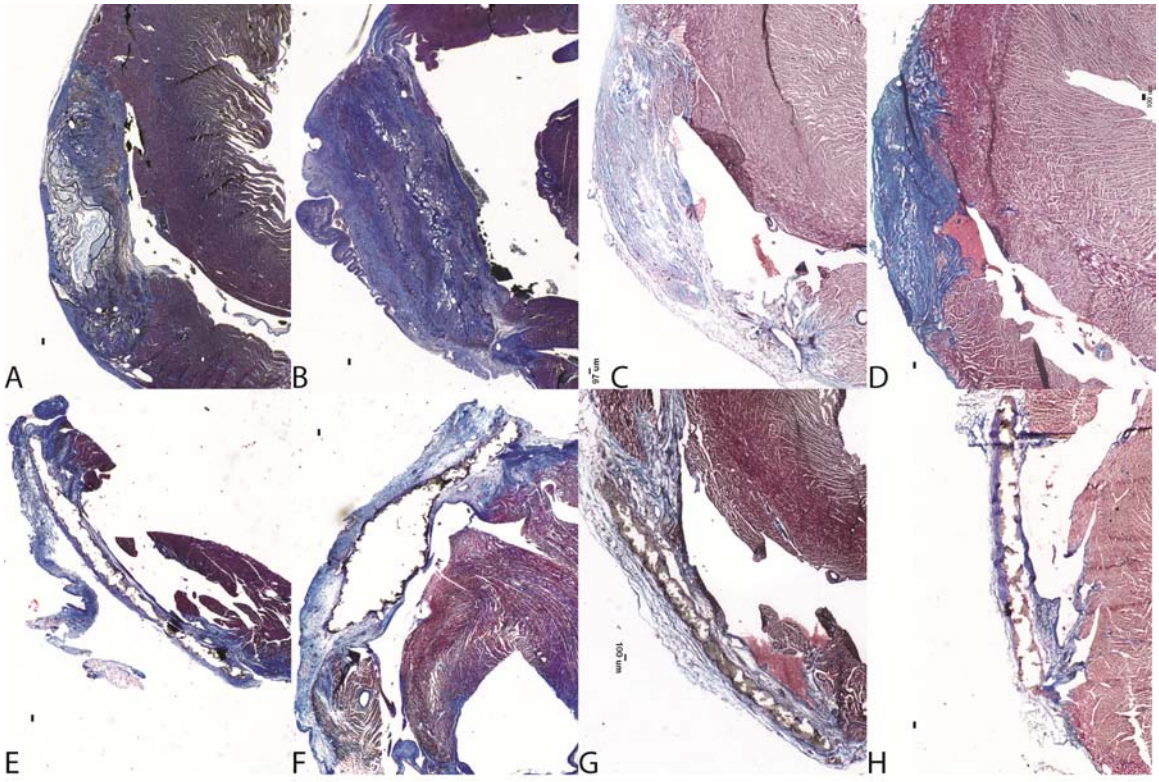

Figure 28. Masson's Trichrome C-ECM Patch at 2, 4, 8, 16 wk post surgery. C-ECM patch recellularizes and remodels over 16 wk timepoint whereas there are few changes in the Dacron patched hearts over the 16 wk. A: 2 wk C-ECM, B: 4 wk C-ECM, C: 8 wk C-ECM, D: 16 wk C-ECM, E: 2 wk Dacron, F: 4 wk Dacron, G: 8 wk Dacron, H: 16 wk Dacron. Scale bar: 100 µm.

The connective tissue surrounding the Dacron patch had a continuous endothelial layer on the endocardial surface as shown by the positive staining for VWF. There were few endothelial cells and no smooth muscle cells within the connective tissue surrounding the Dacron patch and no calcification was observed. The Dacron patch showed encapsulation by a thin dense connective tissue layer with few differences between the 2 and 16 wk post surgery time points.

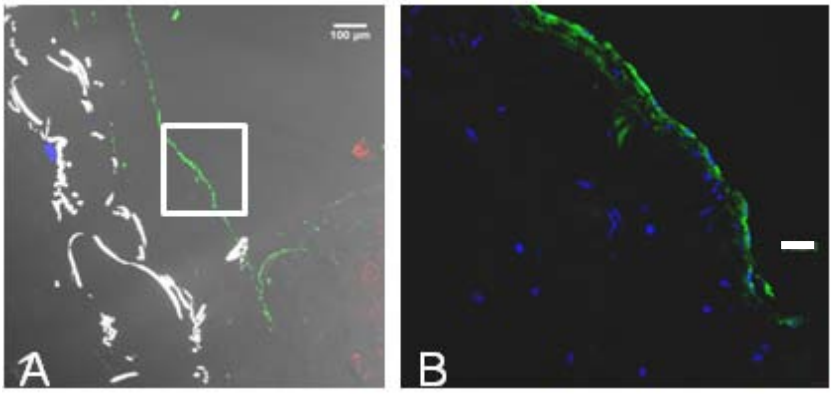

Figure 29. Immunofluorescent staining of the Dacron patched area at 16 wk showing little cellular infiltrate of the tissue surrounding the patch and no cellular infiltrate into the Dacron weave. There is an intact endothelium on the endocardial surface but no cardiomyocytes surrounding patch. A: 10 X with transmission light capture scale: 100 µm. B: 60X from inset area scale: 17 µm. VWF: green, alpha actinin: red, Draq 5: blue.

The C-ECM patch remodeled from an acellular scaffold material containing mostly collagen into densely cellular connective tissue. At 2 wk a portion of the original C-ECM patch could be identified in the Masson's trichrome stained sections as denoted by the acellular area within the center of the patch. By 4 wk, the C-ECM patch was characterized as densely cellular connective tissue. At 8 and 16 wk the trichrome images showed that the C-ECM patch had remodeled into vascularized collagenous tissue with small islands of striated muscle. Von Kossa

staining failed to show any signs of calcification. VWF showed a continuous endothelialized endocardium. Endothelial and smooth muscle cells were visualized throughout the patched regions either localized in the same area or independent from one another.

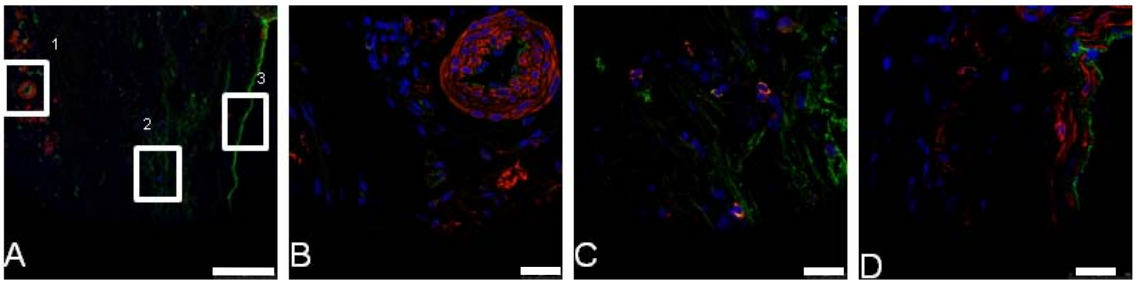

Figure 30. Immunofluorescent staining of the remodeled C-ECM patch showing VWF positive endothelium and vasculature and SMMHCII positive smooth muscle throughout the middle of the patch at 16 wk. A: 10X scale: 250 µm, B: 60X from inset area 1 scale: 25 µm, C: 60X from inset area 2 scale: 25 µm, D: 60X from inset area 3 scale: 25 µm, VWF: green, SMMHCII: red, Draq 5: blue.

There were small islands of cells stained positive for alpha actinin, cardiac troponin T, and connexin 43 both on the epicardium and endocardium. These islands of cardiomyocytes also contained blood vessels as shown by the positive staining of SMMHC II and VWF.

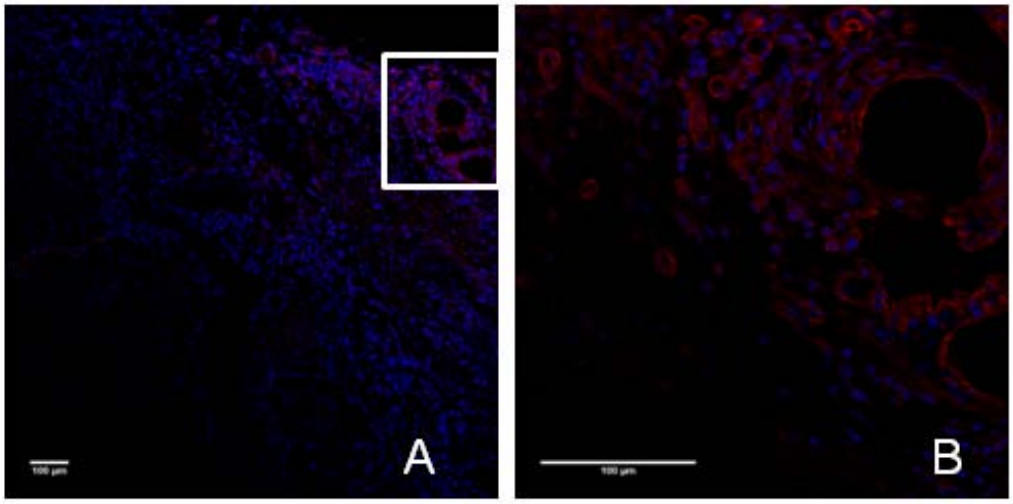

Figure 31. Immunofluorescent staining of the remodeled C-ECM patch showing α-actinin positive cardiomyocytes in the middle of the patch on the epicardial surface at 16 wks. α-actinin: red, Nuclei: blue, A:10X scale: 100 µm, B: 40X from inset area scale: 100 µm.

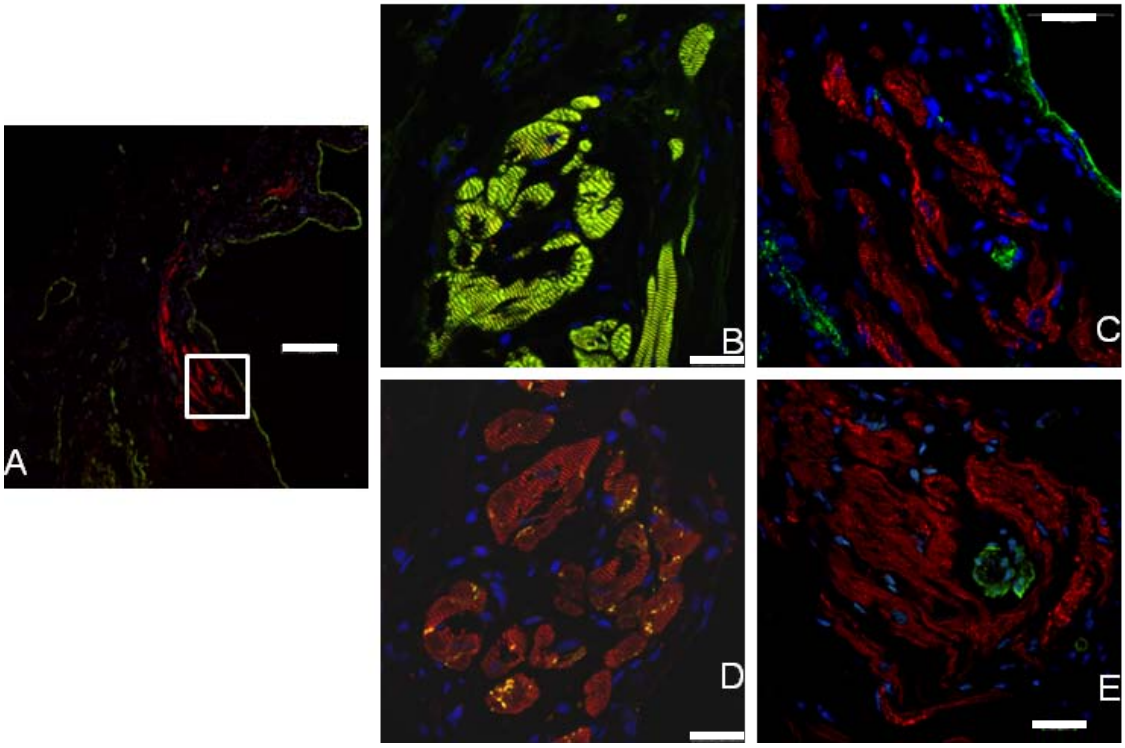

Figure 32. Immunofluorescent staining of the remodeled C-ECM patch showing α-actinin and cardiac troponin T positive cardiomyocytes with connexin 43 labeled gap junctions, VWF labeled endothelium and SMMHCII labeled smooth muscle in the middle of the patch on the endocardial surface at 16 wk. A: 10X scale: 200 µm vwf: green, alpha actinin: red, DAPI: blue. B, C, D, and E from inset area on sequential slides scale: 30 µm. B: 63X Alpha actinin: green, Card Troponin T: red, Draq 5: blue. C: 60X vwf: green, alpha actinin: red, DAPI: blue. D: 63X Connexin 43: green, alpha actinin: red, Draq 5: blue. E: 60X SMMHCII: green, alpha actinin: red, DAPI: blue.

4.3.3 *Echocardiographic Assessment of RVOT*

The RV minimum and maximum diameters were greater for the Dacron patched hearts at 16 wk compared to pre-surgery ($p<0.05$). At 16 wk post surgery, the RV minimum diameter was 150 % greater than pre-surgery and RV maximum diameter was 130% greater than pre-surgery. The

C-ECM patched heart at either time point showed no statistical differences in functional or dimensional measurements to pre-surgery.

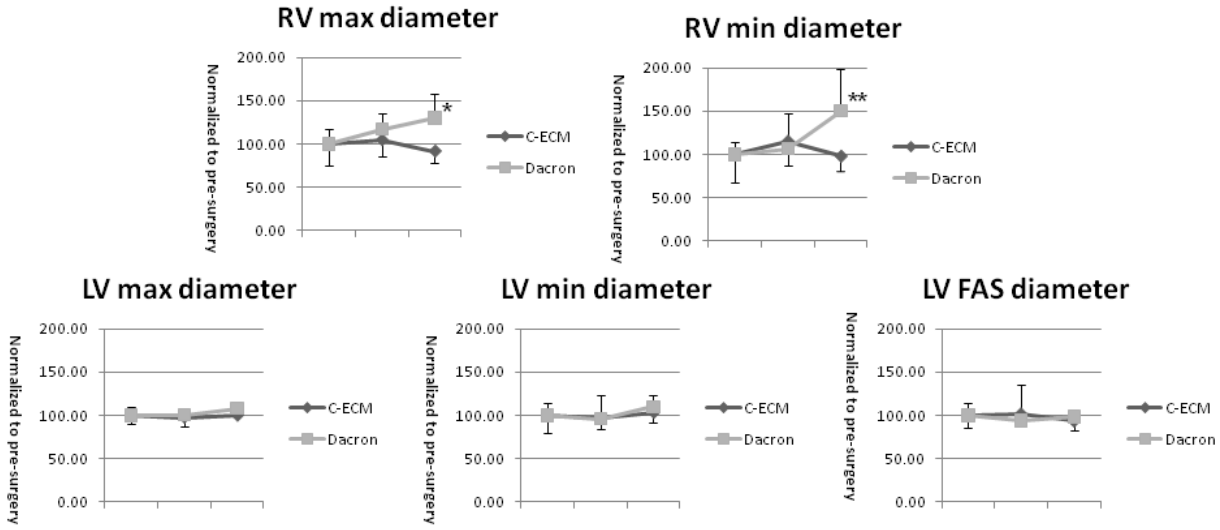

Figure 33. Echocardiographic analysis at pre surgery and 4 and 16 wk post surgery with one standard deviation shown. A: RV max diameter. B: RV min diameter. C: LV max diameter. D: LV min diameter E: Fractional area shortening. For the C-ECM patch, none of the measures were different to pre-surgery at either the 4 or 16 wk time point. For the Dacron patch the RV minimum and maximum diameter had dilated by the 12 wk time point. C-ECM: red line. Dacron: blue line.* $p < 0.05$ to pre-surgery. ** $p < 0.05$ to pre-surgery and 4 wk post surgery.

4.4 DISCUSSION

A biologic scaffold composed of cardiac ECM was shown to be suitable as a replacement material for a full thickness RVOT defect in this rat model. The C-ECM was completely degraded and replaced by host tissue including small islands of cardiomyocytes. By the 16 wk time point, the 2.5 mm thick C-ECM patch had remodeled such that the thickness was similar to the native RVOT and the function and global dimensions of the heart were normal at 4 and 16

wk post surgery. In contrast, the Dacron material was surrounded by a dense fibrous capsule and negatively impacted RV dimensions at 16 wk.

This is the first study reporting the use of cardiac specific ECM to positively impact the repair of a ventricular defect. Previous studies investigating the remodeling of non-cardiac ECM scaffolds following implantation in cardiac applications have been associated with the presence of c-kit positive cells, angiogenesis, small patches of cardiomyocytes, and partially organized collagenous connective tissue (43, 123, 126). Kochupura et al. reported local contractility of the remodeled ECM scaffolds but the percentage of the patch to the free wall was only 5% (123) so global measurements of ventricle function were of limited value (181). With the 25% replacement of the RV freewall, this study was able to assess global dimensional and functional differences. The present study also had a longer endpoint than other degradable cardiac patch remodeling studies (38, 43, 123, 126) allowing assessment of long term maturation of the defect. The cellular infiltrate and neovascularization that was observed in the remodeled C-ECM material is typical of the *in vivo* host response to non-crosslinked ECM biologic scaffold materials, such as small intestinal submucosa (SIS) and urinary bladder matrix (UBM) (39, 41, 43). Particularly, the C-ECM material showed similar cellular infiltration, angiogenic response, and degradation rate to those for SIS an UBM, and promoted the presence of site appropriate cells. Angiogenesis is a common occurrence following ECM placement in many anatomic locations (123, 182-185). Singelyn et al. showed migration of endothelial and smooth muscle cells toward C-ECM in the rat heart with increased arteriole formation; specifically they used a gel form of C-ECM in a non-defect LV rat model (81). Zhao et al. recently described the time course of cellular infiltration in response to SIS particulate injection in an acute infarction with reperfusion rat model; the cellular infiltration included initial migration of macrophages followed

by myofibroblasts and angiogensis (185). Suggested mechanisms of angiogenesis include release of cytokines such as transforming growth factor-β (TGF-β), basic fibroblast growth factor (b-FGF), vascular endothelial growth factor (VEGF), and stem cell factor (SCF) (74, 76, 185-186), chemoattractive properties of ECM degradation products to endothelial, progenitor cells (47, 53, 187), and the suitability of the ECM as a substrate for endothelial cell attachment and proliferation (77, 188-189).

The remodeled C-ECM scaffold in the present study showed focal regions of cardiomyocytes along the edges of the repair site and across the endocardial and epicardial surfaces, suggesting that the presence of these cells was dependent upon a vascular supply. The small islands of cardiomyocytes within the C-ECM patched area lacked syncytium, representing immature myocardium that was most likely not capable of actively contributing to cardiac function. Possible sources of the cardiomyocytes are resident islet1 positive (isl1+) (152, 170) cells or circulating bone marrow mesenchymal stem cells (165, 190), both of which have been shown to form cardioblasts. The possibility also exists that iatrogenic effects caused a limited seeding of both patches, but that the cardiomyocytes were only able to populate the C-ECM due to the presence of cell attachment sites and rapid angiogenesis. Further study is required to determine the origin of the cardiomyocytes, and whether they would continue to mature with time.

The hearts repaired with the C-ECM patch had superior echocardiographic results as compared to the hearts repaired with the Dacron patch. The Dacron RV minimum and maximum diameter increased in size by the 16 wk time point which could be an early indication of aneurysm as the LV dimensions remained constant. While there was no difference at the 4 or 16 wk time point for the C-ECM patched heart indicating the patched area had constructively

remodeled. A possible mechanism for the Dacron dilation is the stiffness mismatch to the native ventricle. Kochupura et al. showed almost no change in Dacron dimensions throughout the cardiac cycle whereas the ECM deformed with the surrounding tissue (123). Due to this stiffness mismatch of Dacron, the ventricle could have dilated to minimize wall stress similar to the negative remodeling that occurs after a myocardial infarction (191-193). The C-ECM patch did not impact LV function and was not dilated; these measures are critical for a RVOT reconstruction patch.

While the present study does show the potential for organ specific ECM for cardiac applications, it does not explicitly show that C-ECM is better than ECM derived from other sources since head to head comparisons were not performed. However, ECM of each tissue is synthesized by the resident cells and is in a state of dynamic equilibrium with these cells (64, 69). Hepatocytes have shown superior structure and function when seeded upon liver derived ECM scaffolds compared to ECM scaffolds derived from non-hepatic sources (194). Hydrated decellularized tracheal matrix (HDTM) supported the formation of site-specific epithelium and provided sufficient short term mechanical integrity to withstand physiologic pressures (176). Based on the tissue specific structure and composition of C-ECM (78, 80) and previous data showing advantages of tissue specific ECM (176, 194), it is logical that C-ECM would be a preferred scaffold material for myocardial reconstruction over ECM derived from non-homologous sources.

C-ECM produced by the described method possesses morphological advantages over current clinical materials for reconstructive surgeries due to the macroscopic and ultrastructural similarities to the region being replaced. For example, it may be possible to reconstruct the entire outflow tract, valve, and pulmonary artery from a decellularized porcine heart since coronary

perfusion allows for better decellularization of dense cardiac tissue (78, 80) than alternative approaches (79, 117-118). Furthermore, the advantageous mechanical behavior of the C-ECM relative to the normal heart (78) and subsequent remodeling could reduce the incidence of aneurysm formation (179). The use of decellularized xenogeneic tissue would also eliminate the current issues associated with homografts, specifically insufficient supply and limited size availability (16, 178). Numerous studies have shown the lack of an adverse immune response when an appropriately decellularized non-crosslinked ECM biologic scaffold is placed within a xenogeneic recipient (183-184, 195). These non-crosslinked ECM scaffolds could eliminate issues of sensitization and rejection that are currently experienced with the use homografts in pediatric patients, thereby increasing the potential for successful donor matching in a population that may require an orthotopic heart transplant (19). Finally, it may be possible to use a 3D C-ECM patch seeded with stem cell derived cardiomyocytes (26, 155) to obtain an actively contracting patch as ECM in multiple *in vitro* investigations has been shown to support synchronously contractile cardiomyocytes (79-80, 140-141).

4.5 CONCLUSIONS

The improved echocardiographic findings of the C-ECM patch over the Dacron patch appeared to be related to the morphometric differences seen in the patched region. Additional studies are needed to assess the potential of C-ECM biologic scaffold material, but the possibility of using 3D C-ECM for the correction of congenital heart defects is promising.

4.6 LIMITATIONS AND FUTURE WORK

Limitations of this study were that it was a small animal model with one primary endpoint (i.e. 16 wks) and the source of the cells populating the patched region was not specifically determined. While the rats did increase their weight by about 25%, a 6 month juvenile sheep model is the standard for congenital heart defect reconstruction due to similar calcification issues and growth rates to children (196). A limited number of animals were employed for histological evaluation at the early time points, which restricted analysis of cellular remodeling over time, but echocardiographic measurements enabled functional analysis of the tissue remodeling time course. Studies are ongoing to elucidate possible sources of the cells within the C-ECM patched area and to compare RVOT remodeling with different sources of ECM; this may provide further information leading to a beneficial CHD treatment.

5.0 DISSERTATION SYNOPSIS

5.1 MAJOR FINDINGS

The present work described the manufacture and use of cardiac extracellular matrix (C-ECM) biologic scaffold produced by perfusion decellularization. When this study was started, there were no publications on ventricular decellularization for tissue engineering applications. The biochemical composition and structure of C-ECM was determined and mechanical performance was tested. The *in vitro* growth of multiple cell types was compared with immunolabeling and metabolic assays between C-ECM and a well characterized biologic scaffold material, urinary bladder matrix (UBM). Finally, C-ECM was compared to a standard cardiac reconstruction material, Dacron™, to repair a full thickness defect in the right ventricle outflow tract in a rat model.

The following are the major findings of the present work:

Specific Aim 1

- Use of retrograde aortic perfusion can decellularize heart in less than 10 hrs.
- Removal of cells and DNA confirmed.
- Presence of collagen IV, GAG, and elastin.
- C-ECM ball burst force was not different than native tissue.

Specific Aim 2

- Cardiomyocytes can be maintained in culture on 2D and 3D C-ECM scaffolds
    a. In 2D culture an organized sarcomere structure of cardiomyocytes were visualized on C-ECM scaffolds but not on UBM scaffolds
    b. An intact decellularized rat heart maintained striated cardiomyocytes in 3D culture
- Myoblasts and endothelial cell counts on C-ECM sheet and gel similar to UBM
    a. C-ECM produced by the described method enabled cell survival

Specific Aim 3

- Dacron successfully patched the RVOT defect but there was a negative impact on global function at 4 weeks and RV diameter at 16 weeks.
- C-ECM can successfully patch and remodel in a full thickness RVOT defect
    a. No negative impact on RV or LV dimension or LV function
    b. Native tissues at site (collagenous connective tissue, smooth muscle, endothelium, and cardiac muscle)
        i. Small numbers of cardiomyocytes within patched region

5.2 OVERALL CONCLUSIONS

The innovative portion of the decellularization method described in this chapter is the optimization of sytematic decellularization solutions in combination with retrograde aortic perfusion to produce a biologic scaffold that maintained much of the macroscopic and

microscopic structures as well as the C-ECM composition. Since the C-ECM biaxial rupture strength force was not different than the native tissue and was significantly larger than 4 layers of UBM, the mechanical integrity of C-ECM should be sufficient to withstand the pressure of the right or left ventricle as constructive remodeling progresses. While there is much work to be done, the methodology described herein provides a useful step to fully realizing an engineered complex organ.

C-ECM supported *in vitro* culture of cardiomyocytes, endothelial and myoblast cells. Only on the C-ECM scaffold did the cardiomyocytes show an organized sarcomere structure showing maintenance of their differentiated state. The 3D C-ECM was shown to be a suitable substrate for cardiac cell attachment with maintenance of cardiomyocyte phenotype and is suitable for *in vivo* experimentation.

The improved echocardiographic findings of the C-ECM patch over the Dacron patch appeared to be related to the morphometric differences seen in the patched region. Additional studies are needed to assess the potential of C-ECM biologic scaffold material, but the possibility of using 3D C-ECM for the correction of congenital heart defects is promising.

APPENDIX A

SOP P0055 vr 1 Preparation of Cardiac Extracellular Matrix

Objective: To prepare Extracellular Matrix (ECM) from heart using retrograde perfusion

Requirements: Must have completed the following training modules based on the tissue source used.

All procedures:

Research Integrity – general must be completed to work in the research laboratory

Chemical Hygiene – general must be completed to work in the research laboratory

Animal Tissue:

Use of Animal in Research and Education – when source is animal tissue

Small Animal Research and Training – when source is small animal tissue

Large animal training – when source is large animal tissue

Human tissue:

Bloodborne Pathogen Training – when source is human tissue (obtained through an honest broker)

1. SOP# P1004 DAPI Staining of Tissue for Determination of DNA

2. SOP# D2000 PAA Disinfection and Depyrogenation: Mechanical Shaker
3. SOP# H3000 Fixation, Dehydration, and Paraffin Embedding of Tissue Specimens

NOTE: Record all steps and observations on Heart Production Sheet *(See attached sheet for example*)

Solutions:

Label all solution bottles with solution name, your initials, date of preparation, and date of expiration.

3% (v/v) Triton X-100/0.05% EDTA/0.05%Sodium Azide (NaN_3) (expiration 1 month)

Triton X 100 (source :Spectrum TR135 or equivalent)……..90.0 ml

EDTA (source: Fisher BP120 or equivalent)……...1.5 g

Sodium Azide (source: Sigma S8032-100G or equivalent)…….....1.5g

Type I water…….2910.0 ml

The Triton X-100 is viscous, so it will be necessary to do a repeated backwashing of the graduated cylinder to remove residual Triton X-100. Mix on shaker to thoroughly dissolve.

Caution: Sodium Azide is very hazardous in case of skin contact (irritant), Hazardous in case of ingestion, of inhalation, slightly hazardous in case of skin contact (permeator).

0.1% PAA (expiration 2 days)

15% PAA (SOP#D2000 PAA)……20.0 ml

Type I water…….2860.0 ml

Alcohol……..120.0 ml

4% (w/v) Deoxycholic Acid (expiration 1 month)

Deoxycholic acid[source: Spectrum S1066 or equivalent] (sodium salt minimum 97%) 120.0 g

Type I water……3000.0 ml

Caution: Deoxycholic Acid is a lung irritant. Solution must be made under the hood.

0.2% trypsin/0.05% EDTA/0.05%Sodium Azide (expiration 1 day)

trypsin[source: Sigma T-4549 or equivalent] (10X solution).....24.0 ml

EDTA[source: Fisher BP120 or equivalent]……...1.5 g

Sodium Azide[source: Sigma S8032-100G or equivalent]…….. 1.5 g

Type I water…… 2973.0 ml

The trypsin is commonly packaged in a concentration of 25g/L. Therefore, for a 0.02% solution of trypsin in 500 ml, 0.1 grams of trypsin is required. This is equivalent to 0.004 L, or 4 ml of the concentrated trypsin per 500 ml DI water. 0.05% EDTA is produced by adding 0.25 g of EDTA (4 ml of trypsin) to 495.75 ml of DI water. Place on shaker to ensure adequate mixing.

2X PBS (expiration 6 months)

Type 1 water…… 3000.0 ml

1X PBS[source: Sigma #P3813 or equivalent]……6 pouches
According to manufacture's procedure one pouch is used to make 1 L of 1X PBS, but for the purpose of the heart decellularization the hypertonicity of the solution was increased.

Procedure:

The following procedure is for an approximately 400g porcine heart or a rat heart. Flows, times, and solution quantity can be adjusted as needed for different size hearts.

Contact appropriate source to obtain fresh heart.
Transport heart on ice back to the laboratory or MIRM necropsy room. Trim the heart of excess fat and tissue.

Before beginning the decellularization process the heart must be frozen. Wrap heart in freezer paper and store in the -80ºC freezer. The heart will be completely frozen after approximately 24 hours.

Obtain production sheet and begin recording all processes (see attached sheet for example).

Take frozen heart and thaw in Type 1 water. Weigh heart and record weight. Once thawed, suture or zip tie the tube fitting/cannulae to aorta. **Note:** Make sure the tube is above the aortic valve.

1. Flush porcine heart with Type 1 water for five minutes (approx 2000 ml/min), (rat heart approx 5 ml/min). Flushing allows influx of clean solution and removal of effluent. Heart can be connected directly to a Barnstead or similar water filtration system to flush heart.

2. Use peristaltic pump to pump the following solutions through the heart (**Note:** pump speed ranges from about 1000 ml/min-1700 ml/min usually increasing through the decell process, flow rate for the rat heart stays at 5 ml/min):

- 2X PBS for 15 min
- 0.02% trypsin/0.05% EDTA/ 0.05% NaN_3 at 37°C for 2 hours (**Note:** 1 hr for the rat heart)
- Ensure heart is not sitting on bottom of beaker
- 3% Triton X-100/0.05% EDTA/ 0.05% NaN_3 for 2 hours (**Note:** 1 hr for the rat heart)
- 4% Deoxycholic acid for 2 hours (**Note:** 1 hr for the rat heart)
- 0.1% Peracetic acid for 1 hour (**Note:** 30 min for the rat heart)

After each chemical solution Type 1 water is flushed through the heart for approximately 5 mins and then 2X PBS is pumped through for 15 mins. This removes cellular debris, chemical residues, and aids in cell lysis.

After the final PAA solution is pumped through the heart, 1X PBS and Type1 water washes follow (see SOP# D2000 vr2 PAA):

- 15 min 1X PBS pump
- 5 min Type 1 water flush
- 5 min Type 1 water flush
- 15 min 1X PBS pump
- 5 min Type 1 water flush
- Record weight once most water removed.

Optional:
Decellularization of the organ can be confirmed through DAPI (SOP# P1004) and H/E staining (SOP# H3006). The best histological analysis is obtained when approximately 1 cm piece from each chamber free wall (outside wall of the heart) and the ventricular septum are submitted for this analysis. The absence of cellular remnants in each of the four chambers and the ventricular septum indicated that the organ has been decellularized.

End of Procedure

APPENDIX B

LANGENDORFF PREPARATION FOR MEASUREMENT OF LV PRESSURE

OBJECTIVE

To validate Langendorff preparation setup with adult rat hearts so that system can be used to measure LV pressure volume relationships in the reseeded rat heart described in chapter 3.

METHODS

FILTER PERFUSATE BEFORE STARTING

Prep of perfusate

1. **MacGowan Perfusate Solution - 1 Liters**

Solute	Concentration	Amount (grams)
		1 L
NaCl	112 mM	6.5400
KCl	4.7 mM	0.3500
CaCl2	2.5 mM	0.2777
MgSO4	1.2 mM	0.1447
Na-EDTA	0.5 mM	0.1860
NaHCO3	25.0 mM	2.1000
Glucose	5.5 mM	0.9900
Pyruvate	5.0 mM	0.5500
Caprylic Sodium Octanoate Sigma C5038-10G	50 uM	0.0087
Insulin	90 U/L 27 u/mg	0.0011
Metoprolol	5.0 uM	0.0032
Sigma M5391	*MW 684*	

- *Filter after mixing*

Prep of system

- *Check pH (7.4) after oxygenation.*
- *Check oxygenation and adjust O2 flow as needed to reach > 650 mmHg*

- *Temperature of perfusate should be 38 °C; adjust water bath temp approx 43 C and 600 ml/min recirculation rate*
- *Pressure equal to 60-70 mmHg adjust height of water bath.*
- *Ensure balloon system has no air and pressure gauge zeroed and calibrated*
- *Coronary flow (CF) should be 6-8 ml/min based on Heart Weight (HW) in grams.*

  *CF=7.43*HW^0.56 (Doring and Dehnert 1988)*

Pressure and volume calibration

The 5F Millar used for pressure measurements has to be warmed up and wetted for several minutes before connecting it into the balloon system. If this is not the case, there will be a drift in pressure readings.

Calibrate the Millar for the 0 and 100 readings then turn the box to transducer. Before the transducer is clamped into the volume control, take the wetted Millar and hold it right underneath the surface of the liquid in the bowl. This is the zero on the transducer.

Isolation of heart

Induce a surgical plane of anesthesia with 5% isoflurane for 2-5 min (until the animal does not respond to stimuli). Place animal on table and place a hard object behind the base of the skull. Then pull the tail until popping sound heard followed by lifting the rear 90° while keeping hard object in place. Next place animal on its back. Excise rib cage and fill thoracic cavity and cannulae with ice cold perfusate. Isolate ascending aorta and dissect halfway through at carotid bifurcation. Insert cannulae into aorta making sure not to pass the aortic valve. Suture the

cannulae in place with 5-0 silk or equivalent. Excise heart and immediately hang on Langendorff apparatus and start flow of perfusate. Excise both atriums and insert stimulation electrodes near RV and apex of the heart.

Experimental protocol

Crush AV node by squeezing top of septal wall (Inset one end of tweezer into each atrium.)

The insertion of the balloon usually takes two people. One person is holding the balloon away from the heart and the other is inserting the straightened needle connected to the bottom of the balloon into the ventricle and through the apex. In order for the balloon to enter the ventricle with minimal damage, the balloon has to be deflated and great care must be taken to insert the balloon in as straight as possible. Once the bottom of the balloon is visible exiting the apex, the balloon should be seated by quickly infusing and withdrawing approximately 25 microliters.

- *Place an electrode in the right atrium and the apex of the heart to prevent puncturing a coronary.*

- *Increase voltage until get sinus rhythm then return to the following parameters: 1BPS, 10 ms, 15 V.*
- *Fill volume of balloon 0.025 ml*

- *Increase volume of balloon then take 10 measurements. Repeat until diastolic pressure is 30- 40 mmHg. Deflate the balloon all the way and repeat two more times.*

Calculations

Average systolic pressure for 3 beats for each balloon volume step. Plot pressure over time.

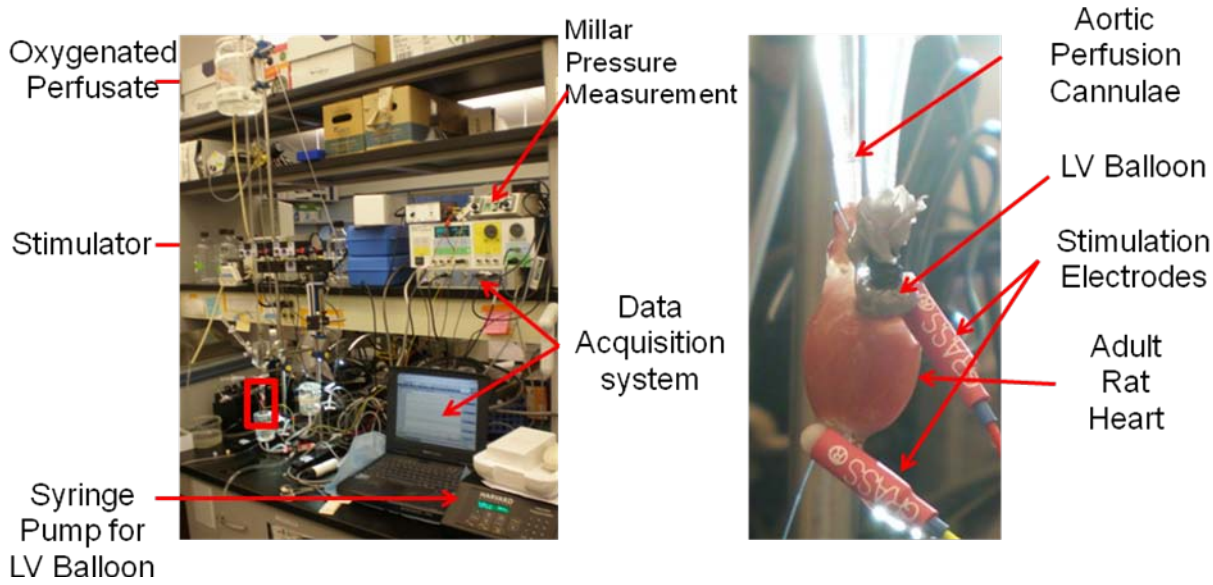

Figure 34. Setup of Langendorff Preparation System. Adult rat heart from inset.

<u>Preparation of balloon</u>

For the balloon prep, you will need the following materials:

• plastic garbage bag (Sears, or any stiff thin polyethylene material)

• 0.25 glass hypodermic syringe plunger

• white sewing thread

• black 00 silk

• 23 gauge serrated metal rod or other cannulae

• silicone tubing, large enough to fit over the 23 gauge rods

• 4-0 black silk suture, needle straightened

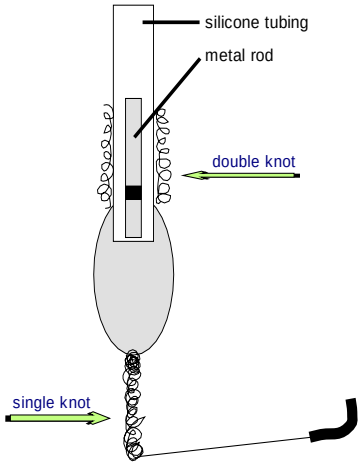

Figure 35. Preparation of balloon

Take the syringe plunger and sequentially stretch out the plastic bag into a tube approximately 1-1.5 cm in length. Cut the plastic tube out of the bag. Cut a 3 cm length of the small silicone tubing and fit the serrated 23-gauge rod into one end, making sure the serrated end is closer to the opening. The plastic balloon should be fitted on the rod/tubing end and tied with the white sewing thread. To ensure a tight grip of the thread without ripping the plastic, the thread should be tied with double looped knots and by alternating sides. The bottom of the balloon should be tied with single knots and alternating sides. The knots have to be sequential in order to make it as thin as possible; otherwise the width of the knots will damage the apex of the heart as it passes through.

Connect the balloon/tubing to the custom made pressure and volume control. Tie the tubing with black 00 silk. Do the same with the tubing connecting the volume control syringe and metal holder. The easiest way to get rid of air in the system is to fill a bowl with an alconox/degassed water solution and leave the balloon in overnight.

RESULTS

After 10 attempts at isolating heart and recording pressure measurements the procedure was refined to that listed. With this procedure pressure volume measurements were obtained on an adult rat heart. This concluded development of the Langendorff preparation system.

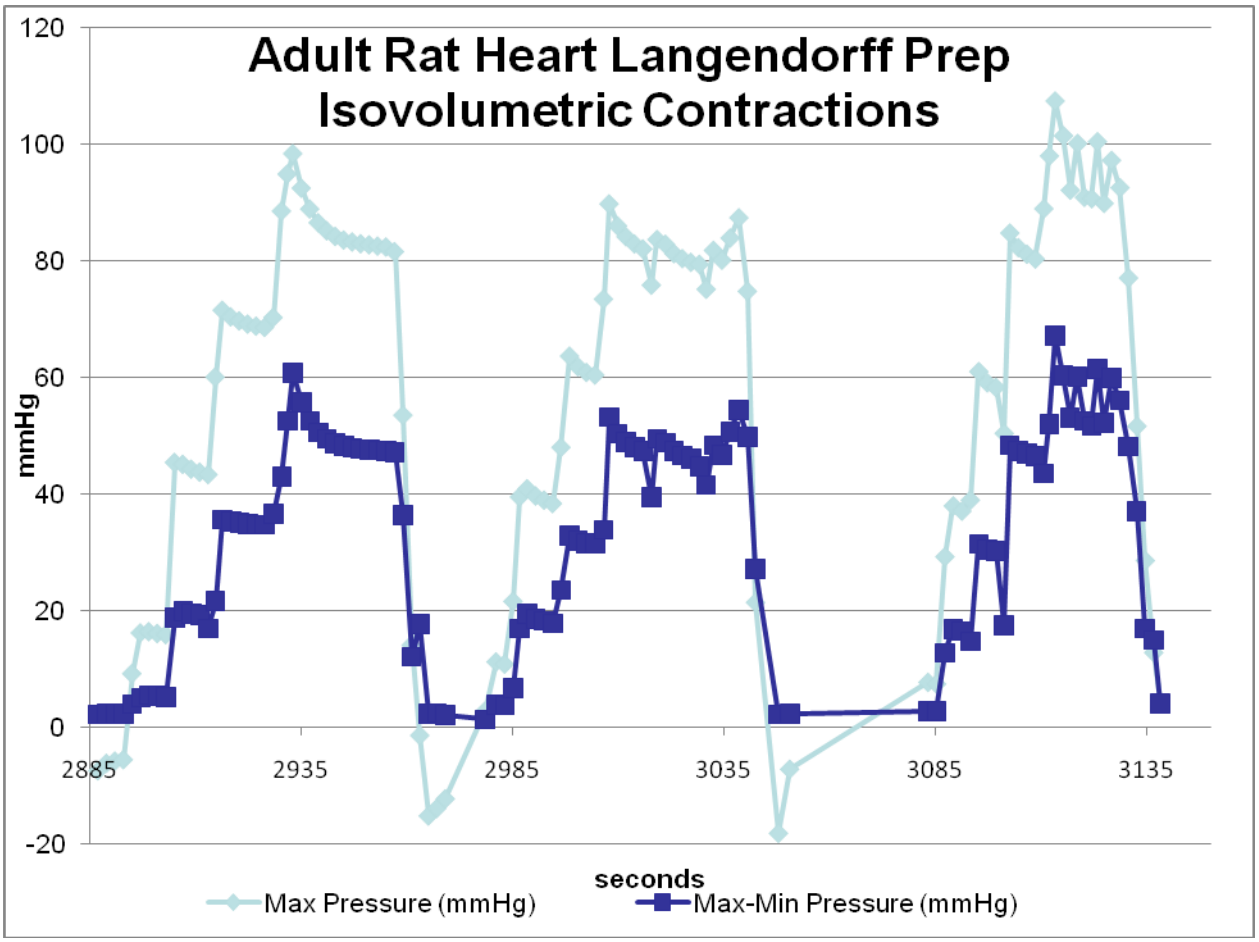

Figure 36. LV pressure measurements of adult rat heart with changing LV balloon volume.

If the reseeded decellularized rat heart described in chapter 2 generated measurable pressure, this system would have been used to measure the pressure volume relations ships and compare the reseeded heart to the adult rat heart. In the middle of one reseeding experiment the rat heart generated visible contraction during a media change. Unfortunately, the reseeded 3D C-ECM scaffold had a fungal contamination before the end of the culture period. This result was not replicated over the next two attempts due to issues with cell isolation and a shorter culture period.

APPENDIX C

THE USE OF EXTRACELLULAR MATRIX AS AN ATRIAL SEPTAL DEFECT REPAIR DEVICE

OBJECTIVE

The purpose of this study was to evaluate the ability of an extracellular matrix scaffold to function as a repair device for experimentally produced atrial septal defects (ASD) in a dog model. The device was manufactured from a four layers of vacuum pressed urinary bladder matrix (UBM).

BACKGROUND AND OVERVIEW OF STUDY DESIGN

Septal defects are typically a congenital heart problem in which there is a hole in the wall that separates the chambers of the heart. The word “septal” refers to the wall between the chambers, and “congenital” describes a condition that has been present since before birth. Congenital heart disease occurs in just under 1 of every 100 births.

A prototype for the percutaneous delivery of the UBM ASD patch was created. The prototype was optimized based on in vivo work and benchtop testing.

The animal study investigated the repair of atrial septal defects with a biologic scaffold material. Site specific cellular regeneration after an operation is essentially unknown. An extracellular matrix (ECM) material used as a scaffold represents a major advance in cellular engineering. An important unexplored application is the use of ECM for the reconstruction of healthy tissue for the treatment of myocardial defects: atrial and ventricular wall defects, atrial and ventricular septal defects, aneurysms, and valve leaflet repair. Preliminary evidence has demonstrated that site specific tissue reconstruction occurs in the myocardium similar to that which occurs at other tissue sites (83, 123-124, 126).

This study evaluated the ability for the UBM device to prevent blood flow shunting as a result of the created ASD as well as the morphology of the atrial free wall at 3 months. In addition, histology of the patched areas was evaluated at the 3 month timepoint.

SPECIFIC AIM NO. 1: TO CREATE A PROTOTYPE ASD REPAIR DEVICE FROM AN ECM BIOLOGIC SCAFFOLD AND DEMONSTRATE FUNCTIONALITY IN VITRO.

Rationale: Biologic scaffolds derived from ECM (such as the UBM-ECM derived from porcine urinary bladder proposed for use in this study) have significant adaptability with regard to mechanical and material properties and physical appearance. To create a device that will equal or exceed the success of the existing metal cage devices while eliminating the rare but potentially

catastrophic adverse events, it will be important to maximize the amount of ECM material in the prototype device while minimizing any foreign material that would have the potential to abrade the adjacent atrial and aortic structures. In addition, a prototype device created from an ECM biologic scaffold must have the ability to be folded around a delivery wire, passed through a <14 Fr catheter, deployed at the site of intended use, and retrieved if necessary via catheter-based techniques. These are non-trivial requirements and form the basis of this first Specific Aim.

Voice of the customer (VOC) was obtained from an Interventional Cardiologist and a Cardiac Surgeon on ASD defect sizes and device requirements. From this data an initial prototype was made, revision 1 (See Figure). However, based on benchtop testing, it was determined the waist region of the ASD device had to be larger to match the defect diameter.

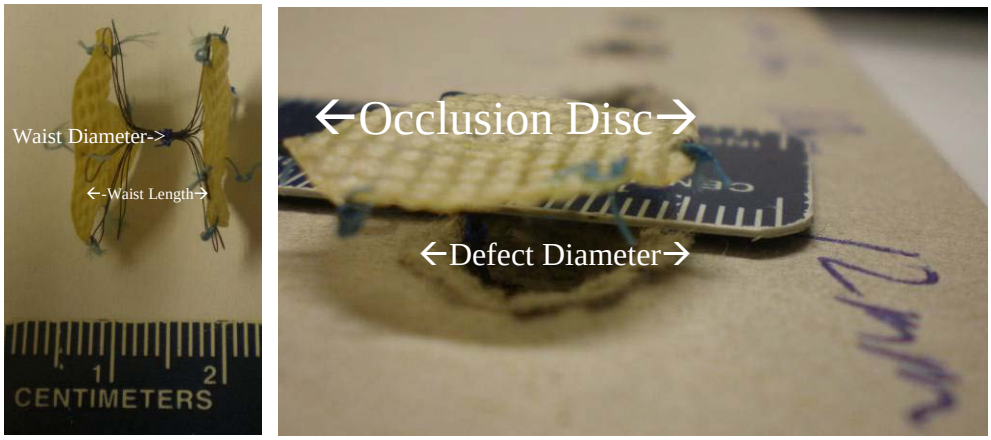

Figure 37. Original ASD Prototype

A multistep forming process was developed to incorporate a self sizing waist length and diameter, revision 2 (See Figure).

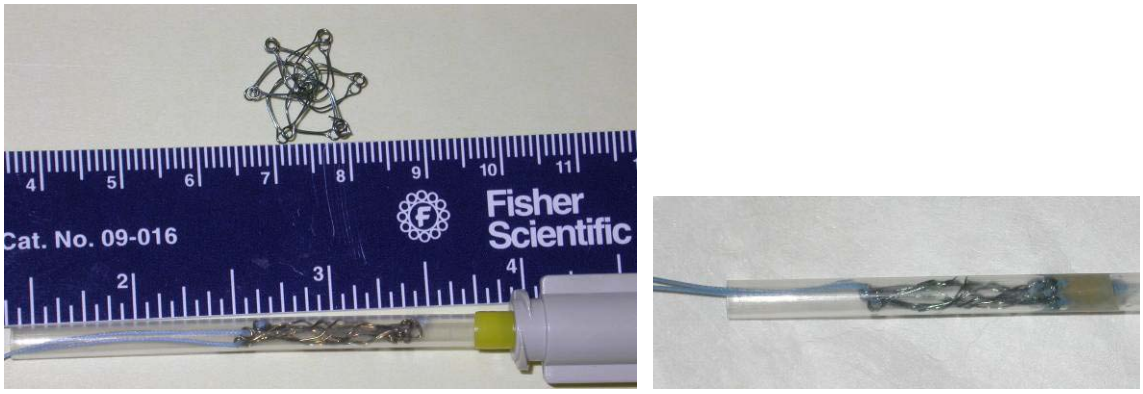

Figure 38. Self-sizing device in expanded form and in 11 Fr. Tube (3.7 mm ID) with and without 4 layer UBM attached.

The self sizing ASD device was then tested in an explanted calf heart. Approximately a 10 mm defect in the atrial septum was made. The self sizing frame was then placed within the defect (See Figure).

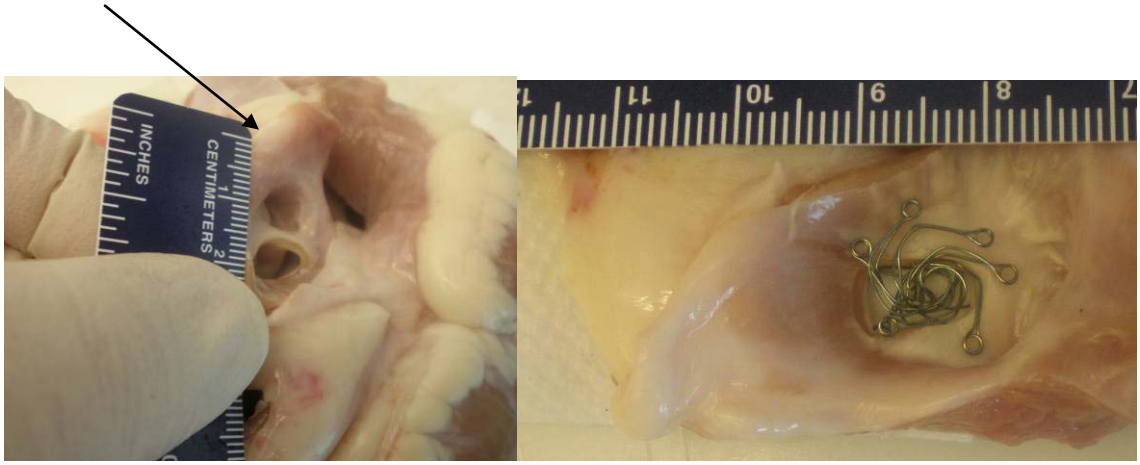

Figure 39. 10 mm ASD in a calf heart, picture taken from the right atrium side. Self sizing NiTi device in ASD

From this data, it was determined that the NiTi device needed a larger occlusion disc than 15 mm due to the flexibility of the tissue. Revision 3 of the device was developed which included a 25 mm occlusion disc (See Figure). This completed development of the frame.

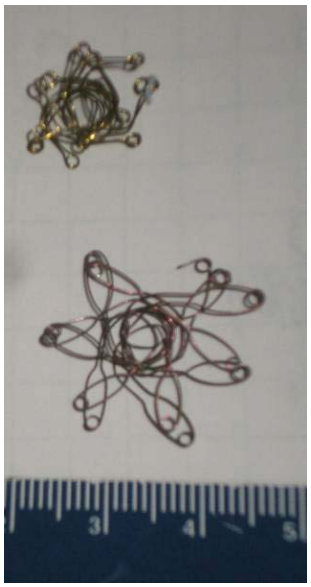

Figure 40. Revision 3 of NiTi ASD frame on top and Revision 4 of NiTi ASD frame on bottom

SPECIFIC AIM NO. 2: TO CONDUCT MECHANICAL PROPERTIES TESTING UPON THE MULTILAMINATE ECM PROTOTYPE TO DETERMINE SUITABILITY FOR USE AS AN ASD REPAIR DEVICE.

Rationale: The UBM-ECM device functions *in vivo* as an inductive template for autologous tissue repair. Stated differently, the device degrades *in vivo* and is replaced by site-appropriate host tissue. The handling characteristics and the mechanical properties of the device at the time of implantation should closely match the native tissue so that immediate functionality is realized. The work conducted for this Specific Aim will determine the size, shape, thickness, and strength (number of layers) needed to prepare the most suitable prototype ASD repair device.

As described in Specific Aim 1, the NiTi frame went through multiple iterations to obtain a suitable design. A single layer or a four layer of UBM was considered for the UBM Occluder disc. The four layer UBM sheet was manufactured by layering wet sheets of UBM alternating between laying the luminal side up or down. This created a construct that had the luminal side of UBM facing outwards on both sides. Being the luminal side of UBM is the basement membrane, the natural attachment for endothelial cells; it was hypothesized that this orientation could reduce thrombosis and encourages endothelialization. The wet construct was then vacuum pressed at approximately -30 mmHg for 8 hours until dry. The ball burst test (BBS) was used to compare the devices single layer or a four layer of UBM sheets (101-102). The BBS test is described by the Standard Test Method for Bursting Strength of Knitted Goods, Constant-Rate-of-Traverse (CRT) Ball-burst Test (ASTM D 3797–89). Briefly, an Instron was equipped with a ball-burst

compression cage in which a 25.4 mm polished steel hemisphere was pushed against the material until failure. The burst strength was defined as the force required to rupture the material. Table 1 shows the (BBS) values of the single and four layer UBM sheets (101-102).

Table 4. BBS values of the single and four layer UBM sheets

	BBS (N)
Single layer UBM	11.32 ± 1.88 (n=6)
Four Layer UBM	35±2 (n=3)

While the single layer UBM has been shown to remodel without failure in the canine right ventricle (83, 123-125, 197), a four layer sheet was chosen for both occluder disks. The four layer sheet was chosen based on the fact that the 4 layer UBM device had a significantly higher BBS the single layer UBM and the fact that the basement membrane would cover all surfaces.

SPECIFIC AIM NO. 3: TO CONDUCT AN ANIMAL STUDY TO REPAIR AN ASD DEFECT WITH A FOUR LAYER UBM BIOLOGIC SCAFFOLD.

Animal Husbandry

Each animal was fed appropriate amounts of Nutro dog food. The dogs were supplied with tap water ad libitum. The animals were checked daily for eating, drinking, urine production, feces, and general appearance. The results were recorded on the appropriate data collection sheet. Approval for this study was granted by the Institutional Animal Care and Use Committee, IACUC. IACUC approval # 0806636

Device Implants

Test article: 4 layer UBM patch with luminal layer facing outward on both surfaces.

All grafts produced in Dr. Badylak's laboratory

Procedure

Surgical Procedure:

Dogs were anesthetized (dog, sodium thiopental, 12-25 mg/kg IV for induction and intubation. Animals were then be maintained at a surgical plane of anesthesia with Isoflurane (1-3% in oxygen). Blood pressure (via femoral artery) and ECG was monitored throughout the surgical procedure. The animals were infused with 2 ml/kg/h of lactated Ringer's solution or equivalent solution throughout the procedure.

Prior to undergoing thoracotomy the wound edges were infiltrated with local anesthetic (marcaine or bupivicaine, ~10-15 ml) effectively blocking the intercostal nn., (This has been shown to decrease pain in the early post-op period thereby improving comfort and decreasing the requirements for narcotic analgesics in patients undergoing thoracotomy). A right thoracotomy was made at the third intercostal space, followed by a pericardiotomy and placement of suspension sutures to cradle the heart. Visualization of the heart, the pulmonary valve outflow tract, aorta, and right atrium was accomplished. Heparin was administered IV (25-75 IU/kg). The animal was then be placed on cardiopulmonary bypass (CPB) by cannulation of the vena cava

and the outflow cannulae for the cardiopulmonary bypass was inserted into either the carotid artery using a cutdown or into the aorta based on the individual anatomy of the animal. Ventricular fibrillation was induced by standard cardioplegia. For the creation of an ASD the right atrium was opened and a portion of the intra-atrial septum in the fossa ovalis was excised (approximately 2cm x2cm). The defect was repaired using a ECM scaffold material. The ECM scaffold device was sewn into its place with 7-0 non-absorbable suture material (e.g. Prolene). The hole in the right atrium was closed with ECM scaffold in the same manner as the ASD. At the conclusion of surgery, defibrillation was achieved and the dogs were weaned from CPB. A chest tube was placed prior to closing the chest and maintained up to 72 hours to ensure negative pressure compliance in the chest and to remove any excess drainage present after a procedure of this type. The chest wall was closed using routine thoracic closure technique (1-0 Prolene for closure of the ribs, 2-0 PDS for SQ and 2-0 Prolene or staples for skin closure). Skin staples/suture will be removed 10 days post-op.

Post-Operative Care:

Following the surgical procedure and cessation of inhalation anesthesia, the animal was continually monitored for 24 hours, recording the following parameters every hour: pulse rate, strength of pulse, capillary refill time, amount of fluid removed from chest via the chest drain, respiratory rate & ability to maintain an open airway, urinary output, and defecation. Body temperature was determined and recorded every 2 hours. The animal was kept warm and dry to prevent hypothermia and was rotated once per half-hour until it can maintain a sternal position.

Extubation of an animal was based on the following criteria: the presence of a swallowing reflex and the protective cough reflexes that are functional. The pulse, respiration,

body temperature, jaw tone, capillary refill time, and mucous membrane color was evaluated prior to removing the endotracheal tube. An animal's overall health status was stable prior to extubation, and after extubation the animal must continue to maintain an open airway, stable heart rate, respiration rate, body temperature, jaw tone, capillary refill time (3-4sec), and good (pink) mucous membrane color. Following extubation, the animal responded to touch and sound, and achieved sternal recumbency (i.e., the animal was alert and able to sit up and balance itself on its sternum).

Dogs were held in a recovery cage for up to 72 hours. The dog was moved to a run when it demonstrated normal respiration, did not demonstrate pain, and was bright, alert, and responsive. At this time the cephalic vein line was removed.

Buprenorphine hydrochloride (dogs, 0.01-0.02 mg/kg, SQ, q12h; pigs, 0.005-0.01 mg/kg, IM or IV, q12h), was administered at regular intervals for 4 days for pain, and then was continued to be administered for pain management if signs of pain are exhibited. Acute pain in animals is expressed by guarding, vocalization, mutilation, restlessness, recumbency for an unusual length of time, depression (reluctance to move or difficulty in rising), or abnormal appearance (head down, tucked abdomen, hunched, facial distortion).

Non invasive echocardiograms were performed at 1 week and at the time of sacrifice. In addition, the implants were harvested after euthanasia for mechanical properties testing and macroscopic and microscopic examination. The measured endpoints were evaluated at the following time point: 3 months.

Following the first 24 hours, the animal was evaluated and assessed for the need for additional continuous monitoring. If the animal is unstable (unable to maintain a stable pulse, respiration, clotting time, hematocrit), continual monitoring will follow for an additional 24

hours. Once the animal is considered stable, monitoring frequency will decrease to once every 2-4 hours, then once every 4-12 hours, and finally, once every 24 hours.

At three months following surgery, a final echocardiogram was performed prior to euthanasia while the animal was under anesthesia. Once the dog has been euthanized graft sites were analyzed grossly and tissues harvested for morphologic evaluation.

Euthanasia

Animal Sacrifice: At the 3 month time point animals was evaluated for flow from the left and right atrium as well as visual inspection. Heparin was administered IV (110-500 IU/kg). A sternotomy, followed by a pericardiotomy and placement of suspension sutures to cradle the heart. Visualization of the heart, the pulmonary valve outflow tract, aorta, and right atrium was accomplished. Trans-esophageal echocardiogram was used to visualize the defect. Isoflurane was increased to 5% for 5 minutes. The vena cava, pulmonary arteries, and aorta were clamped. The heart was then excised and perfusate flushed through. The scaffold placement site and the adjacent native tissue will be excised, divided, and placed in neutral buffered formalin for routine H&E and Masson's trichrome staining or 4% Paraformaldehyde for immunofluorescence.

Methods of Evaluation

The response variables for this study included:

- Surgical assessment to determine feasibility of new graft
- Echocardiogram to assess graft efficacy
- Histology to determine the degree (qualitative morphologic assessment) of remodeling of the patched areas

Results

Surgical assessment:

The first two attempts to create the defect in a dog were unsuccessful. During the first surgery the AV node was crushed while creating the ASD defect and during the second surgery a vein was irreparably punctured during the cannulation.

On the third attempt, a 10 mm patch was placed in the septal wall and a 30 mm patch on the atrial free wall. The rehydrated device was easy to manipulate and suture. Both patches were competent at initial surgery and at 3 months.

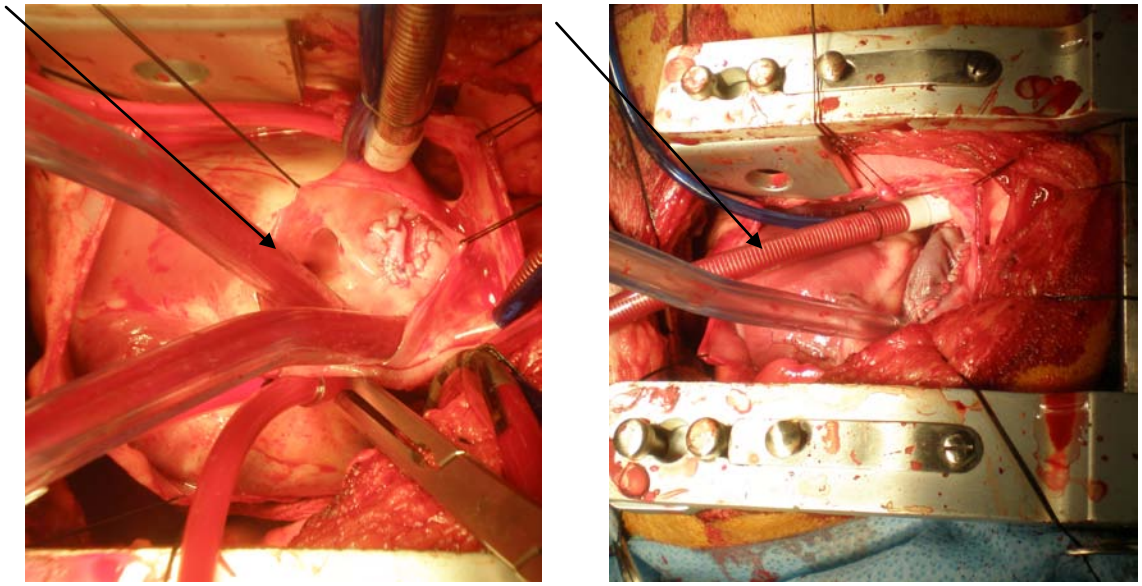

Figure 41. Grafts at implantation. ASD and right atrium free wall patch

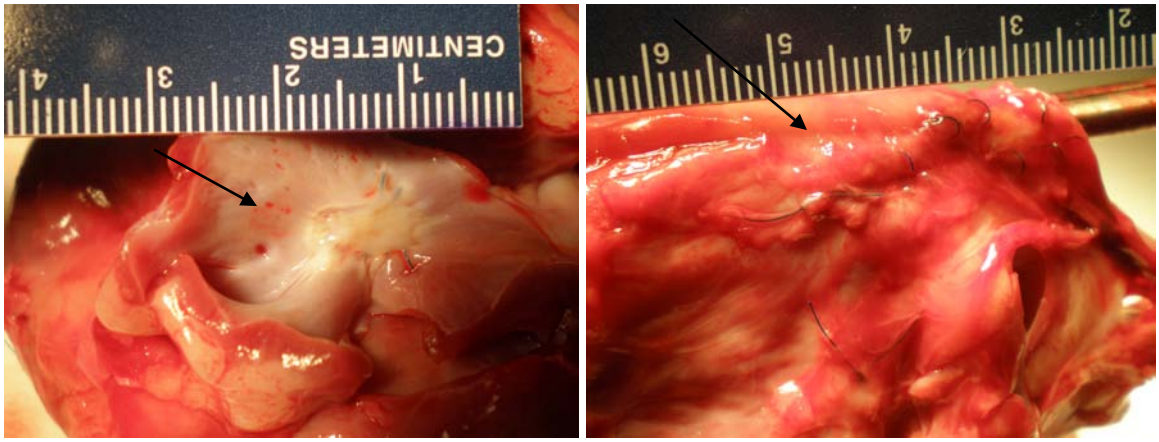

Figure 42. Grafts at 3 months. ASD and right atrium free wall patch

Echo Results: There was no shunting between the atriums as determined by microbubble test at 1 week or 3 months. This result indicates that the device was clinically successful.

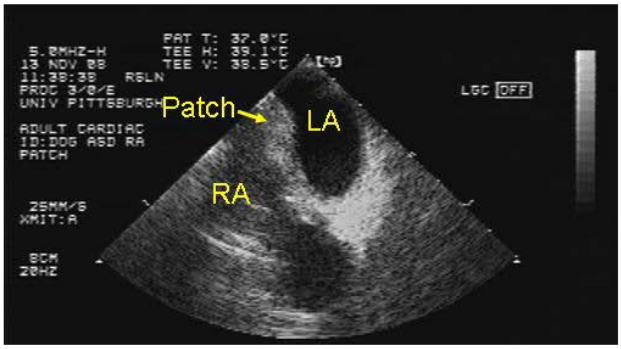

Color Doppler with No Shunt

Saline Bubbles with No Shunt

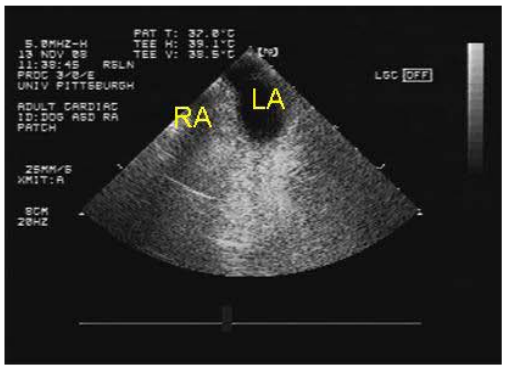

Figure 43. Trans Esophageal Echocardiogram of ASD area patched with the UBM device 1 week post surgery.

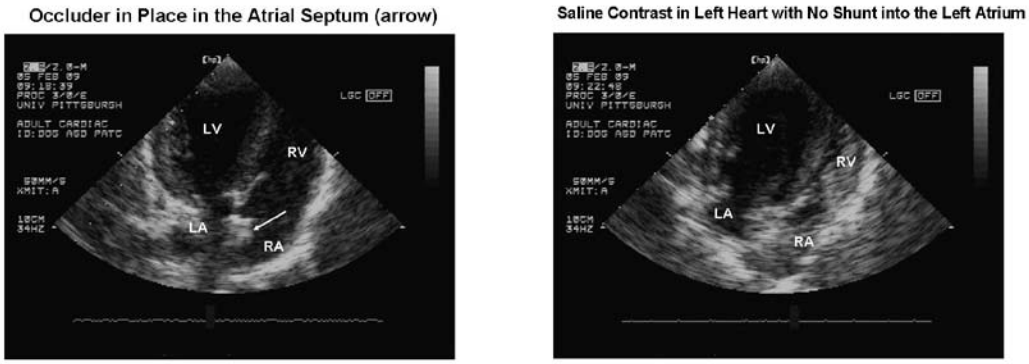

Figure 44. Epicardial Echocardiogram of ASD area patched with the UBM device 3 months post surgery.

Histological Evaluation:

The UBM ECM patches had smooth intact endothelialized non-thrombogenic surface. The patched areas were well vascularized and integrated into the adjacent myocardium. The device was replaced by a mixture of connective tissues: dense collagenous tissue and adipose tissue. The freewall also had small islands of muscle and fingers of muscle from the adjacent native tissue. There were also some chondrocytes in the freewall as noted by the arrow in figure.

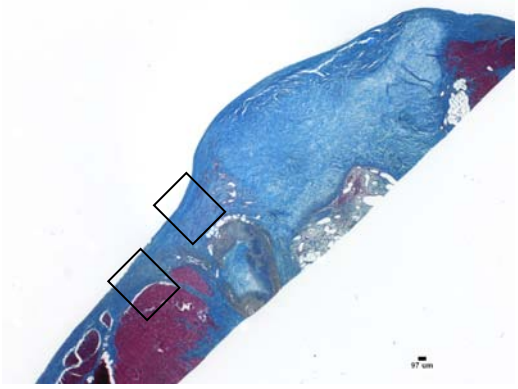

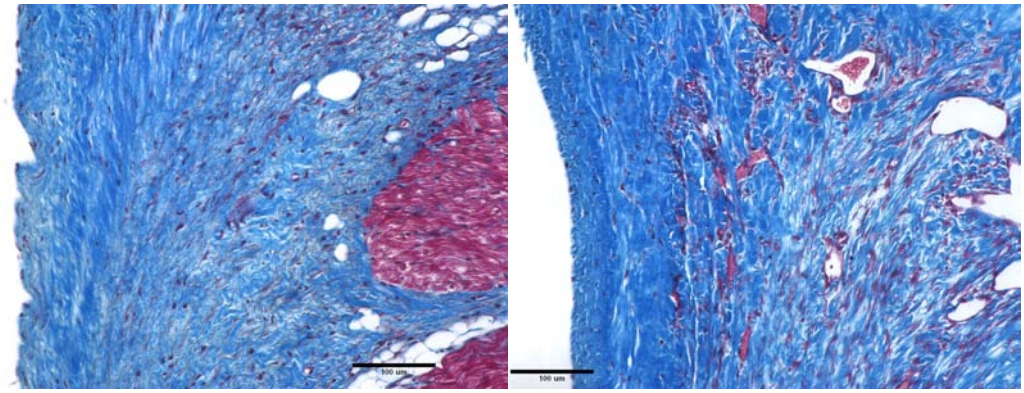

Figure 45. Trichrome cross section of ASD patched area at 2 and 20 X magnification

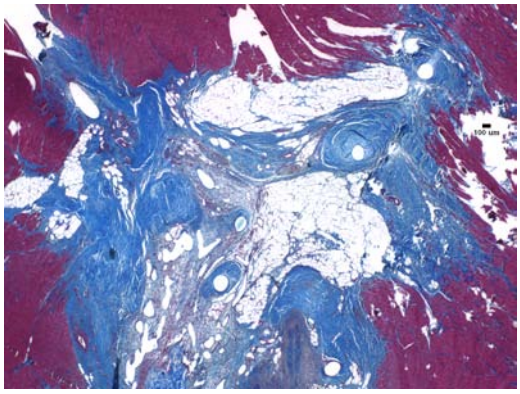

Figure 46. Face section of ASD patched area showing integration of the connective tissue matrix with the adjacent tissue 2X.

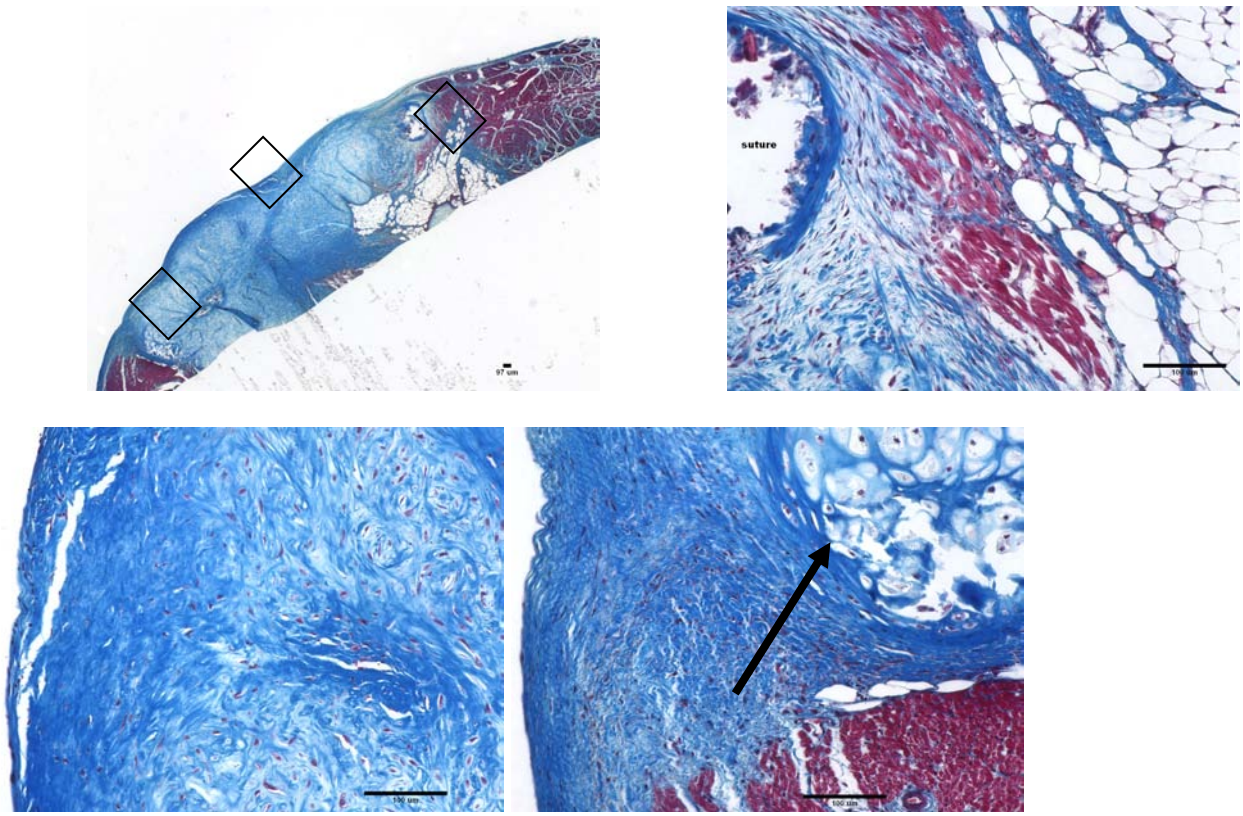

Figure 47. Trichrome cross section of atrial free wall patched area at 2 and 20 X magnification

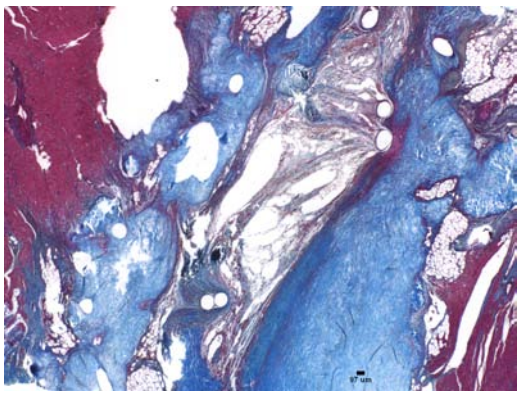

Figure 48. Face section of atrial free wall patched area showing integration of the connective tissue matrix with the adjacent tissue 2X.

Summary

- A novel ASD percutaneous device was developed.
- The surgical procedure was feasible with the 4 layer UBM test article to close a defect in both the atrial septum and right atrium free wall.
- The device was remodeled within the 3 month timeframe and prevented shunting.
- Device Patent Application submitted: Biologic Matrix for Cardiac Repair (International Pub No.: WO/2009/137755 published 11/12/09)

(12) INTERNATIONAL APPLICATION PUBLISHED UNDER THE PATENT COOPERATION TREATY (PCT)

(19) World Intellectual Property Organization
International Bureau

(43) International Publication Date
12 November 2009 (12.11.2009)

PCT

(10) International Publication Number
WO 2009/137755 A2

(51) International Patent Classification:
A61F 2/24 (2006.01)

(21) International Application Number:
PCT/US2009/043264

(22) International Filing Date:
8 May 2009 (08.05.2009)

(25) Filing Language: English

(26) Publication Language: English

(30) Priority Data:
61/051,734 9 May 2008 (09.05.2008) US

(71) Applicant *(for all designated States except US)*: **UNIVERSITY OF PITTSBURGH- COMMONWEALTH SYSTEM OF HIGHER EDUCATION** [US/US]; 200 Gardener Steel Conference Center, Thackery And O'hara Streets, Pittsburgh, PA 15217 (US).

(72) Inventors; and
(75) Inventors/Applicants *(for US only)*: **ANDERSON, William** [US/US]; 202 Woodcock Dr., Pittsburgh, PA 15215 (US). **BADYLAK, Steven** [US/US]; 4713 Bayard St., Pittsburgh, PA 15213 (US). **GILBERT, Thomas** [US/US]; 893 Harrison Ave., Pittsburgh, PA 15221 (US).

(72) Inventor; and
(75) Inventor/Applicant *(for US only)*: **WAINWRIGHT, John** [US/US]; 3808 Henley Dr., Churchill, PA 15235 (US).

(74) Agent: **HIRSHMAN LAW, LLC**; 1722 Murray Avenue, 3rd Floor, Pittsburgh, PA 15217 (US).

(81) Designated States *(unless otherwise indicated, for every kind of national protection available)*: AE, AG, AL, AM, AO, AT, AU, AZ, BA, BB, BG, BH, BR, BW, BY, BZ, CA, CH, CN, CO, CR, CU, CZ, DE, DK, DM, DO, DZ, EC, EE, EG, ES, FI, GB, GD, GE, GH, GM, GT, HN, HR, HU, ID, IL, IN, IS, JP, KE, KG, KM, KN, KP, KR, KZ, LA, LC, LK, LR, LS, LT, LU, LY, MA, MD, ME, MG, MK, MN, MW, MX, MY, MZ, NA, NG, NI, NO, NZ, OM, PG, PH, PL, PT, RO, RS, RU, SC, SD, SE, SG, SK, SL, SM, ST, SV, SY, TJ, TM, TN, TR, TT, TZ, UA, UG, US, UZ, VC, VN, ZA, ZM, ZW.

(84) Designated States *(unless otherwise indicated, for every kind of regional protection available)*: ARIPO (BW, GH,

[Continued on next page]

(54) Title: BIOLOGIC MATRIX FOR CARDIAC REPAIR

(57) Abstract: Provided herein is a device to occlude a hole in a wall of an organ or tissue. In another embodiment, a device is provided which comprises an extracellular matrix-derived material and an adhesive to occlude a hole in a wall of an organ or tissue. Provided are devices prepared from extracellular matrix-derived cell-growth scaffolding to repair defects in walls of organs or tissues. Also provided are methods for preparing the device as well as for using the device.

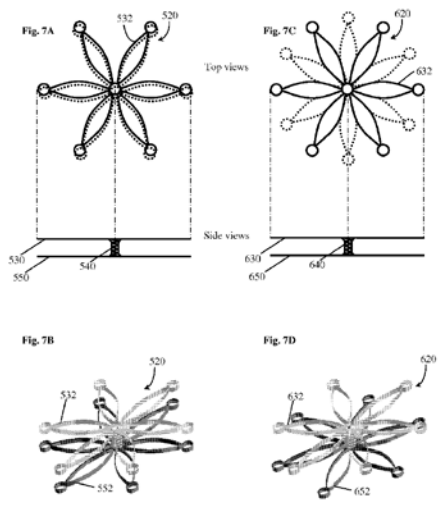

WO 2009/137755 A2

Figure 49. Device Patent Application submitted: Biologic Matrix for Cardiac Repair (International Pub No.: WO/2009/137755 published 11/12/09)

BIBLIOGRAPHY

1. Wolter JR, Meyer RF. Sessile macrophages forming clear endothelium-like membrane on inside of successful keratoprosthesis. Trans Am Ophthalmol Soc. 1984;82:187-202. PMCID: 1298663.

2. Katz A. Physiology of the Heart. 4th ed. Philadelphia: Lippincot Williams & Wilkins; 2006.

3. Writing Group Members, Rosamond W, Flegal K, Furie K, Go A, Greenlund K, et al. Heart Disease and Stroke Statistics--2008 Update: A Report From the American Heart Association Statistics Committee and Stroke Statistics Subcommittee. Circulation. 2008;117(4):e25-146.

4. Hoffman JI, Kaplan S. The incidence of congenital heart disease. J Am Coll Cardiol. 2002;39(12):1890-900.

5. Hoffman JI, Kaplan S, Liberthson RR. Prevalence of congenital heart disease. Am Heart J. 2004;147(3):425-39.

6. Gheorghiade M, Bonow RO. Chronic Heart Failure in the United States : A Manifestation of Coronary Artery Disease. 1998. p. 282-9.

7. Taylor DO, Edwards LB, Boucek MM, Trulock EP, Aurora P, Christie J, et al. Registry of the International Society for Heart and Lung Transplantation: Twenty-fourth Official Adult Heart Transplant Report--2007. The Journal of Heart and Lung Transplantation. 2007;26(8):769-81.

8. Charles E. Murry LJF, and Philippe Menasche. Cell-Based Cardiac Repair: Reflections at the 10-year Point. Circulation. 2005:3174-83.

9. Park SJ, Tector A, Piccioni W, Raines E, Gelijns A, Moskowitz A, et al. Left ventricular assist devices as destination therapy: A new look at survival. Journal of Thoracic and Cardiovascular Surgery. 2005;129(1):9-17.

10. Levy D, Kenchaiah S, Larson MG, Benjamin EJ, Kupka MJ, Ho KK, et al. Long-term trends in the incidence of and survival with heart failure. N Engl J Med. 2002;347(18):1397-402.

11. Pignone M, Earnshaw S, Tice JA, Pletcher MJ. Aspirin, Statins, or Both Drugs for the Primary Prevention of Coronary Heart Disease Events in Men: A Cost–Utility Analysis. Annals of Internal Medicine. 2006;144(5):326-36.

12. Taylor DO, Edwards LB, Aurora P, Christie JD, Dobbels F, Kirk R, et al. Registry of the International Society for Heart and Lung Transplantation: twenty-fifth official adult heart transplant report--2008. J Heart Lung Transplant. 2008;27(9):943-56.

13. Lloyd-Jones D, Adams R, Carnethon M, De Simone G, Ferguson TB, Flegal K, et al. Heart disease and stroke statistics--2009 update: a report from the American Heart Association Statistics Committee and Stroke Statistics Subcommittee. Circulation. 2009;119(3):e21-181.

14. Kirk R, Edwards LB, Aurora P, Taylor DO, Christie JD, Dobbels F, et al. Registry of the International Society for Heart and Lung Transplantation: Twelfth Official Pediatric Heart Transplantation Report-2009. J Heart Lung Transplant. 2009;28(10):993-1006.

15. Boening A, Scheewe J, Paulsen J, Regensburger D, Kramer HH, Hedderich J, et al. Tetralogy of Fallot: influence of surgical technique on survival and reoperation rate. Thorac Cardiovasc Surg. 2001;49(6):355-60.

16. Hickey EJ, Veldtman G, Bradley TJ, Gengsakul A, Manlhiot C, Williams WG, et al. Late risk of outcomes for adults with repaired tetralogy of Fallot from an inception cohort spanning four decades. Eur J Cardiothorac Surg. 2009;35(1):156-64; discussion 64.

17. Uva MS, Lacour-Gayet F, Komiya T, Serraf A, Bruniaux J, Touchot A, et al. Surgery for tetralogy of Fallot at less than six months of age. J Thorac Cardiovasc Surg. 1994;107(5):1291-300.

18. Laing BJ, Meyer SR, Halpin AM, Campbell PM, Ross DB, West LJ, et al. 313: HLA-Sensitization in Infants after Repair of Hypoplastic Left Heart Syndrome (HLHS) Is Prevented by Use of Glutaraldehyde-Treated Homografts. The Journal of Heart and Lung Transplantation. 2008;27(2, Supplement 1):S173-S.

19. Rajani B, Mee RB, Ratliff NB. Evidence for rejection of homograft cardiac valves in infants. J Thorac Cardiovasc Surg. 1998;115(1):111-7.

20. Menicanti L, Di Donato M. The Dor procedure: What has changed after fifteen years of clinical practice? The Journal of Thoracic and Cardiovascular Surgery. 2002;124:886-90.

21. Constantine L. Athanasuleas M, Alfred W. H. Stanley, Jr., MD, Gerald D. Buckberg, MD,, Vincent Dor M, Marissa DiDonato, MD, Eugene H. Blackstone, MD, and the RESTORE group. Surgical Anterior Ventricular Endocardial Restoration (SAVER) in the Dilated Remodeled Ventricle After Anterior Myocardial Infarction. Journal of the American College of Cardiology. 2001;37(5):1199-209.

22. Lietz K, Long JW, Kfoury AG, Slaughter MS, Silver MA, Milano CA, et al. Impact of Center Volume on Outcomes of Left Ventricular Assist Device Implantation as Destination

Therapy: Analysis of the Thoratec HeartMate Registry, 1998 to 2005. Circ Heart Fail. 2009;2(1):3-10.

23. Heart Assist Devices - Texas Heart Institute. [cited 2009 9/20]; Available from: http://www.texasheart.org/Research/Devices/.

24. Hare JM, Traverse JH, Henry TD, Dib N, Strumpf RK, Schulman SP, et al. A randomized, double-blind, placebo-controlled, dose-escalation study of intravenous adult human mesenchymal stem cells (prochymal) after acute myocardial infarction. J Am Coll Cardiol. 2009;54(24):2277-86.

25. Kehat I, Kenyagin-Karsenti D, Snir M, Segev H, Amit M, Gepstein A, et al. Human embryonic stem cells can differentiate into myocytes with structural and functional properties of cardiomyocytes. J Clin Invest. 2001;108(3):407-14. PMCID: 209357.

26. Yang L, Soonpaa MH, Adler ED, Roepke TK, Kattman SJ, Kennedy M, et al. Human cardiovascular progenitor cells develop from a KDR+ embryonic-stem-cell-derived population. Nature. 2008;453(7194):524-8.

27. Lesman A, Habib M, Caspi O, Gepstein A, Arbel G, Levenberg S, et al. Transplantation of a Tissue-Engineered Human Vascularized Cardiac Muscle. Tissue Eng Part A. 2009.

28. Ohtsuka M, Takano H, Zou Y, Toko H, Akazawa H, Qin Y, et al. Cytokine therapy prevents left ventricular remodeling and dysfunction after myocardial infarction through neovascularization. FASEB J. 2004;18(7):851-3.

29. Loot AE, Roks AJ, Henning RH, Tio RA, Suurmeijer AJ, Boomsma F, et al. Angiotensin-(1-7) attenuates the development of heart failure after myocardial infarction in rats. Circulation. 2002;105(13):1548-50.

30. McMurray J, Davie AP. Angiotensin-(1-7) attenuates the development of heart failure after myocardial infarction in rats. Circulation. 2002;106(20):e147; author reply e.

31. Ota T, Gilbert TW, Schwartzman D, McTiernan CF, Kitajima T, Ito Y, et al. A fusion protein of hepatocyte growth factor enhances reconstruction of myocardium in a cardiac patch derived from porcine urinary bladder matrix. The Journal of Thoracic and Cardiovascular Surgery. 2008;136(5):1309-17.

32. Wong DA, Kumar A, Jatana S, Ghiselli G, Wong K. Neurologic impairment from ectopic bone in the lumbar canal: a potential complication of off-label PLIF/TLIF use of bone morphogenetic protein-2 (BMP-2). Spine J. 2008;8(6):1011-8.

33. Akhyari P, Kamiya H, Haverich A, Karck M, Lichtenberg A. Myocardial tissue engineering: the extracellular matrix. Eur J Cardiothorac Surg. 2008;34(2):229-41.

34. Oku H, Shirotani H, Yokoyama T, Yokota Y, Kawai J, Makino S, et al. Right ventricular outflow tract prosthesis in total correction of tetralogy of Fallot. Circulation. 1980;62(3):604-9.

35. Payne WS, Kirklin JW. Late complications after plastic reconstruction of outflow tract in tetralogy of Fallot. Ann Surg. 1961;154:53-7. PMCID: 1465854.

36. Zong X, Bien H, Chung CY, Yin L, Fang D, Hsiao BS, et al. Electrospun fine-textured scaffolds for heart tissue constructs. Biomaterials. 2005;26(26):5330-8.

37. Guan J, Sacks MS, Beckman EJ, Wagner WR. Synthesis, characterization, and cytocompatibility of elastomeric, biodegradable poly(ester-urethane)ureas based on poly(caprolactone) and putrescine. J Biomed Mater Res. 2002;61(3):493-503.

38. Fujimoto KL, Guan J, Oshima H, Sakai T, Wagner WR. In vivo evaluation of a porous, elastic, biodegradable patch for reconstructive cardiac procedures. Ann Thorac Surg. 2007;83(2):648-54.

39. Nieponice A, McGrath K, Qureshi I, Beckman EJ, Luketich JD, Gilbert TW, et al. An extracellular matrix scaffold for esophageal stricture prevention after circumferential EMR. Gastrointest Endosc. 2008.

40. Huber JE, Spievack A, Simmons-Byrd A, Ringel RL, Badylak SF. Extracellular matrix as a scaffold for laryngeal reconstruction. Ann Otol Rhinol Laryngol. 2003;112(5):428-33.

41. Gilbert TW, Nieponice A, Spievack AR, Holcomb J, Gilbert S, Badylak SF. Repair of the thoracic wall with an extracellular matrix scaffold in a canine model. J Surg Res. 2008;147(1):61-7.

42. Badylak SF, Freytes DO, Gilbert TW. Extracellular matrix as a biological scaffold material: Structure and function. Acta Biomater. 2009;5(1):1-13.

43. Kelly DJ, Rosen AB, Schuldt AJ, Kochupura PV, Doronin SV, Potapova IA, et al. Increased myocyte content and mechanical function within a tissue-engineered myocardial patch following implantation. Tissue Eng Part A. 2009;15(8):2189-201. PMCID: 2743237.

44. Gilbert TW, Stewart-Akers AM, Simmons-Byrd A, Badylak SF. Degradation and remodeling of small intestinal submucosa in canine Achilles tendon repair. J Bone Joint Surg Am. 2007;89(3):621-30.

45. Record RD, Hillegonds D, Simmons C, Tullius R, Rickey FA, Elmore D, et al. *In vivo* degradation of ^{14}C-labeled small intestinal submucosa (SIS) when used for urinary bladder repair. Biomaterials. 2001;22(19):2653-9.

46. Brennan EP, Reing J, Chew D, Myers-Irvin JM, Young EJ, Badylak SF. Antibacterial activity within degradation products of biological scaffolds composed of extracellular matrix. Tissue Eng. 2006.

47. Li F, Li W, Johnson S, Ingram D, Yoder M, Badylak SF. Low-molecular-weight peptides derived from extracellular matrix as chemoattractants for primary endothelial cells. Endothelium. 2004;11(3-4):199-206.

48. Sarikaya A, Record R, Wu CC, Tullius B, Badylak SF, Ladisch M. Antimicrobial activity associated with extracellular matrices. Tissue Eng. 2002;8(1):63-71.

49. Badylak SF, Coffey AC, Lantz GC, Tacker WA, Geddes LA. Comparison of the resistance to infection of intestinal submucosa arterial autografts versus polytetrafluoroethylene arterial prostheses in a dog model. J Vasc Surg. 1994;19(3):465-72.

50. Badylak SF, Wu CC, Bible M, McPherson E. Host protection against deliberate bacterial contamination of an extracellular matrix bioscaffold versus Dacron mesh in a dog model of orthopedic soft tissue repair. J Biomed Mater Res B Appl Biomater. 2003;67(1):648-54.

51. Jernigan TW, Croce MA, Cagiannos C, Shell DH, Handorf CR, Fabian TC. Small intestinal submucosa for vascular reconstruction in the presence of gastrointestinal contamination. Ann Surg. 2004;239(5):733-8; discussion 8-40.

52. Shell DH, 4th, Croce MA, Cagiannos C, Jernigan TW, Edwards N, Fabian TC. Comparison of small-intestinal submucosa and expanded polytetrafluoroethylene as a vascular conduit in the presence of gram-positive contamination. Ann Surg. 2005;241(6):995-1001; discussion -4.

53. Badylak SF, Park K, Peppas N, McCabe G, Yoder M. Marrow-derived cells populate scaffolds composed of xenogeneic extracellular matrix. Exp Hematol. 2001;29(11):1310-8.

54. Zantop T, Gilbert TW, Yoder MC, Badylak SF. Extracellular matrix scaffolds are repopulated by bone marrow-derived cells in a mouse model of Achilles tendon reconstruction. J Orthop Res. 2006;24(6):1299-309.

55. Agrawal V, Johnson SA, Reing J, Zhang L, Tottey S, Wang G, et al. Regenerative Medicine Special Feature: Epimorphic regeneration approach to tissue replacement in adult mammals. Proc Natl Acad Sci U S A. 2010;107(8):3351-5.

56. Badylak SF, Gilbert TW. Immune response to biologic scaffold materials. Semin Immunol. 2007.

57. Badylak S. The extracellular matrix as a scaffold for tissue reconstruction. Semin Cell Dev Biol. 2002;5:377-83.

58. S.F.Badylak. Xenogeneic extracellular matrix as a scaffold for tissue reconstruction. . Transpl Immunol. 2004;12:367-77.

59. Badylak SF, Kochupura PV, Cohen IS. The use of Extracellular Matrix as an Inductive Scaffold for the Partial Replacement of Functional Myocardium. Cell Transplantation. 2006;Vol. 15, Supplement 1:1-100.

60. Rosen M, Roselli EE, Faber C, Ratliff NB, Ponsky JL, Smedira NG. Small Intestinal Submucosa Intracardiac Patch: An Experimental Study. Surgical Innovation. 2005;12(3):227-31.

61. Paul Kochupura EA, Damon Kelly, Sergey Doronin, Stephen Badylak, Irvin Krukenkamp, Ira Cohen, and Glenn Gaudette. Tissue-Engineered Myocardial Patch Derived From Extracellualr Matrix Provides Regional Mechanical Function. Circulation. 2005;Vol 112:144-9.

62. Keith A. Robinson JL, Stephen F. Badylak et. al. Extracellular Matrix Scaffold for Cardiac Repair. Circulation. 2005;Vol 112, Suppl I:I-135-I-43.

63. Crapo PM, Wang Y. Small Intestinal Submucosa Gel as a Potential Scaffolding Material for Cardiac Tissue Engineering. Acta Biomater. 2009.

64. Bornstein P, McPherson J, Sage H, editors. Synthesis and secretion of structural macromolecules by endothelial cells in culture. New York: Academic Press; 1982.

65. Sage H. Collagens of basement membranes. J Invest Dermatol. 1982;79 Suppl 1:51s-9s.

66. Bornstein P. Cell-matrix interactions: the view from the outside. Methods Cell Biol. 2002;69:7-11.

67. Bissell MJ, Aggeler J. Dynamic reciprocity: how do extracellular matrix and hormones direct gene expression? Prog Clin Biol Res. 1987;249:251-62.

68. Bissell MJ, Hall HG, Parry G. How does the extracellular matrix direct gene expression? J Theor Biol. 1982;99(1):31-68.

69. Nelson CM, Bissell MJ. Of extracellular matrix, scaffolds, and signaling: tissue architecture regulates development, homeostasis, and cancer. Annu Rev Cell Dev Biol. 2006;22:287-309.

70. Sellaro T, Ravindra A, Beer-Stolz D, Badylak S. Maintenance of Hepatic Sinusoidal Endothelial Cell Phenotype In Vitro Using Organ-Specific Extracellular Matrix Scaffolds. Tissue Engineering. 2007;13(9):2301-10.

71. Lin CS, Lai LP, Lin JL, Sun YL, Hsu CW, Chen CL, et al. Increased expression of extracellular matrix proteins in rapid atrial pacing-induced atrial fibrillation. Heart Rhythm. 2007;4(7):938-49.

72. Dobaczewski M, Gonzalez-Quesada C, Frangogiannis NG. The extracellular matrix as a modulator of the inflammatory and reparative response following myocardial infarction. Journal of Molecular and Cellular Cardiology.In Press, Corrected Proof.

73. Hodde JP, Badylak SF, Brightman AO, Voytik-Harbin SL. Glycosaminoglycan content of small intestinal submucosa: A bioscaffold for tissue replacement. Tissue Eng. 1996;2(3):209-17.

74. Hodde JP, Record RD, Liang HA, Badylak SF. Vascular endothelial growth factor in porcine-derived extracellular matrix. Endothelium. 2001;8(1):11-24.

75. Sacks MS, Gloeckner DC. Quantification of the fiber architecture and biaxial mechanical behavior of porcine intestinal submucosa. J Biomed Mater Res. 1999;46(1):1-10.

76. Voytik-Harbin SL, Brightman AO, Kraine MR, Waisner B, Badylak SF. Identification of extractable growth factors from small intestinal submucosa. J Cell Biochem. 1997;67(4):478-91.

77. Brown B, Lindberg K, Reing J, Stolz DB, Badylak SF. The basement membrane component of biologic scaffolds derived from extracellular matrix. Tissue Eng. 2006;12(3):519-26.

78. Wainwright JM, Czajka CA, Patel UB, Freytes DO, Tobita K, Gilbert TW, et al. Preparation of Cardiac Extracellular Matrix from an Intact Porcine Heart. Tissue Eng Part C Methods. 2009.

79. Eitan Y, Sarig U, Dahan N, Machluf M. Acellular cardiac extracellular matrix as a scaffold for tissue engineering: In-vitro cell support, remodeling and biocompatibility. Tissue Engineering Part C: Methods. 2009.

80. Ott HC, Matthiesen TS, Goh SK, Black LD, Kren SM, Netoff TI, et al. Perfusion-decellularized matrix: using nature's platform to engineer a bioartificial heart. Nat Med. 2008;14(2):213-21.

81. Singelyn JM, Dequach JA, Seif-Naraghi SB, Littlefield RB, Schup-Magoffin PJ, Christman KL. Naturally derived myocardial matrix as an injectable scaffold for cardiac tissue engineering. Biomaterials. 2009;30(29):5409-16.

82. Pettigrew AB. Design in Nature. Volume II. London: Longmans, Green and Co.; 1908.

83. Badylak SF, Kochupura PV, Cohen IS, Doronin SV, Saltman AE, Gilbert TW, et al. The use of extracellular matrix as an inductive scaffold for the partial replacement of functional myocardium. Cell Transplant. 2006;15 Suppl 1:S29-40.

84. Badylak SF, Vorp DA, Spievack AR, Simmons-Byrd A, Hanke J, Freytes DO, et al. Esophageal reconstruction with ECM and muscle tissue in a dog model. J Surg Res. 2005;128(1):87-97.

85. Gilbert TW, Gilbert S, Madden M, Reynolds SD, Badylak SF. Morphologic assessment of extracellular matrix scaffolds for patch tracheoplasty in a canine model. Ann Thorac Surg. 2008;86(3):967-74; discussion -74.

86. Nieponice A, Gilbert TW, Badylak SF. Reinforcement of esophageal anastomoses with an extracellular matrix scaffold in a canine model. Ann Thorac Surg. 2006;82(6):2050-8.

87. Ota T, Gilbert TW, Badylak SF, Schwartzman D, Zenati MA. Electromechanical characterization of a tissue-engineered myocardial patch derived from extracellular matrix. J Thorac Cardiovasc Surg. 2007;133(4):979-85.

88. Dejardin LM, Arnoczky SP, Ewers BJ, Haut RC, Clarke RB. Tissue-engineered rotator cuff tendon using porcine small intestine submucosa. Histologic and mechanical evaluation in dogs. Am J Sports Med. 2001;29(2):175-84.

89. MacLeod TM, Sarathchandra P, Williams G, Sanders R, Green CJ. Evaluation of a porcine origin acellular dermal matrix and small intestinal submucosa as dermal replacements in preventing secondary skin graft contraction. Burns. 2004;30(5):431-7.

90. Wainwright DJ. Use of an acellular allograft dermal matrix (AlloDerm) in the management of full-thickness burns. Burns. 1995;21(4):243-8.

91. Hudson TW, Liu SY, Schmidt CE. Engineering an improved acellular nerve graft via optimized chemical processing. Tissue Eng. 2004;10(9-10):1346-58.

92. Macchiarini P, Jungebluth P, Go T, Asnaghi MA, Rees LE, Cogan TA, et al. Clinical transplantation of a tissue-engineered airway. Lancet. 2008;372(9655):2023-30.

93. Montoya CV, McFetridge PS. Preparation of Ex Vivo-Based Biomaterials Using Convective Flow Decellularization. Tissue Eng Part C Methods. 2009.

94. Omae H, Zhao C, Sun YL, An KN, Amadio PC. Multilayer tendon slices seeded with bone marrow stromal cells: A novel composite for tendon engineering. J Orthop Res. 2008.

95. Ott HC, Matthiesen TS, Goh SK, Black LD, Kren SM, Netoff TI, et al. Perfusion-decellularized matrix: using nature's platform to engineer a bioartificial heart. Nat Med. 2008.

96. Ozeki M, Narita Y, Kagami H, Ohmiya N, Itoh A, Hirooka Y, et al. Evaluation of decellularized esophagus as a scaffold for cultured esophageal epithelial cells. J Biomed Mater Res A. 2006;79(4):771-8.

97. Sellaro TL, Ravindra AK, Stolz DB, Badylak SF. Maintenance of hepatic sinusoidal endothelial cell phenotype in vitro using organ-specific extracellular matrix scaffolds. Tissue Eng. 2007;13(9):2301-10.

98. Xu CC, Chan RW, Tirunagari N. A biodegradable, acellular xenogeneic scaffold for regeneration of the vocal fold lamina propria. Tissue Eng. 2006.

99. Freytes D, Badylak S, Webster T, Geddes L, Rundell A. Biaxial strength of multilaminated extracellular matrix scaffolds. Biomaterials. 2004;25:2353-61.

100. Gilbert TW, Freund JM, Badylak SF. Quantification of DNA in biologic scaffold materials. J Surg Res. 2009;152(1):135-9.

101. Freytes DO, Tullius RS, Badylak SF. Effect of storage upon material properties of lyophilized porcine extracellular matrix derived from the urinary bladder. J Biomed Mater Res B Appl Biomater. 2006;78(2):327-33.

102. Freytes DO, Stoner RM, Badylak SF. Uniaxial and biaxial properties of terminally sterilized porcine urinary bladder matrix scaffolds. J Biomed Mater Res B Appl Biomater. 2008;84(2):408-14.

103. Horan RL, Bramono DS, Stanley JR, Simmons Q, Chen J, Boepple HE, et al. Biological and biomechanical assessment of a long-term bioresorbable silk-derived surgical mesh in an abdominal body wall defect model. Hernia. 2009;13(2):189-99.

104. Coburn JC, Brody S, Billiar KL, Pandit A. Biaxial mechanical evaluation of cholecyst-derived extracellular matrix: A weakly anisotropic potential tissue engineered biomaterial. J Biomed Mater Res A. 2007;81(1):250-6.

105. Derwin KA, Baker AR, Spragg RK, Leigh DR, Iannotti JP. Commercial extracellular matrix scaffolds for rotator cuff tendon repair. Biomechanical, biochemical, and cellular properties. J Bone Joint Surg Am. 2006;88(12):2665-72.

106. Daly KA, Stewart-Akers AM, Hara H, Ezzelarab M, Long C, Cordero K, et al. Effect of the alphaGal epitope on the response to small intestinal submucosa extracellular matrix in a nonhuman primate model. Tissue Eng Part A. 2009;15(12):3877-88.

107. Gilbert T, Sellaro T, Badylak S. Decellularization of tissues and organs. Biomaterials. 2006;27(19):3675-83.

108. Ota T, Taketani S, Iwai S, Miyagawa S, Furuta M, Hara M, et al. Novel method of decellularization of porcine valves using polyethylene glycol and gamma irradiation. Ann Thorac Surg. 2007;83(4):1501-7.

109. Grauss RW, Hazekamp MG, Oppenhuizen F, van Munsteren CJ, Gittenberger-de Groot AC, DeRuiter MC. Histological evaluation of decellularised porcine aortic valves: matrix changes due to different decellularisation methods. Eur J Cardiothorac Surg. 2005;27(4):566-71.

110. Voet D, Voet J, Pratt C. Fundamentals of biochemistry. New

York: Wiley; 2002.

111. Jason Hodde MH. Virus safety of a porcine-derived medical device: Evaluation of a viral inactivation method. Biotechnology and Bioengineering. 2002;79(2):211-6.

112. Koivunen J, Heinonen-Tanski H. Peracetic acid (PAA) disinfection of primary, secondary and tertiary treated municipal wastewaters. Water Research. 2005;39(18):4445-53.

113. Pruss A, Kao M, Kiesewetter H, Von Versen R, Pauli G. Virus Safety of Avital Bone Tissue Transplants: Evaluation of Sterilization Steps of Spongiosa Cuboids Using a Peracetic Acid-Methanol Mixture. Biologicals. 1999;27(3):195-201.

114. DEPT. OF HEALTH E, AND , SERVICE WPH, ADMINISTRATION FAD, *ORA/ORO/DEIO/IB. Pyrogens, Still a Danger. 4/30/2009 [updated 4/30/2009; cited]; Available from:

http://www.fda.gov/iceci/inspections/inspectionguides/inspectiontechnicalguides/ucm072906.htm.

115. Sarafian TA, Tsay KK, Fluharty AL, Kihara H. A procedure for pyrogen decontamination of Sephacryl S-300. Biochemical Medicine. 1982;28(2):237-40.

116. Grauss RW, Hazekamp MG, van Vliet S, Gittenberger-de Groot AC, DeRuiter MC. Decellularization of rat aortic valve allografts reduces leaflet destruction and extracellular matrix remodeling. Journal of Thoracic and Cardiovascular Surgery. 2003;126(6):2003-10.

117. Simon P, Kasimir MT, Seebacher G, Weigel G, Ullrich R, Salzer-Muhar U, et al. Early failure of the tissue engineered porcine heart valve SYNERGRAFT in pediatric patients. Eur J Cardiothorac Surg. 2003;23(6):1002-6; discussion 6.

118. Hilbert SL, Yanagida R, Souza J, Wolfinbarger L, Jones AL, Krueger P, et al. Prototype anionic detergent technique used to decellularize allograft valve conduits evaluated in the right ventricular outflow tract in sheep. J Heart Valve Dis. 2004;13(5):831-40.

119. Harrison RD, Gratzer PF. Effect of extraction protocols and epidermal growth factor on the cellular repopulation of decellularized anterior cruciate ligament allografts. Journal of Biomedical Material Research. 2005;75A:841–54.

120. Woods T, Gratzer PF. Effectiveness of three extraction techniques in the development of a decellularized bone-anterior cruciate ligament-bone graft. Biomaterials. 2005;26(35):7339-49.

121. Rieder E, Kasimir MT, Silberhumer G, Seebacher G, Wolner E, Simon P, et al. Decellularization protocols of porcine heart valves differ importantly in efficiency of cell removal and susceptibility of the matrix to recellularization with human vascular cells. J Thorac Cardiovasc Surg. 2004;127(2):399-405.

122. Brendel K, Meezan E, Nagle R. The acellular Perfused Kidney: A model for basement membrane permiability. Biology and Chemistry of Basement Membrane: Academic Press; 1978.

123. Kochupura PV, Azeloglu EU, Kelly DJ, Doronin SV, Badylak SF, Krukenkamp IB, et al. Tissue-engineered myocardial patch derived from extracellular matrix provides regional mechanical function. Circulation. 2005;112(9 Suppl):I144-9.

124. Potapova IA, Doronin SV, Kelly DJ, Rosen AB, Schuldt AJ, Lu Z, et al. Replacing damaged myocardium. J Electrocardiol. 2007;40(6 Suppl):S199-201.

125. Potapova IA, Doronin SV, Kelly DJ, Rosen AB, Schuldt AJ, Lu Z, et al. Enhanced Recovery of Mechanical Function in the Canine Heart by Seeding an Extracellular Matrix Patch with Mesenchymal Stem Cells Committed to a Cardiac Lineage. Am J Physiol Heart Circ Physiol. 2008.

126. Robinson KA, Li J, Mathison M, Redkar A, Cui J, Chronos NA, et al. Extracellular matrix scaffold for cardiac repair. Circulation. 2005;112(9 Suppl):I135-43.

127. Freytes DO, Martin J, Velankar SS, Lee AS, Badylak SF. Preparation and rheological characterization of a gel form of the porcine urinary bladder matrix. Biomaterials. 2008;29(11):1630-7.

128. Badylak S, Kokini K, Tullius B, Whitson B. Strength over Time of a Resorbable Bioscaffold for Body Wall Repair in a Dog Model. Journal of Surgical Research. 2001;99(2):282-7.

129. Boruch AV, Nieponice A, Qureshi IR, Gilbert TW, Badylak SF. Constructive Remodeling of Biologic Scaffolds is Dependent on Early Exposure to Physiologic Bladder Filling in a Canine Partial Cystectomy Model. J Surg Res. 2009.

130. Freytes DO, Badylak SF, Webster TJ, Geddes LA, Rundell AE. Biaxial strength of multilaminated extracellular matrix scaffolds. Biomaterials. 2004;25(12):2353-61.

131. Tobita K, Liu LJ, Janczewski AM, Tinney JP, Nonemaker JM, Augustine S, et al. Engineered early embryonic cardiac tissue retains proliferative and contractile properties of developing embryonic myocardium. Am J Physiol Heart Circ Physiol. 2006;291(4):H1829-37.

132. Sreejit P, Kumar S, Verma RS. An improved protocol for primary culture of cardiomyocyte from neonatal mice. In Vitro Cell Dev Biol Anim. 2008;44(3-4):45-50.

133. Petty RD, Sutherland LA, Hunter EM, Cree IA. Comparison of MTT and ATP-based assays for the measurement of viable cell number. Journal of Bioluminescence and Chemiluminescence. 1995;10(1):29-34.

134. Crouch SP, Kozlowski R, Slater KJ, Fletcher J. The use of ATP bioluminescence as a measure of cell proliferation and cytotoxicity. J Immunol Methods. 1993;160(1):81-8.

135. Simpson P, Savion S. Differentiation of rat myocytes in single cell cultures with and without proliferating nonmyocardial cells. Cross-striations, ultrastructure, and chronotropic response to isoproterenol. Circulation Research. 1982;50:101-16.

136. Cannizzaro C, Tandon N, Figallo E, Park H, Gerecht S, Radisic M, et al. Practical aspects of cardiac tissue engineering with electrical stimulation. Methods Mol Med. 2007;140:291-307.

137. Radisic M, Marsano A, Maidhof R, Wang Y, Vunjak-Novakovic G. Cardiac tissue engineering using perfusion bioreactor systems. Nat Protocols. 2008;3(4):719-38.

138. Lula L. Hilenski, Xuehui M, Vinson N, Terracio L, Borg TK. The role of beta-integrin in spreading and myofibrillogenesis in neonatal rat cardiomyocytes in vitro. Cell Motility and the Cytoskeleton. 1992;21(2):87-100.

139. Brenner RM, Slayden OD, Rodgers WH, Critchley HO, Carroll R, Nie XJ, et al. Immunocytochemical assessment of mitotic activity with an antibody to phosphorylated histone H3 in the macaque and human endometrium. Hum Reprod. 2003;18(6):1185-93.

140. Hata H, Bar A, Dorfman S, Vukadinovic Z, Sawa Y, Haverich A, et al. Engineering a novel three-dimensional contractile myocardial patch with cell sheets and decellularised matrix. Eur J Cardiothorac Surg. 2010.

141. Shah U, Bien H, Entcheva E. Microtopographical effects of natural scaffolding on cardiomyocyte function and arrhythmogenesis. Acta Biomater. 2010.

142. Gilbert TW, Stewart-Akers AM, Badylak SF. A quantitative method for evaluating the degradation of biologic scaffold materials. Biomaterials. 2007;28(2):147-50.

143. ELLEN P. BRENNAN JR, DOUGLAS CHEW, JULIE M., MYERS-IRVIN EJY, and STEPHEN F. BADYLAK. Antibacterial Activity within Degradation Products of Biological Scaffolds Composed of Extracellular Matrix. Tissue Engineering. 2006;12(10):2949- 55.

144. VanWinkle WB, Snuggs MB, Buja LM. Cardiogel: a biosynthetic extracellular matrix for cardiomyocyte culture. In Vitro Cell Dev Biol Anim. 1996;32(8):478-85.

145. Davis RA, van Winkle WB, Buja LM, Poindexter BJ, Bick RJ. Effect of a simple versus a complex matrix on the polarity of cardiomyocytes in culture. J Burns Wounds. 2006;5:e3. PMCID: 1687145.

146. Vartanian KB, Kirkpatrick SJ, Hanson SR, Hinds MT. Endothelial cell cytoskeletal alignment independent of fluid shear stress on micropatterned surfaces. Biochem Biophys Res Commun. 2008;371(4):787-92.

147. Badylak S, Obermiller J, Geddes L, Matheny R. Extracellular matrix for myocardial repair. Heart Surg Forum. 2003;6(2):E20-6.

148. Adler CP, Costabel U. Cell number in human heart in atrophy, hypertrophy, and under the influence of cytostatics. Recent Adv Stud Cardiac Struct Metab. 1975;6:343-55.

149. Sandritter W, Adler CP. Numerical hyperplasia in human heart hypertrophy. Experientia. 1971;27(12):1435-7.

150. Li F, Wang X, Capasso JM, Gerdes AM. Rapid transition of cardiac myocytes from hyperplasia to hypertrophy during postnatal development. J Mol Cell Cardiol. 1996;28(8):1737-46.

151. Matsuda T, Takahashi K, Nariai T, Ito T, Takatani T, Fujio Y, et al. N-cadherin-mediated cell adhesion determines the plasticity for cell alignment in response to mechanical stretch in cultured cardiomyocytes. Biochem Biophys Res Commun. 2005;326(1):228-32.

152. Bu L, Jiang X, Martin-Puig S, Caron L, Zhu S, Shao Y, et al. Human ISL1 heart progenitors generate diverse multipotent cardiovascular cell lineages. Nature. 2009;460(7251):113-7.

153. Li W, Ding S. Small molecules that modulate embryonic stem cell fate and somatic cell reprogramming. Trends Pharmacol Sci. 2010;31(1):36-45.

154. Lin T, Ambasudhan R, Yuan X, Li W, Hilcove S, Abujarour R, et al. A chemical platform for improved induction of human iPSCs. Nat Methods. 2009;6(11):805-8.

155. Kamp TJ, Lyons GE. On the road to iPS cell cardiovascular applications. Circ Res. 2009;105(7):617-9. PMCID: 2771209.

156. Tateishi K, Takehara N, Matsubara H, Oh H. Stemming heart failure with cardiac- or reprogrammed-stem cells. J Cell Mol Med. 2008;12(6A):2217-32.

157. Segers VFM, Lee RT. Stem-cell therapy for cardiac disease. Nature. 2008;451(7181):937-42.

158. Abdel-Latif A, Bolli R, Tleyjeh IM, Montori VM, Perin EC, Hornung CA, et al. Adult Bone Marrow-Derived Cells for Cardiac Repair: A Systematic Review and Meta-analysis. Arch Intern Med. 2007;167(10):989-97.

159. Zammaretti P, Jaconi M. Cardiac tissue engineering: regeneration of the wounded heart. Curr Opin Biotechnol. 2004;15(5):430-4.

160. Dinsmore JH, Dib N. Stem cell therapy for the treatment of acute myocardial infarction. Cardiol Clin. 2010;28(1):127-38.

161. Schabort EJ, Myburgh KH, Wiehe JM, Torzewski J, Niesler CU. Potential Myogenic Stem Cell Populations: Sources, Plasticity, and Application for Cardiac Repair. Stem Cells Dev. 2009.

162. Pasquet S, Sovalat H, Henon P, Bischoff N, Arkam Y, Ojeda-Uribe M, et al. Long-term benefit of intracardiac delivery of autologous granulocyte-colony-stimulating factor-mobilized blood CD34+ cells containing cardiac progenitors on regional heart structure and function after myocardial infarct. Cytotherapy. 2009;11(8):1002-15.

163. Mollmann H, Nef H, Elsasser A, Hamm C. Stem cells in myocardial infarction: from bench to bedside. Heart. 2009;95(6):508-14.

164. Lam JT, Moretti A, Laugwitz KL. Multipotent progenitor cells in regenerative cardiovascular medicine. Pediatr Cardiol. 2009;30(5):690-8.

165. Barile L, Cerisoli F, Frati G, Gaetani R, Chimenti I, Forte E, et al. Bone marrow-derived cells can acquire cardiac stem cells properties in damaged heart. Journal of Cellular and Molecular Medicine. 2009.

166. Bergmann O, Bhardwaj RD, Bernard S, Zdunek S, Barnabe-Heider F, Walsh S, et al. Evidence for cardiomyocyte renewal in humans. Science. 2009;324(5923):98-102.

167. Nakano A, Nakano H, Chien KR. Multipotent islet-1 cardiovascular progenitors in development and disease. Cold Spring Harb Symp Quant Biol. 2008;73:297-306.

168. Laugwitz KL, Moretti A, Caron L, Nakano A, Chien KR. Islet1 cardiovascular progenitors: a single source for heart lineages? Development. 2008;135(2):193-205.

169. Qyang Y, Martin-Puig S, Chiravuri M, Chen S, Xu H, Bu L, et al. The renewal and differentiation of Isl1+ cardiovascular progenitors are controlled by a Wnt/beta-catenin pathway. Cell Stem Cell. 2007;1(2):165-79.

170. Laugwitz KL, Moretti A, Lam J, Gruber P, Chen Y, Woodard S, et al. Postnatal isl1+ cardioblasts enter fully differentiated cardiomyocyte lineages. Nature. 2005;433(7026):647-53.

171. Zimmermann W-H, Didie M, Doker S, Melnychenko I, Naito H, Rogge C, et al. Heart muscle engineering: An update on cardiac muscle replacement therapy. Cardiovascular Research. 2006;71(3):419-29.

172. Clause KC, Tinney JP, Liu LJ, Keller BB, Tobita K. Engineered early embryonic cardiac tissue increases cardiomyocyte proliferation by cyclic mechanical stretch via p38-MAP kinase phosphorylation. Tissue Eng Part A. 2009;15(6):1373-80.

173. Gupta V, Grande-Allen KJ. Effects of static and cyclic loading in regulating extracellular matrix synthesis by cardiovascular cells. Cardiovascular Research. 2006;72(3):375-83.

174. Tandon N, Cannizzaro C, Chao PH, Maidhof R, Marsano A, Au HT, et al. Electrical stimulation systems for cardiac tissue engineering. Nat Protoc. 2009;4(2):155-73.

175. Radisic M, Fast VG, Sharifov OF, Iyer RK, Park H, Vunjak-Novakovic G. Optical mapping of impulse propagation in engineered cardiac tissue. Tissue Eng Part A. 2009;15(4):851-60.

176. Remlinger NT, Czajka CA, Juhas ME, Vorp DA, Stolz DB, Badylak SF, et al. Hydrated xenogeneic decellularized tracheal matrix as a scaffold for tracheal reconstruction. Biomaterials. 2010;31(13):3520-6.

177. Dvir T, Kedem A, Ruvinov E, Levy O, Freeman I, Landa N, et al. Prevascularization of cardiac patch on the omentum improves its therapeutic outcome. Proc Natl Acad Sci U S A. 2009.

178. Konuma T, Devaney EJ, Bove EL, Gelehrter S, Hirsch JC, Tavakkol Z, et al. Performance of CryoValve SG decellularized pulmonary allografts compared with standard cryopreserved allografts. Ann Thorac Surg. 2009;88(3):849-54; discussion 554-5.

179. Breymann T, Blanz U, Wojtalik MA, Daenen W, Hetzer R, Sarris G, et al. European Contegra multicentre study: 7-year results after 165 valved bovine jugular vein graft implantations. Thorac Cardiovasc Surg. 2009;57(5):257-69.

180. Brown BN, Barnes CA, Kasick RT, Michel R, Gilbert TW, Beer-Stolz D, et al. Surface characterization of extracellular matrix scaffolds. Biomaterials. 2010;31(3):428-37. PMCID: 2783670.

181. Pfeffer M, Pfeffer J, Fishbein M, Fletcher P, Spadaro J, Kloner R, et al. Myocardial infarct size and ventricular function in rats. Circ Res 1979;44:503–12.

182. Thai HM, Juneman E, Lancaster J, Hagerty T, Do R, Castellano L, et al. Implantation of a three-dimensional fibroblast matrix improves left ventricular function and blood flow after acute myocardial infarction. Cell Transplant. 2009;18(3):283-95. PMCID: 2739416.

183. Chen F, Yoo JJ, Atala A. Acellular collagen matrix as a possible "off the shelf" biomaterial for urethral repair. Urology. 1999;54(3):407-10.

184. Reddy PP, Barrieras DJ, Wilson G, Bagli DJ, McLorie GA, Khoury AE, et al. Regeneration of functional bladder substitutes using large segment acellular matrix allografts in a porcine model. J Urol. 2000;164(3 Pt 2):936-41.

185. Zhao ZQ, Puskas JD, Xu D, Wang NP, Mosunjac M, Guyton RA, et al. Improvement in Cardiac Function With Small Intestine Extracellular Matrix Is Associated With Recruitment of C-Kit Cells, Myofibroblasts, and Macrophages After Myocardial Infarction. J Am Coll Cardiol. 2010;55(12):1250-61.

186. McDevitt CA, Wildey GM, Cutrone RM. Transforming growth factor-beta1 in a sterilized tissue derived from the pig small intestine submucosa. J Biomed Mater Res A. 2003;67(2):637-40.

187. Reing JE, Zhang L, Myers-Irvin J, Cordero KE, Freytes DO, Heber-Katz E, et al. Degradation products of extracellular matrix affect cell migration and proliferation. Tissue Eng Part A. 2009;15(3):605-14.

188. Kalluri R. Basement membranes: structure, assembly and role in tumour angiogenesis. Nat Rev Cancer. 2003;3(6):422-33.

189. Badylak SF, Liang A, Record R, Tullius R, Hodde JP. Endothelial cell adherence to small intestinal submucosa: an acellular bioscaffold. Biomaterials. 1999;20(23-24):2257-63.

190. Mangi AA, Noiseux N, Kong D, He H, Rezvani M, Ingwall JS, et al. Mesenchymal stem cells modified with Akt prevent remodeling and restore performance of infarcted hearts. Nat Med. 2003;9(9):1195-201.

191. Lerman RH, Apstein CS, Kagan HM, Osmers EL, Chichester CO, Vogel WM, et al. Myocardial healing and repair after experimental infarction in the rabbit. Circ Res. 1983;53(3):378-88.

192. McCormick RJ, Musch TI, Bergman BC, Thomas DP. Regional differences in LV collagen accumulation and mature cross-linking after myocardial infarction in rats. Am J Physiol. 1994;266(1 Pt 2):H354-9.

193. Jugdutt BI. Ventricular remodeling after infarction and the extracellular collagen matrix: when is enough enough? Circulation. 2003;108(11):1395-403.

194. Sellaro T, Ranade A, Faulk D, McCabe GP, Dorko K, Badylak SF, et al. Maintenance of Human Hepatocyte Function in Vitro by Liver-Derived Extracellular Matrix Gels. Tissue Eng Part A. 2009.

195. Brown BN, Valentin JE, Stewart-Akers AM, McCabe GP, Badylak SF. Macrophage phenotype and remodeling outcomes in response to biologic scaffolds with and without a cellular component. Biomaterials. 2009;30(8):1482-91.

196. Hopkins RA, Jones AL, Wolfinbarger L, Moore MA, Bert AA, Lofland GK. Decellularization reduces calcification while improving both durability and 1-year functional results of pulmonary homograft valves in juvenile sheep. J Thorac Cardiovasc Surg. 2009;137(4):907-13, 13e1-4.

197. Kelly DJ, Rosen AB, Schuldt AJT, Kochupura PV, Doronin SV, Potapova IA, et al. Increased Myocyte Content and Mechanical Function Within a Tissue-Engineered Myocardial Patch Following Implantation. Tissue Engineering Part A.0(0).